



Scuola Internazionale Superiore di Studi Avanzati - Trieste



INTERNATIONAL SCHOOL FOR ADVANCED STUDIES

STATISTICAL PHYSICS CURRICULUM
ACADEMIC YEAR 2014-2015

Phase Separation and Interfaces

Exact Results

Thesis submitted for the degree of
DOCTOR PHILOSOPHIÆ

Advisor
PROF. GESUALDO DELFINO

Candidate
ALESSIO SQUARCINI

SISSA - Via Bonomea 265 - 34136 TRIESTE - ITALY



INTERNATIONAL SCHOOL FOR ADVANCED STUDIES

STATISTICAL PHYSICS CURRICULUM
ACADEMIC YEAR 2014-2015

Phase Separation and Interfaces

Exact Results

Thesis submitted for the degree of
DOCTOR PHILOSOPHIÆ

Advisor

PROF. GESUALDO DELFINO

Candidate

ALESSIO SQUARCINI

Outlook

This thesis conveys the exact theory of phase separation and interfaces in two dimensions developed in the research articles:

- G. Delfino and J. Viti, *Phase separation and interface structure in two dimensions from field theory*, J. Stat. Mech. (2012) P10009 ([1]);
- G. Delfino and A. Squarcini, *Interfaces and wetting transition on the half plane. Exact results from field theory*, J. Stat. Mech. (2013) P05010 ([2]);
- G. Delfino and A.Squarcini, *Exact theory of intermediate phases in two dimensions*, Annals of Physics 342 (2014) 171-194 ([3]);
- G. Delfino and A.Squarcini, *Phase separation in a wedge. Exact results*, Physical Review Letters 113, (2014) 066101 ([4]);
- G. Delfino and A.Squarcini, *Multiple phases and vicious walkers in a wedge*, arXiv:1509.00310v1([5]);
- G. Delfino and A.Squarcini, *Bulk and boundary effects on the decay of the thermodynamic Casimir force*, Europhysics Letters 109 (2015) 16001 ([6]).

We will devote Chapter 1 to a short review of traditional approaches to interfacial phenomena. This starts with an overview on phenomenological descriptions and terminates with a discussion on mean field theories of interfaces. In Chapter 2 we recall some essential notions of scattering theory in two dimensions on which we will rely in the rest of the thesis. In Chapter 3 we will pose the basis of the exact field-theoretic approach to phase separation in two dimensions. In particular, we will develop the formalism for the study of interfaces in a strip geometry. Drops on a flat substrate and the corresponding wetting transition will be discussed in Chapter 4. In Chapter 5 we will analyze phase separation in presence of a wedge-shaped substrate and its field-theoretical implications.

The exposition will cover phase separation both with and without the occurrence of intermediate phases. These two regimes will be discussed in detail for

the strip, half-plane and wedge geometries. Our study is based on universal properties of the scaling limit and accounts exactly for the properties of the different universality classes.

The field-theoretical approach to near-critical behavior does not exhaust its applications to interfacial phenomena. We will conclude in Chapter 6 with a further application in which we will consider the thermal Casimir effect, *i.e.* the analogue of the quantum Casimir effect for statistical systems near criticality. We will show how bulk and boundary effects, jointly with the symmetry of boundary conditions, play a role in the determination of the long-distance decay of the Casimir force.

Contents

Outlook	i
1 Introduction to phase separation, interfaces and wetting	1
1.1 Phase separation: preliminary notions	1
1.2 Phenomenology of interfacial phenomena	3
1.2.1 Wetting	3
1.2.2 Capillary wave theory	6
1.3 Surface critical behavior in mean field theory	8
1.3.1 A free domain wall	10
1.3.2 Cahn-Landau theory	11
2 Notions of two-dimensional scattering theory	15
2.1 Bulk scattering	15
2.1.1 Elastic amplitude	16
2.1.2 Analytic properties	17
2.2 The integrable case	20
2.3 Boundary scattering	22
3 Exact theory of phase separation in two dimensions	25
3.1 Introduction	25
3.2 Adjacent phases and single interfaces	26
3.2.1 Order parameter profile	26
3.2.2 Interface structure and passage probability	32
3.3 Intermediate phases	34
3.4 Application to the q -state Potts model	43

3.5	Exact interfacial wetting transition: Ashkin-Teller model	49
3.6	Summary	54
3.7	Appendix A: computation of integrals	56
3.8	Appendix B: Critical interfaces	60
4	Interfaces and wetting on the half plane	63
4.1	Introduction	63
4.2	Single interface	64
4.3	Wetting transition	70
4.4	Intermediate phases	73
4.5	Summary	78
4.6	Appendix A: computation of integrals	79
5	Phase separation and filling transition in a wedge	85
5.1	Introduction	85
5.2	Two phases in a wedge	86
5.3	Filling transition	92
5.4	Third phase and double interface	94
5.5	Summary	100
6	Decay of the thermodynamic Casimir force: bulk and boundary effects	105
6.1	Introduction	105
6.2	Below the critical temperature	108
6.2.1	Identical boundary conditions	108
6.2.2	Mixed boundary conditions	111
6.3	Above the critical temperature	112
6.4	Summary	114
	Bibliography	120

Chapter 1

Introduction to phase separation, interfaces and wetting

Before turning to the exact results in two dimensions which are the subject of this thesis, in this chapter we recall some general notions, as well as the phenomenological and mean-field descriptions of wetting and surface critical behavior.

1.1 Phase separation: preliminary notions

Phase separation is a common phenomenon of everyday life. A typical example is a glass of water in which the liquid phase is in contact with its saturated vapor phase. Many other similar phenomena include binary mixtures below the consolute point, binary alloys, domain walls in magnetic systems, etc. The examples above provide an intuitive view of the phenomenon, which finds a macroscopic formalization in the framework of classical thermodynamics. Thermodynamic systems at equilibrium are characterized by homogeneous domains of states of matter and chemical composition termed *phases*. Phase coexistence means the simultaneous existence of more phases of the same system in thermodynamic equilibrium¹ [7]. The coexistence of different phases naturally leads to the notions of *phase separation* and *interface*, the latter being defined as the surface of common contact that separates two coexisting phases. In a continuum picture

¹In the examples we gave at the beginning the phase can be identified either with the state of matter (liquid-air) or with the chemical composition (binary mixtures).

the surface can be regarded as a D -dimensional manifold embedded in a $D + 1$ dimensional bulk.

Consider the thermodynamic equilibrium of a fluid system. The thermodynamic state is uniquely determined by the pressure P , volume V and temperature T . All these quantities are related among each other through the equation of state $f(P, V, T) = 0$ whose graphical representation is summarized in the phase diagram of that substance [7]. We report in Fig.1.1 two prototypical phase diagrams¹.

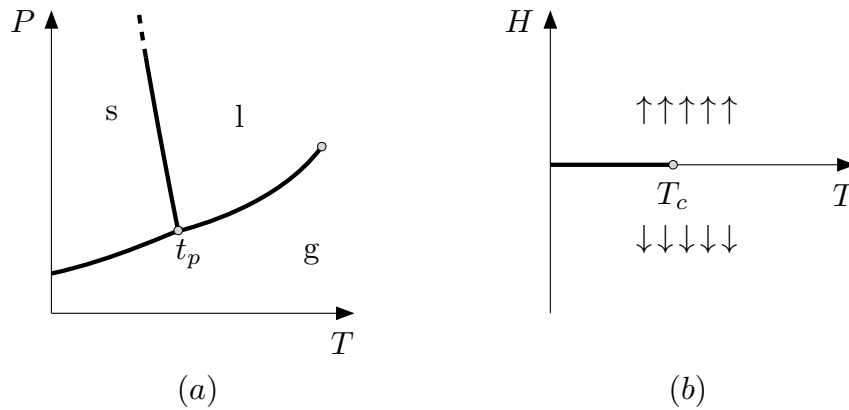


Figure 1.1: Schematic projection of the phase diagram onto the PT variables for fluid (a) and HT variables for a magnetic (b) system (see text). Note that (a) is a qualitative phase diagram of water since the negative slope of the SL coexistence line is at the origin of the increasing pressure upon freezing, while (b) is the phase diagram of the Ising model.

Each phase in the diagram of Fig.1.1(a) is defined by a mass density ρ ; an interface in a fluid system divides two regions with different values of mass density. Phase coexistence takes place along the lines of first-order phase transition where each phase is characterized by a finite correlation length. Three lines of first-order transitions may meet together in a common point known as *triple point* where three phases can coexist (t_p of Fig.1.1(a))².

While interfaces are often studied in the context of fluid systems, the concept of phase coexistence extends straightforwardly to magnetic systems and

¹Further examples for real substances can be found in [8, 9].

²The most common example is the case of the triple point of water, where ice, liquid water and its vapor coexist.

consequently also the study of their interfaces. With the exception of these introductory sections we will normally use the terminology of magnetic systems. To be definite we will consider ferromagnetic spin models of classical statistical mechanics. In close analogy with the fluid case, the thermodynamic state of a magnetic system is defined through the magnetic field H , magnetization M and temperature T . The coexistence curves in the PT plane have the magnetic analogue in the curves on the HT plane [10]. An interface in a magnetic system is thus a domain wall that separates two regions of different magnetization. Along the phase coexistence line ($H = 0, T < T_c$) of Fig.1.1(b) domains of different magnetization can freely coexist at thermodynamic equilibrium. In the phase diagram of Fig.1.1(b) the line of first order transitions terminate in a second-order phase transition point, located in $T = T_c, H = 0$. The distinctive feature of second order phase transition points is the divergence of the correlation length, a phenomenon at the basis of the emergence of scale invariance and universality of critical behavior (see *e.g.* [11]).

1.2 Phenomenology of interfacial phenomena

In this section we present an overview of the phenomenological aspects of the physics of interfaces. The literature on wetting and interfacial phenomena is extremely vast and we only mention some reviews on the subject [12, 13, 14, 15, 16, 17], and [18] as an introductory textbook.

1.2.1 Wetting

Every solid material exposed to the environment is inevitably coated by a gas or a liquid phase. The interplay/competition of molecular forces between solid and fluid can lead to quite distinct surface phenomena such as the formation of isolated liquid drops on the solid substrate or a macroscopically thick layer of liquid adsorbed on it. Consider a liquid drop on a flat and solid substrate as in Fig.1.2. At thermodynamic equilibrium the shape of the drop is such that it attains an *equilibrium contact angle* θ . Each pair of phases - solid-vapor, solid-liquid and liquid-vapor - is characterized by a certain surface tension, that we

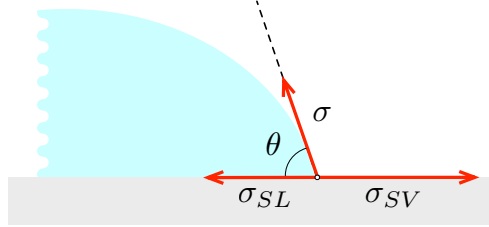


Figure 1.2: Equilibrium contact angle of a sessile drop.

denote with $\sigma_{SV}, \sigma_{SL}, \sigma_{LV} \equiv \sigma$. At equilibrium, these quantities are related by the Young's law [19]:

$$\sigma_{SV} = \sigma_{SL} + \sigma \cos \theta, \quad (1.1)$$

a relation that follows after imposing the mechanical equilibrium of the contact line where the three phases meet. It is worth recalling that such a phenomenological derivation applies considering the contact line as a well defined geometrical entity. Of course this is not very precise since the contact region is affected by strong density inhomogeneities and such a sharp definition of interface between two phases is an artifact. As pointed out in [15], (1.1) can be better derived by the following argument. The energy content of the configuration of Fig.1.2 cannot change after a global shift of the contact line. Such an energy variation is exactly the area of each interface multiplied by the associated surface tension. The free energy does not change if (1.1) holds true. The pictorial representation of Fig.1.2 can be considered valid on length scales much bigger than the typical scales of intramolecular forces. It follows that θ acquires the meaning of contact angle only within this macroscopic perspective¹.

Once the surface tensions are known, (1.1) can be used to predict the wetting state. Two distinct things may happen:

- for $\sigma_{SV} < \sigma_{SL} + \sigma$, a solid-vapor interface is energetically favored and Young's law gives a finite contact angle θ . In this regime the substrate is covered by isolated drops and the corresponding state is termed *partial wetting*;

¹An alternative way to prove the Young's law consist into a minimization of the energy content of an hemispherical-shaped sessile drop on a planar substrate [20].

- for $\sigma_{SV} = \sigma_{SL} + \sigma$ ⁽¹⁾, the contact angle vanishes and the drops spread along the substrate forming a macroscopically thick wetting layer²; in this case we talk about *complete wetting*.

The quantity $S \equiv \sigma_{SV} - \sigma_{SL} - \sigma = -\sigma(1 - \cos\theta)$, called *equilibrium spreading coefficient*, measures the free energy difference associated to the solid-vapor interface with respect to the wet situation. The spreading coefficient is commonly used to determine the wetting state; we have partial wetting for $S < 0$ and complete wetting for $S = 0$. The passage from a partially wet to a completely wet substrate goes under the name of *wetting transition*. Such a transition can be induced upon the variation of a thermodynamic variable of the system, which in general is the temperature. Typically, there exists a wetting temperature T_w lesser than the bulk critical point temperature T_c such that partial wetting occurs for $T < T_w$ while complete wetting at $T_w \leq T < T_c$. Wetting transitions are characterized by the vanishing of the equilibrium contact angle and the divergence of the wetting thickness.

The existence of a wetting temperature smaller than the critical one has been argued by Cahn [21] using a heuristic argument that we report. It is known that close to the critical point the surface tension of the LV interface vanishes as a power law $\sigma \propto (T_c - T)^\mu$. This fact is known since van der Waals, which also predicts a mean field critical exponent $\mu_{MF} = \frac{3}{2}$. From a modern perspective, the surface tension exhibits a critical behavior and μ is called Widom exponent [22]. Cahn argued that also $\sigma_{SV} - \sigma_{SL}$ approaches zero close to criticality through a power law $\sigma_{SV} - \sigma_{SL} \propto (T_c - T)^{\beta_1}$. The surface critical exponent β_1 is associated to the order parameter [23] - mass density in this case. It follows that close to T_c , $\cos\theta \sim (T_c - T)^{\beta_1 - \mu}$. For a three dimensional system Cahn used the values $\mu \approx 1.3$ and $\beta_1 \approx 0.8$. Since the cosine cannot be greater than unity there exist a wetting temperature $T_w < T_c$, such that for $T = T_w$ the cosine reaches unity and the angle vanishes.

¹This condition is known as Antonov rule. The energetic cost of the SV interface equals the sum of free energies of isolated SL and LV interfaces.

²The thickness of the wetting layer may be limited by gravitational effects.

1.2.2 Capillary wave theory

The simplest description of the wetting mechanisms is based on a phenomenological approach. At low temperatures the surface is mildly undulated and therefore it can be suitably described by collective coordinates. A point \mathbf{s} on the surface $\mathfrak{S} \in \mathbb{R}^d$ is parametrized via the *Monge gauge*, which amounts to set $\mathbf{s} = (\mathbf{r}, \ell(\mathbf{r}))$. The height function $\ell(\mathbf{r})$ is a smooth map of a subset of \mathbb{R}^{d-1} to \mathbb{R} or \mathbb{R}^+ , respectively for free and confined interfaces on the half-space (Fig.1.3). We stress that such a parametrization becomes ill-defined at high temperatures where strong undulations may produce overhangs. This is not the situation we are interested in. The free energy content of the interface is thus written as the surface tension

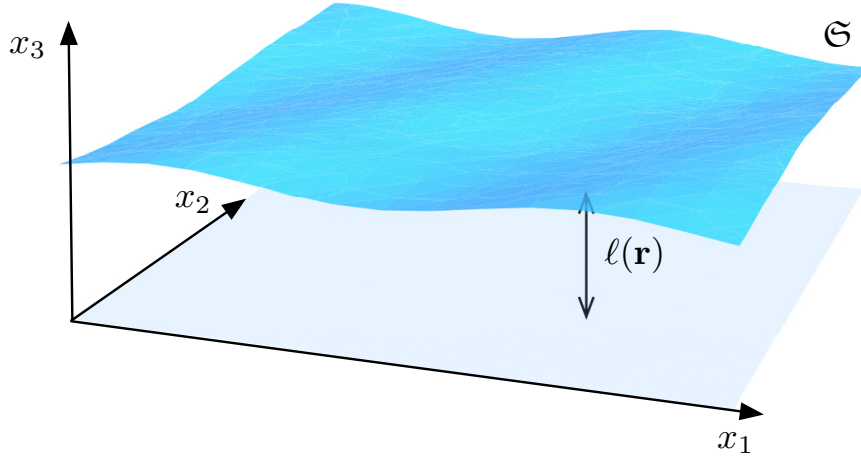


Figure 1.3: A two-dimensional surface in three dimensions.

σ multiplied by the curvilinear area, something that we can write as

$$\beta \mathcal{F}_{DH} = \sigma \int d^{d-1} \mathbf{r} \sqrt{1 + (\nabla \ell)^2}, \quad \beta^{-1} = \kappa_B T, \quad (1.2)$$

which is usually referred as the *drumhead model* [24]. Notice that (1.2) specifies the energy of a height configuration only through the total area, a rather common approach in studies of liquid interfaces¹. The discussion so far considered the

¹We mention that such an approach can be pursued for the study of biological vesicles and lipid membranes. However curvatures are generally not negligible and must be included [25];

surface as isolated, now we introduce a boundary and modify (1.2) accordingly, taking the limit of small curvatures ($|\nabla\ell| \ll 1$) the effective hamiltonian becomes

$$\beta\mathcal{F}_{CW} = \sigma A_\pi + \frac{\sigma}{2} \int d^{d-1}\mathbf{r} [(\nabla\ell)^2 + W(\ell)]. \quad (1.3)$$

The interaction with the boundary is codified through an effective potential $W(\ell)$ and the effective theory (1.3) goes under the name of *Capillary Wave model*. The constant term in (1.3) is the free energy of an isolated flat interface with area A_π given by the projection of \mathfrak{S} onto the remaining $d - 1$ coordinates.

The specific form of the binding potential $W(\ell)$ depends on the interaction forces. Apart from specific features, $W(\ell)$ must decay to a constant (say zero) at $\ell \rightarrow \infty$ and should reproduce the hard-wall repulsion at $\ell \rightarrow 0$. In Fig.1.4 we show two typical forms of the function $W(\ell)$ as the temperature T varies. The minimum of $W(\ell)$ determines the thickness of the wetting layer. For a

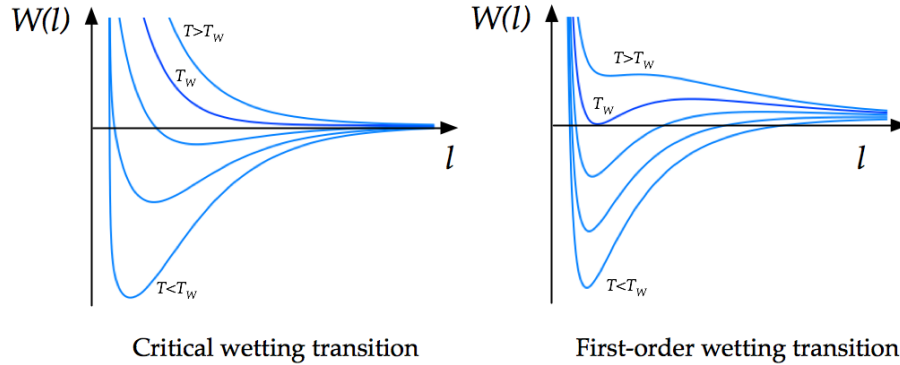


Figure 1.4: Typical forms of the binding potential for: (a) critical wetting and (b) first-order wetting transitions.

critical wetting transition, as T is increased the thickness grows continuously and ultimately diverges for $T \rightarrow T_w$ (Fig.1.4(a)). In contrast, for a first-order wetting transition the minimum jumps discontinuously from a finite value to infinite.

The peculiarity of the wetting transition is a strong sensitivity of the transition order depending on the kind of cohesion forces among solid-liquid molecules and liquid molecules with themselves. One of the first tasks of a theory for wetting is the determination of the equilibrium spreading coefficient and the binding

see also [26].

potential for a given system whose interactions are known, at least qualitatively. It is customary, in the wetting context, to consider as long-ranged the forces characterized by an algebraic decay in the intramolecular distance, while short-ranged forces are generally characterized by an exponential decay. A detailed discussion of these issues can be found in the literature. Long-range forces are examined in [16, 27] and references therein. While for short-range forces we refer the reader to [28, 29] for theoretical analyses and to [30] for experiments.

1.3 Surface critical behavior in mean field theory

It is obviously important to pass from a phenomenological to a more fundamental description. It is thus necessary to formulate a theory for the whole system and all its microscopic degrees of freedom; the effective ones will result only after the coarse-graining procedure. We have in mind a statistical system sufficiently close to a critical point in presence of boundaries. Bulk critical behavior can be adequately described by a continuum formulation based on fields. Therefore surface critical behavior will be described by field theories in presence of boundaries. Before turning to the exact treatment of the two-dimensional case in the following chapters, we mention here the field-theoretical approach to surface critical behavior in d dimensions (see e.g. [31]).

Let us take a near critical system with bulk dimension d , confined by a $d - 1$ dimensional hyperplane. For the sake of simplicity we can consider the case of a scalar field φ (generalizations to vector fields can be found in [31]). This is sufficient to show the essential ideas without formal complications. It is customary to divide bulk degrees of freedom from surface ones as follows

$$\mathcal{H}[\varphi] = \mathcal{H}_s[\varphi] + \mathcal{H}_b[\varphi]. \quad (1.4)$$

The Hamiltonian functionals $\mathcal{H}_{b/s}[\varphi]$ specify the free energy of a generic field configuration $\{\varphi\}$. Keep in mind that this sharp division is not unique since bulk terms can be integrated by parts becoming thus surface contributions. Bulk

degrees of freedom are taken into account thanks to

$$\mathcal{H}_b[\varphi] = \int_V d^d x \mathcal{L}_b(\varphi, \partial\varphi). \quad (1.5)$$

with $\mathcal{L}_b(\varphi, \partial\varphi)$ a function of the field and its derivatives. Close to a second-order phase transition point the free energy density takes the usual form of a φ^4 theory

$$\mathcal{L}_b(\varphi, \partial\varphi) = \frac{1}{2} (\nabla\varphi)^2 + U(\varphi), \quad (1.6)$$

with

$$U(\varphi) = \frac{\tau}{2!} \varphi^2 + \frac{g}{4!} \varphi^4. \quad (1.7)$$

The bare coupling constants τ and g are chosen in order to reproduce the double-well potential below a certain MF critical temperature. Within these notations the excess free energy writes as $\omega(\varphi) = U(\varphi) - U(\varphi_0)$. The surface term specifies the free energy of a field configuration due to the interaction with the boundary. In general one has

$$\mathcal{H}_s[\varphi] = \int_{\partial V} d^{d-1}x \mathcal{L}_s(\varphi, \partial\varphi), \quad (1.8)$$

the specific form of $\mathcal{L}_s(\varphi, \partial\varphi)$ will be specified later. At mean field level, fluctuation effects are not included and the field configuration φ^* follows from the energy minimization. The stationarity condition

$$\left. \frac{\delta\mathcal{H}[\varphi]}{\delta\varphi(x)} \right|_{\varphi=\varphi^*} = 0, \quad (1.9)$$

leads to the MF equation for the field profile

$$\nabla^2\varphi(x) = \tau\varphi + \frac{g}{6}\varphi^3. \quad (1.10)$$

Such a differential equation must be supplemented with the boundary condition generated by the surface term. Standard techniques of field theory allow one to carry out the study of fluctuation effects on top of the mean-field solution. These techniques are based on perturbative techniques such as the ϵ -expansion. Critical exponents and interfacial profile can be computed perturbatively for continuous bulk dimension d . These aspects are well described in the review articles [31,

[32](#)]. In the following sections we recall the solution of (1.10) in absence of a boundary, finding the magnetization profile of a free domain wall. Then we recall the treatment of wetting in presence of boundary.

1.3.1 A free domain wall

Let us determine the mean-field profile in absence of boundaries. We consider a system in d -dimensions on a slab geometry with two parallel plates of area A enclosing a volume V . Let us denote with x the spatial coordinate orthogonal to the plates. Without loss of generality we can assume the field φ to be a function of x alone. Using the definition of excess free energy we can write (1.4) in the form $\mathcal{H}[\varphi] = VU(\varphi_0) + A\sigma[\varphi]$ where volume and surface contributions are clearly separated. The surface tension is given by

$$\sigma[\varphi] = \int_{\mathbb{R}} dx \left[\frac{1}{2} \left(\frac{d\varphi}{dx} \right)^2 + \omega(\phi) \right]. \quad (1.11)$$

Below criticality $\omega(\varphi)$ is a double-well potential with global minima in $\pm\varphi_0$ corresponding to bulk magnetizations. Following the parametrization of [\[33\]](#) we write

$$\omega(\phi) = \frac{\kappa^2}{8\varphi_0^2} (\varphi^2 - \varphi_0^2)^2, \quad (1.12)$$

the bulk correlation length κ^{-1} expresses the concavity of ω at bulk phases. After the functional differentiation of (1.9) we get

$$\frac{d^2\varphi(x)}{dx^2} + \partial_\varphi\omega(\varphi) = 0. \quad (1.13)$$

The solution is fixed after imposing the correct asymptotic behavior of the profile

$$\lim_{x \rightarrow \infty} \varphi(x) = \varphi_0, \quad (1.14)$$

$$\lim_{x \rightarrow \infty} \varphi'(x) = 0, \quad (1.15)$$

and after simple manipulations we find

$$\varphi(x) = \varphi_0 \tanh \left(\kappa \frac{x - \ell}{2} \right). \quad (1.16)$$

The profile (1.16) smoothly interpolates between the asymptotic magnetization $-\varphi_0$ and φ_0 . For $x = \ell$ the field vanishes and we can consider that position as the location of the interface between the bulk phases (*crossing criterion*). Notice that the interface position is a free parameter since boundaries are absent. Still at MF level, we can compute the surface tension of this “liquid-vapor” interface. From (1.11) and (1.16) we obtain after a simple integration $\sigma = \frac{2}{3}\kappa\varphi_0^2$. We recall that close to T_c the surface tension vanishes as $\sigma \sim (T_c - T)^\mu$, with a Widom exponent μ that obeys the scaling and hyper-scaling laws [22]

$$\mu + \nu = 2 - \alpha, \quad (1.17)$$

$$\mu = (d - 1)\nu. \quad (1.18)$$

The exponent μ predicted by this MF calculation is independent on d and takes the value $\frac{3}{2}$. Notice that this result differs from the one found in three-dimensional systems, $\mu = 1.28 \pm 0.06$ [22]. Despite this discrepancy this approach is reliable and possible improvements have provided better results on surface tensions, see [34] and references therein.

1.3.2 Cahn-Landau theory

Short range forces and wetting behavior can be adequately described under a unified picture due to Cahn [21]. The basic ingredients follow from the general recipe. The excess free energy takes the form

$$\mathcal{H}[\varphi] = U_s(\varphi_s) + \int_0^\infty dz \left[\frac{1}{2} (\partial_z \varphi)^2 + \omega(\varphi) \right]. \quad (1.19)$$

The interaction with the wall is codified by the boundary free energy

$$U_s(\varphi_s) = -h_1\varphi_s + \frac{c}{2}\varphi_s^2, \quad (1.20)$$

in which $\varphi_s \equiv \varphi(0)$ is the magnetization on the boundary. A constant boundary magnetic field h_1 couples with the order parameter linearly while the *surface enhancement* c describes, in a fluid analogy, the depletion of liquid particles close

to the wall. Once again, the mean field profile is determined by

$$\frac{d^2\varphi(x)}{dx^2} + \partial_\varphi\omega(\varphi) = 0, \quad (1.21)$$

while the boundary term produces the boundary condition

$$\left. \frac{d\varphi}{dx} \right|_{x=0} = c\varphi(0) - h_1. \quad (1.22)$$

The stationarity condition is actually analogous to the classical motion of a particle on a line. The identification is established by interpreting the spatial coordinate x as the “time”, φ as the “coordinate” and $-\omega$ as the “potential energy”. The analogue of energy conservation gives¹ the “velocity” $\varphi'(x) = \pm\sqrt{2\omega(\varphi)} \equiv Q(\varphi)$. Using this result we can eliminate φ' and work with the field alone. After a simple algebra we determine the surface tension as the free energy computed with the MF profile; it reads

$$\sigma(\varphi_s) = \int_{\varphi_s}^{\varphi_b} d\varphi [Q(\varphi) - Y(\varphi)] + U_s(\varphi_b), \quad (1.23)$$

with $Y(\varphi) \equiv c\varphi - h_1$ and φ_b is the bulk magnetization. We notice that the mechanical analogy admits also a graphical interpretation in terms of areas. The integral (1.23) is actually the area enclosed between the curves Q and Y . The surface magnetization is obtained by the solution of $Q(\varphi_s) = Y(\varphi_s)$. The number of solutions of the above equations characterizes the order of the wetting transition. In the following we describe the interpretation of wetting within this model.

- **Critical wetting.** For $c > \kappa$ there is always a unique intersection of Q with Y . If $|\varphi_s| < \varphi_0$ the profile decrease from φ_s to $-\varphi_0$: the bulk region is occupied by the vapor phase. If $\varphi_s > \varphi_0$ the profile decreases from φ_s to φ_0 and the bulk is now occupied by the liquid phase, see Fig.1.5.
- **First-order wetting.** For $0 < c < \kappa$ there can be at most three solutions. As before, each intersection determines a profile that decreases towards the

¹The choice of the \pm is determined by the bulk phase, i.e. the magnetization must decrease if $-\varphi_0$ is the bulk magnetization.

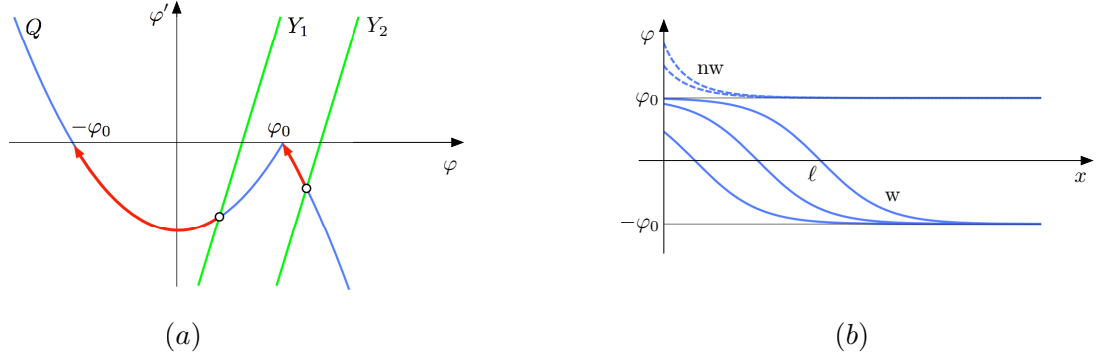


Figure 1.5: The graphical construction for critical wetting (a). Y_1 corresponds to a non-wetting profile as the continuous curves of (b). Y_2 produces a wetting profile as the dashed curves of (b).

closest bulk value. It is possible to show that in the regime of three intersections only two of them correspond to stable configurations (α, γ in Fig.1.6), while the remaining one is metastable (β in Fig.1.6). Stable solutions however compete among themselves and the one with lower surface tension is attained by the system. In the marginal situation the surface tensions become equal and a slight change in h_1 is sufficient to induce a jump from one to the other. This condition can be translated into a Maxwell-like construction of area laws, according to the graphical interpretation. Since the two profiles are characterized by different “traveling times” the jump of the wetting layer is actually discontinuous: the transition is of the first order.

This simplified exposition is sufficient to appreciate the key predictions of the theory. We refer to [21, 17] for an extensive discussion of the graphical constructions for off-coexistence systems. To conclude, the merit of this theory relies on its simplicity compared with the wealth of critical behavior, as summarized in the wetting phase diagram proposed in [35].

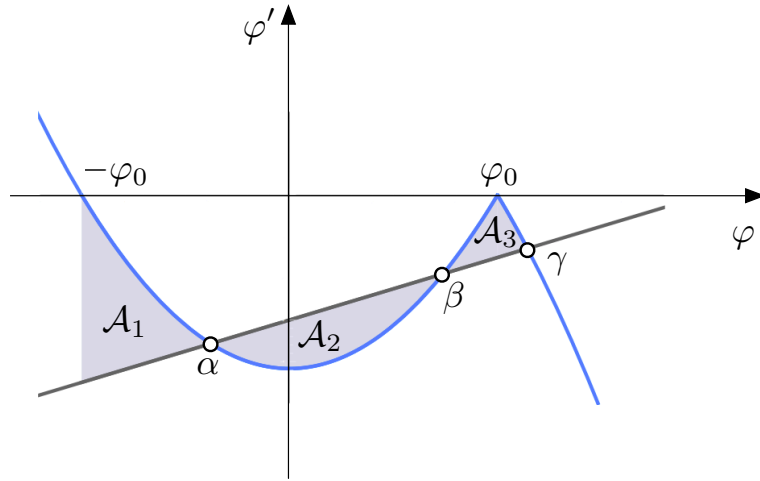


Figure 1.6: Equal area construction for a first-order wetting transition. Stable configurations correspond to a partially wet substrate and their relative stability is dictated by the difference of the areas $\sigma_\alpha - \sigma_\gamma = \mathcal{A}_3 - \mathcal{A}_2$.

Chapter 2

Notions of two-dimensional scattering theory

In this chapter we introduce basic notions of relativistic scattering theory in two dimensions, both in the bulk and at boundaries, to be exploited in the following chapters.

2.1 Bulk scattering

Every lattice structure carries with itself a spatial anisotropy, which is removed near criticality where the typical extent of correlations is much greater than the lattice scale. In such a continuum limit the system becomes isotropic and rotationally invariant¹. The corresponding field theory associated to the scaling limit is a *Euclidean Field Theory*. In $D = 2$ a point on the Euclidean plane \mathbb{E}^2 is regarded as the analytic continuation to imaginary time of a point in $(1 + 1)$ Minkowski space-time. More precisely, a Euclidean field theory with space coordinates (x, y) can be regarded as the analytic continuation of a Quantum Field Theory in Minkowski space-time with coordinates (x, t) under the Wick rotation $y = it$. The square distance $x^2 - t^2$ of an event from the origin is a relativistic invariant that under the analytic continuation turns into the invariance of the Euclidean norm $x^2 + y^2$.

¹We shall not consider boundaries in this section.

The elementary excitations are massive, relativistic and real (not virtual) particles. The latter requirement is enforced by the *on-shell* condition $E^2 - p^2 = m^2$. Energy-momentum can be parametrized through the rapidity variable θ

$$(E, p) = (m \cosh \theta, m \sinh \theta). \quad (2.1)$$

Particles interact among themselves once they come close enough: such a process is a relativistic scattering. It is thus essential to remind some basic properties of relativistic scattering. Let us consider a set of n incoming particles, each with energy-momentum (E_j, p_j) , $j \in \{1, \dots, n\}$. After the collisions the final state will be characterized by momenta (E'_j, p'_j) . Total energy and total momentum must be conserved. In relativistic theories however n may not be conserved.

The probability of such a scattering event is the square modulus of the matrix element

$$S_{a_1, \dots, a_n}^{b_1, \dots, b_n}(p_1, \dots, p_n | p'_1, \dots, p'_n) \equiv {}_{b_1, \dots, b_n} \langle p'_1, \dots, p'_n | \mathcal{S} | p_1, \dots, p_n \rangle_{a_1, \dots, a_n}; \quad (2.2)$$

we used a_j, b_j to denote internal quantum numbers. In such a notation $|p_1, \dots, p_n\rangle_{a_1, \dots, a_n}$ denotes the *incoming state*, while ${}_{b_1, \dots, b_n} \langle p'_1, \dots, p'_n |$ is the *outgoing state*. The operator \mathcal{S} is called *scattering operator*. The short-ranged interactions we are assuming allow us to consider incoming and outgoing states as composed by free particles. In particular, the asymptotic states form a basis of the Hilbert space; orthogonality and completeness are assumed¹.

2.1.1 Elastic amplitude

The scattering is called *elastic* if particle number is conserved. Let us consider the simplest among the elastic scattering events: the diffusion of two particles. In a diffusion the masses do not change, and for the sake of simplicity we take all particles with the same mass m . In two dimensions, energy and momentum conservation forces the final momenta to be equal to the initial ones. The scattering however can redistribute charges. The two-body process we are referring to can be pictorially represented as in Fig.2.1. Let us discuss the corresponding

¹States are normalized through the condition ${}_i \langle p_1 | p_2 \rangle_j = 2\pi E_i \delta(p_1 - p_2) \delta_{ij}$.

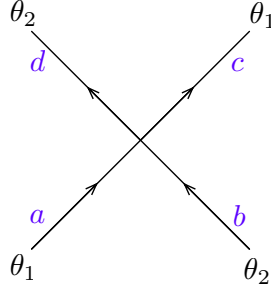


Figure 2.1: Elastic scattering of two particles in $(1 + 1)$ dimensions. Time runs upwards.

scattering amplitude. The amplitude is a relativistically invariant function of the momenta p_1, p_2 , and ultimately of the invariant $s = (E_1 + E_2)^2 - (p_1 + p_2)^2$. In the reference frame of the center of mass, s becomes the square total energy. We denote the scattering amplitude associated to the process of Fig.2.1 as

$$S_{ab}^{cd}(s). \tag{2.3}$$

2.1.2 Analytic properties

The fundamental idea at the basis of the analytic S -matrix approach [36] is to regard s as a complex variable. In Fig.2.2 we show the analytic structure of a typical scattering amplitude $S_{ab}^{cd}(s)$.

The minimum amount of energy needed to produce a state with p particles corresponds to branch points s_p in the complex s -plane. Branch cuts associated to the opening of scattering channels are ultimately originated by the condition of unitarity of the two-particle scattering¹. Apart from branch cuts, a non-analytic behavior may also occur through poles, again with a precise physical meaning. In fact, a pole in the s -plane at $s^* \in (0, s_2)$ corresponds to a bound state particle. The relation

$$S_{ab}^{cd}(s + i\epsilon) = \bar{S}_{da}^{bc}(4m^2 - s^2 - i\epsilon) \tag{2.4}$$

is known as *crossing symmetry* and expresses the fact that interchanging the

¹Notice that branch cuts are actually an infinite sequence. The cuts corresponding to s_p show the nested structure of Fig.2.2.

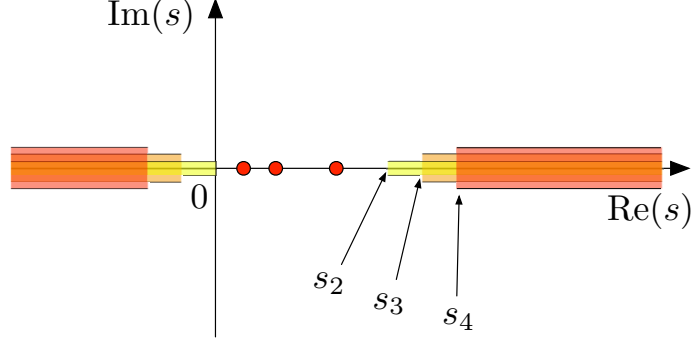


Figure 2.2: The complex s -plane and the singularities of the scattering amplitude. Branch cuts along the real axis correspond to opening of scattering channels. The poles in the region $0 < s < s_2$ are stable bound states.

role of space and time in Fig.2.1 corresponds to an analytic continuation of the amplitude. The symbol $\bar{a} = \mathcal{C}a$ stands for the internal quantum numbers obtained upon change conjugation \mathcal{C} .

Conservation of probability reflects into the *unitarity* of the S -matrix, $\mathcal{S}\mathcal{S}^\dagger = \mathbb{I}$. The collision of two particles may produce intermediate states with n particles if sufficient energy is available. If we restrict our attention to energies below the two-particle threshold, the unitarity condition reads

$$\sum_{e,f} \begin{array}{c} \begin{array}{c} \curvearrowright c \\ \curvearrowright d \\ \curvearrowleft f \\ \curvearrowleft e \end{array} \\ \begin{array}{c} \curvearrowleft a \\ \curvearrowleft b \end{array} \end{array} = \sum_{e,f} S_{ab}^{ef}(s+i\epsilon) [S_{ef}^{cd}(s+i\epsilon)]^* = \delta_{ac}\delta_{bd}. \quad (2.5)$$

Real analyticity is a further requirement. This condition translates into $S_{ab}^{cd}(s+i\epsilon) = [S_{ab}^{cd}(s-i\epsilon)]^*$, and connects upper and lower edges of the cut. The invariant s can be expressed in terms of the rapidity variables as $s = 4m^2 \cosh^2 \frac{\theta_i - \theta_j}{2}$. Notice that a Lorentz boost with rapidity Λ acts as the shift $\theta \rightarrow \theta + \Lambda$. Hence scattering amplitudes depend on rapidities differences because of the Lorentz invariance. Rapidity differences will be denoted with $\theta_{ij} := \theta_i - \theta_j$. With a bit of

abuse of notation we shall write (2.3) as $S_{ab}^{cd}(\theta)$, where $\theta \equiv \theta_{ij}$.

The above properties can be expressed through the θ parametrization as follows:

- *Unitarity*: $\sum_{e,f} S_{ab}^{ef}(\theta) S_{ef}^{cd}(-\theta) = \delta_{ac} \delta_{bd}$,
- *Crossing*: $S_{ab}^{cd}(\theta) = S_{\bar{a}a}^{\bar{b}c}(i\pi - \theta)$,

Finally we quote the parity \mathcal{P} and time-reversal \mathcal{T} symmetries of the S -matrix

- \mathcal{P} : $S_{ab}^{cd}(\theta) = S_{ba}^{dc}(\theta)$,
- \mathcal{T} : $S_{ab}^{cd}(\theta) = S_{cd}^{ab}(\theta)$.

As we just discussed, poles in the physical strip at $\text{Re}(\theta) = 0$ correspond to bound states. Let us suppose the existence of a simple pole for $S_{ab}^{cd}(\theta)$ at $\theta = iu_{ab}^e$ with $u_{ab}^e \in (0, \pi)$. Close to that singularity the scattering amplitude behaves as

$$S_{ab}^{cd} \sim \frac{i\Gamma_{ab}^e \Gamma_{cd}^e}{\theta - iu_{ab}^e}, \quad (2.6)$$

Γ_{ab}^e and Γ_{cd}^e are coupling constants at the three-particle vertex of Fig.2.3(a). The

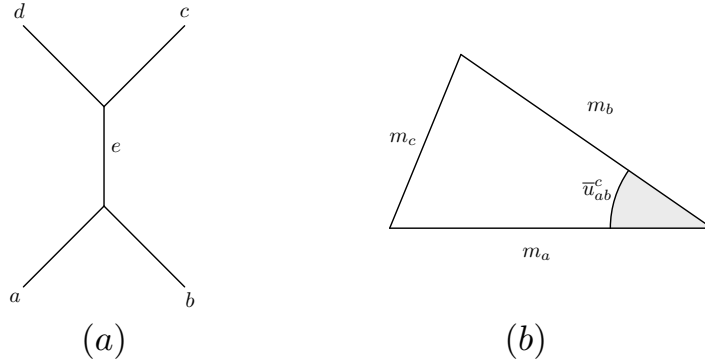


Figure 2.3: (a) graphical representation of a pole in the direct channel corresponding to (2.6) and the mass triangle (b).

location of the pole is determined by the so called *mass-triangle*

$$m_c^2 = m_a^2 + m_b^2 - 2m_a m_b \cos \bar{u}_{ab}^c, \quad (2.7)$$

the angle $\bar{u}_{ab}^c = \pi - u_{ab}^c$ has a clear geometrical meaning (Fig.2.3(b)).

Correlation functions of local fields can be expanded on the complete basis of asymptotic particle states. We recall that Hamiltonian and momentum operators act as the generators of space-time translations

$$\mathcal{O}(x, y) = e^{yH+ixP} \mathcal{O}(0, 0) e^{-ixP-yH}, \quad (2.8)$$

in which we already specified the analytic continuation to the Euclidean space. Form factors are defined as the matrix elements of a local operator \mathcal{O} on the asymptotic n -particle state as follows

$$F_n^{\mathcal{O}}(\theta_1, \dots, \theta_n) = \langle 0 | \mathcal{O}(0, 0) | \theta_1, \dots, \theta_n \rangle. \quad (2.9)$$

The state without particles, i.e. the *vacuum*, is indicated with $|0\rangle$. The two-point correlation function $\langle \mathcal{O}(\mathbf{x}) \mathcal{O}(\mathbf{0}) \rangle$ can be expanded as

$$\begin{aligned} \langle \mathcal{O}(\mathbf{x}) \mathcal{O}(\mathbf{0}) \rangle &= \langle 0 | \mathcal{O}(\mathbf{x}) \mathcal{O}(\mathbf{0}) | 0 \rangle, \\ &= \sum_{n=0}^{\infty} \frac{1}{n!} \int \prod_{j=1}^n \frac{d\theta_j}{2\pi} |F_n^{\mathcal{O}}(\theta_1, \dots, \theta_n)|^2 e^{-|\mathbf{x}| \sum_{j=1}^n E_j}, \end{aligned} \quad (2.10)$$

where $|\mathbf{x}|$ is the Euclidean distance between the two operators. At large distances the exponential decay of the two-point function $\langle \mathcal{O}(\mathbf{x}) \mathcal{O}(\mathbf{0}) \rangle$ is dominated by the lightest particles. This leads to the identification of the inverse of the lowest mass with the bulk correlation length ξ .

2.2 The integrable case

Quantum field theory in $1 + 1$ dimensions allow for integrable theories whose distinctive feature is the presence of infinitely many conservation laws other than energy and momentum. We recall a fundamental difference with respect to the $(3 + 1)$ dimensional case. In that case Coleman-Mandula theorem [37] ensures that a conserved quantity of tensor rank greater than two immediately leads to a trivial scattering, $S = 1$. For $(1 + 1)$ -dimensional theories such a theorem cannot be applied, and the existence of extra conservation laws reflects in a drastic sim-

plification of the scattering processes, which turn out to be extremely constrained. The final state in such a theory has exactly the same number of particles of the initial state with the same set of momenta and a possible redistribution of charges (*complete elasticity*).

An additional property of scattering in integrable theories is *factorization*. Let us denote with P_s a conserved operator with spin s such that it acts on the state $|p\rangle$ as $P_s|p\rangle = \gamma_s(E + p)^s|p\rangle$. A particle around the origin with momentum p is described by the wave-packet

$$\psi_p(x) \sim \int dk f(k)e^{i\kappa x}, \quad (2.11)$$

with $|f(k)|^2$ peaked around p . Applying the operator $e^{iP_s a}$ and performing a stationary-phase approximation of the integrand around $k = p$, the phase becomes $k\partial_k(kx + \gamma_s k^s a)|_{k=p} = kx + k\Delta x(p)$ with $\Delta x(p) = s\gamma_s p^{s-1}$. This last property means that Δx does not depend on the momentum only for the momentum operator ($s = 1$), while in general it does for $s > 1$: this is a non-trivial conservation law. Acting with $e^{iP_s a}$ with $s > 1$ we can resolve the region where three particles meet obtaining a factorization into 3 two-body processes. The factorizability of the scattering process is codified by the *Yang-Baxter* equation

$$\sum_{\beta_1, \beta_2, \beta_3} S_{\alpha_2 \alpha_3}^{\beta_2 \beta_3}(\theta_{23}) S_{\alpha_1 \beta_3}^{\beta_1 \gamma_3}(\theta_{13}) S_{\beta_1 \beta_2}^{\gamma_1 \gamma_2}(\theta_{12}) = \sum_{\beta_1, \beta_2, \beta_3} S_{\alpha_1 \alpha_2}^{\beta_1 \beta_2}(\theta_{12}) S_{\beta_1 \alpha_3}^{\gamma_1 \beta_3}(\theta_{13}) S_{\beta_2 \beta_3}^{\gamma_2 \gamma_3}(\theta_{23}), \quad (2.12)$$

which admits the graphical representation of Fig.2.4.

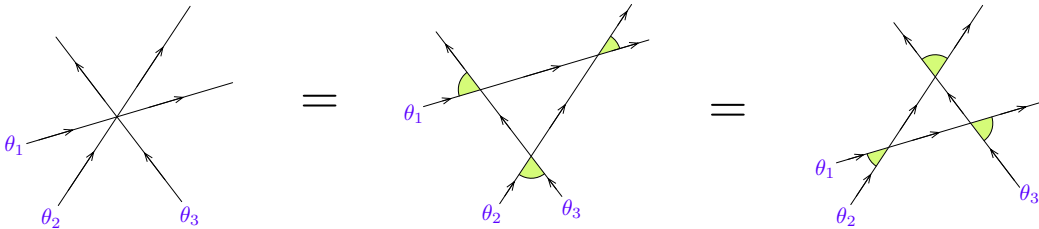


Figure 2.4: The resolution of a three-body scattering and the graphical representation of (2.12). Notice the different chronological order in the scatterings.

2.3 Boundary scattering

As we emphasized in the first chapter, a satisfactory theory for interfacial phenomena must take into account the interplay of bulk excitations with the boundary. The scattering framework, that we outlined in the previous sections, can be suitably generalized to encompass the boundary effects. We consider the half-plane geometry, characterized by the coordinates $(x \geq 0, y)$. The locus of points $(x = 0, y \in \mathbb{R})$ constitutes an infinitely extended and impenetrable boundary. The half-plane with Euclidean time y corresponds to a motion on the half-line $x \geq 0$. Particles in this geometry can scatter among themselves and with the boundary when they reach the position $x = 0$. The boundary itself can be viewed as an infinitely massive particle sitting at $x = 0$. If we consider boundary conditions preserving translation invariance in the y direction, the scattering with the boundary conserves the energy. For elastic scattering, a particle moving towards the wall with rapidity $-\theta$ bounces and reverses the rapidity to θ . The scattering amplitude goes under the name of *reflection amplitude* and it is denoted with $R(\theta)$ (see Fig.2.5(a)). In integrable theories the knowledge of the bulk dynamics encoded by the S -matrix allows for the determination of $R(\theta)$ [38], [39]. The unitarity condition takes the form

$$R(\theta)R(-\theta) = 1, \tag{2.13}$$

and is graphically depicted as in Fig.2.6(a).

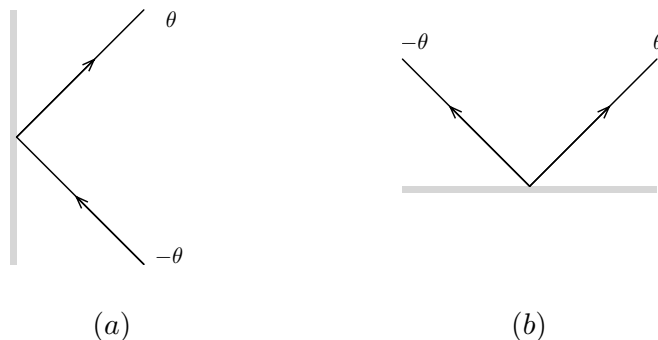


Figure 2.5: (a) reflection amplitude $R(\theta)$ and (b) pair emission amplitude $K(\theta)$.

Boundary crossing requires a bit of care as first pointed out in [38]. The crossed-view of the reflection corresponds to the emission of a pair of particles with opposite momenta. While the reflection process is characterized by energy conservation, the pair emission preserves the total momentum rather than energy. As a consequence of this identification, the reflection amplitude in the direct channel $R(\theta)$ can be analytically continued to define the pair emission amplitude $K(\theta)$ of Fig.2.5(b) as follows

$$K(\theta) = R\left(\frac{i\pi}{2} - \theta\right). \quad (2.14)$$

The replacement $\theta \rightarrow i\pi/2 - \theta$ interchanges energy and momentum as we can see directly from the rapidity parametrization. As realized in [38], crossing symmetry is implemented by imposing the invariance of the pair emission after the interchange of the particles in the bulk, something that takes the concise form

$$K(\theta) = S(2\theta)K(-\theta), \quad (2.15)$$

and the pictorial representation of Fig.2.6(b).

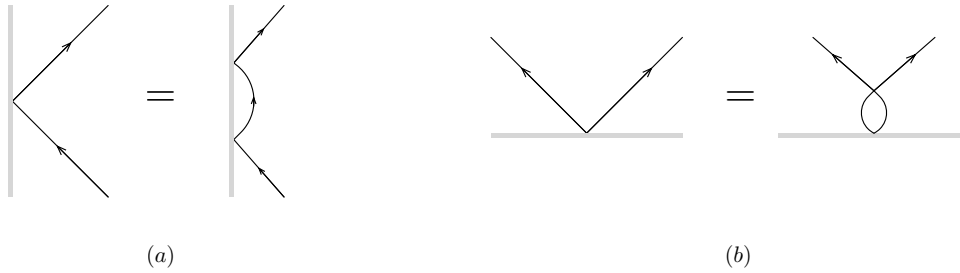


Figure 2.6: Boundary unitarity (a) and boundary crossing symmetry (b).

Chapter 3

Exact theory of phase separation in two dimensions

In this chapter we will illustrate how the formalism of Chapter 2 can be used as starting point for the exact study of phase separation in two dimensions. We will present the fundamental ideas and then we will apply them for the case of a strip geometry. For such a spatial configuration we will investigate first the separation of two phases; then we will extend our approach to systems allowing for the appearance of intermediate phases

3.1 Introduction

Statistical systems at a first order phase transition point allow for phase coexistence. Boundary conditions can be chosen to select a phase a on the left half of the system and a phase b on the right half, the two phases being separated by an interfacial region whose characterization is a particularly interesting problem.

The physics of phase separation is known to be sensitive to dimensionality. The two-dimensional case, in particular, possesses specific features originating from especially strong fluctuations of the interfaces. A key role in establishing the existence of these peculiarities was played by exact results for the planar Ising model [40], which then were used to test the reliability of heuristic descriptions (see in particular [41]). While the technical complexity of lattice derivations has

restricted them to the Ising case, field theory should provide the natural framework for a general study of universal properties in the scaling limit. Nonetheless, a field theory of phase separation in two dimensions has been missing, arguably because the aforementioned peculiarities involve field theoretical counterparts. We now show how the Ising results, as well as new ones, follow as particular cases of the general and exact field theoretical formalism which consistently takes into account the fact that interfaces in two dimensions correspond to trajectories of topological excitations (kinks) propagating in imaginary time.

3.2 Adjacent phases and single interfaces

3.2.1 Order parameter profile

To be definite we refer to a spin model with short range ferromagnetic interactions, at a first order phase transition point. The spin variable can take discrete values labelled by an integer $a = 1, \dots, n$, and the system can be brought into a pure (translationally invariant) phase of type a fixing the boundary spins to the value a and then removing the boundary to infinity.

We consider the scaling limit close to a continuous phase transition point, which yields a Euclidean field theory on the plane with coordinates (x, y) . Such a theory amounts to the continuation to imaginary time $t = iy$ of a relativistic field theory in one space dimension. Phase coexistence corresponds in the relativistic theory to the presence of degenerate vacua $|\Omega_a\rangle$ associated to the pure phases of the system. In $1 + 1$ dimensions the elementary excitations are stable kink states $|K_{ab}(\theta)\rangle$ which interpolate between two different vacua $|\Omega_a\rangle$ and $|\Omega_b\rangle$. These topological excitations are relativistic particles with energy-momentum

$$(e, p) = m_{ab} (\cosh \theta, \sinh \theta) , \quad (3.1)$$

where θ is called rapidity and m_{ab} is the kink mass. Two vacua (phases) are not necessarily connected by an elementary kink, and in this case we call them non-adjacent; non-adjacent vacua will be connected by a multi-kink excitation $|K_{av_1}(\theta_1)K_{v_1v_2}(\theta_2) \dots K_{v_{n-1}b}(\theta_n)\rangle$ which visits other vacua along the way.

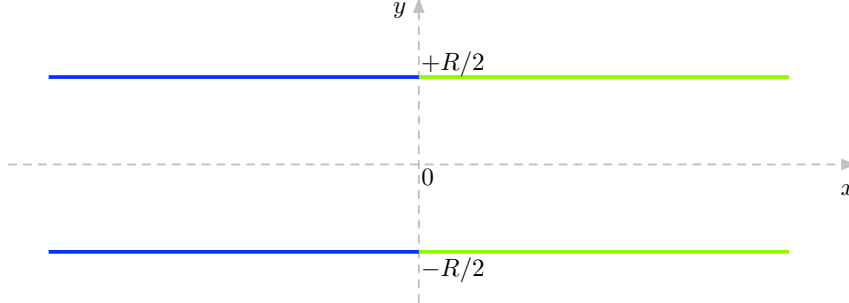


Figure 3.1: ab boundary conditions: the boundary spins are fixed to the value a for $x < 0$ and to a different value b for $x > 0$. We will denote by $\langle \sigma(x, y) \rangle_{ab}$ the magnetization on the strip with these boundary conditions.

We now consider the system on a horizontal strip of width R and fix the boundary spins to a value a for $x < 0$ and to a value $b \neq a$ for $x > 0$ (ab boundary conditions, Fig. 3.1). Phase separation is expected to emerge when R becomes much larger than the correlation length of the pure phases, which is inversely proportional to m_{ab} . In this section we review the case of separation between adjacent phases a and b studied in [1].

The boundary condition at time t switching from a to b at $x = x_0$ is implemented by a boundary state $|B_{ab}(x_0; t)\rangle$ which can be decomposed over the complete basis of states of the bulk theory (the kink states). Since the states entering the decomposition have to interpolate between the phases a and b and the latter are adjacent, we have

$$|B_{ab}(x_0; t)\rangle = e^{-itH + ix_0P} \left[\int_{\mathbb{R}} \frac{d\theta}{2\pi} f_{ab}(\theta) |K_{ab}(\theta)\rangle + \dots \right], \quad (3.2)$$

where H and P are the energy and momentum operators of the (1+1)-dimensional theory, and the dots correspond to states with total mass larger than m_{ab} . The

partition function on the strip with ab boundary conditions then reads¹

$$\begin{aligned} \mathcal{Z}_{ab}(R) &= \langle B(x_0; iR/2) | B(x_0; -iR/2) \rangle \\ &\simeq \int_{\mathbb{R}} d\theta |f_{ab}(\theta)|^2 e^{-m_{ab}R \cosh \theta} \simeq \frac{|f_{ab}(0)|^2 e^{-m_{ab}R}}{\sqrt{2\pi m_{ab}R}}, \end{aligned} \quad (3.3)$$

where in the second line we took the large R limit which projects onto the lightest (single kink) state² in (3.2) and makes the integral dominated by small rapidities. Phase separation amounts to the creation of two pure phases on the far left and on the far right, separated by an interfacial region. The excess free energy due to the creation of the interface divided by R is called interfacial tension and corresponds to

$$\Sigma_{ab} = - \lim_{R \rightarrow \infty} \frac{1}{R} \ln \frac{\mathcal{Z}_{ab}(R)}{\mathcal{Z}_a(R)}, \quad (3.4)$$

where $\mathcal{Z}_a(R)$ is the partition function with all the boundary spin fixed to the value a . The corresponding boundary state expands over bulk states interpolating between a and a , the lightest of which is the vacuum $|\Omega_a\rangle$, so that for large R we have $\mathcal{Z}_a(R) \simeq \langle \Omega_a | \Omega_a \rangle = 1$; (3.3) then yields

$$\Sigma_{ab} = m_{ab}. \quad (3.5)$$

The local magnetization at a point (x, y) on the strip with ab boundary conditions reads

$$\langle \sigma(x, y) \rangle_{ab} = \frac{\langle B_{ab}(0; iR/2) | \sigma(x, y) | B_{ab}(0; -iR/2) \rangle}{\langle B_{ab}(0; iR/2) | B_{ab}(0; -iR/2) \rangle}, \quad (3.6)$$

where $\sigma(x, y)$ is the magnetization operator, satisfying

$$\sigma(x, y) = e^{ixP+yH} \sigma(0, 0) e^{-ixP-yH}. \quad (3.7)$$

¹Kink states are normalized by $\langle K_{ab}(\theta) | K_{b'a'}(\theta') \rangle = 2\pi \delta_{aa'} \delta_{bb'} \delta(\theta - \theta')$. In (3.3) and below the symbol \simeq referred to functions of R indicates omission of terms subleading for R large.

²The minimal energy of an asymptotic state is its total mass.

Use of the boundary state (3.2) gives

$$\begin{aligned} \langle \sigma(x, y) \rangle_{ab} &= \frac{1}{\mathcal{Z}_{ab}(R)} \int_{\mathbb{R}^2} \frac{d\theta}{2\pi} \frac{d\theta'}{2\pi} f_{ab}^*(\theta) \langle K_{ab}(\theta) | e^{(-\frac{R}{2}+y)H} \sigma(x, 0) \\ &\quad e^{-(\frac{R}{2}+y)H} | K_{ab}(\theta') \rangle f_{ab}(\theta') + \dots; \end{aligned} \quad (3.8)$$

the dots stay for the contribution coming from states with higher mass, which for any fixed $|y| < R/2$ becomes negligible as $R \rightarrow \infty$. Then in this limit we have

$$\langle \sigma(x, y) \rangle_{ab} \simeq \frac{1}{\mathcal{Z}_{ab}(R)} \int_{\mathbb{R}^2} \frac{d\theta}{2\pi} \frac{d\theta'}{2\pi} f_{ab}^*(\theta) f_{ab}(\theta') \mathcal{M}_{ab}^\sigma(\theta|\theta') \mathcal{O}(\theta, \theta'), \quad (3.9)$$

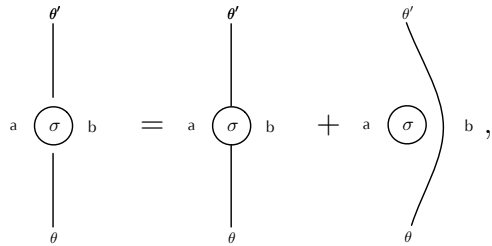
where¹ $\mathcal{O}(\theta, \theta') = e^{-M_- \cosh \theta - M_+ \cosh \theta'} e^{imx(\sinh \theta - \sinh \theta')}$, $M_\pm = m(R/2 \pm y)$, and

$$\mathcal{M}_{ab}^\sigma(\theta|\theta') \equiv \langle K_{ab}(\theta) | \sigma(0, 0) | K_{ba}(\theta') \rangle. \quad (3.10)$$

The matrix element (3.10) decomposes as

$$\mathcal{M}_{ab}^\sigma(\theta|\theta') = \mathcal{F}_{ab}^{\sigma, R}(\theta|\theta') + 2\pi \delta(\theta - \theta') \langle \sigma \rangle_a, \quad (3.11)$$

into the sum of a connected and a disconnected part; $\langle \sigma \rangle_a$ denotes the magnetization in the pure phase a . Such a decomposition corresponds to the pictorial representation



$$\text{Diagram (3.12):} \quad \begin{array}{c} \theta' \\ | \\ \text{a} \circ \sigma \text{ b} \\ | \\ \theta \end{array} = \begin{array}{c} \theta' \\ | \\ \text{a} \circ \sigma \text{ b} \\ | \\ \theta \end{array} + \begin{array}{c} \theta' \\ \curvearrowright \\ \text{a} \circ \sigma \text{ b} \\ \curvearrowleft \\ \theta \end{array}, \quad (3.12)$$

where the disconnected trajectory passes to the right of the insertion point of the magnetization operator, which is then evaluated in the phase a . Of course, the decomposition in which the disconnected trajectory passes to the left of the inser-

¹From now on we will most of the times drop the indices on the kink mass to simplify the notation.

tion point is also allowed, and in this case $\mathcal{F}_{ab}^{\sigma,L}(\theta|\theta')$ and $\langle\sigma\rangle_b$ replace $\mathcal{F}_{ab}^{\sigma,R}(\theta|\theta')$ and $\langle\sigma\rangle_a$ in (3.11). It follows that $\mathcal{F}_{ab}^{\sigma,R}(\theta|\theta')$ and $\mathcal{F}_{ab}^{\sigma,L}(\theta|\theta')$ coincide for $\theta \neq \theta'$, while for $\theta \rightarrow \theta'$ they behave as¹

$$i \frac{\langle\sigma\rangle_a - \langle\sigma\rangle_b}{\theta - \theta' \mp i\epsilon}, \quad (3.13)$$

with the upper (resp. lower) sign referring to $\mathcal{F}_{ab}^{\sigma,R}(\theta|\theta')$ (resp. $\mathcal{F}_{ab}^{\sigma,L}(\theta|\theta')$). For the purpose of generalization in subsequent sections we use the pictorial representation²

$$-i \operatorname{Res}_{\theta_1=\theta_2} \begin{array}{c} \theta_2 \\ | \\ \text{a} \text{---} \textcircled{\sigma} \text{---} \text{b} \\ | \\ \theta_1 \end{array} = \begin{array}{c} \theta_2 \\ \diagdown \\ \text{a} \text{---} \textcircled{\sigma} \text{---} \text{b} \\ \diagup \\ \theta_1 \end{array} - \begin{array}{c} \theta_2 \\ \diagup \\ \text{a} \text{---} \textcircled{\sigma} \text{---} \text{b} \\ \diagdown \\ \theta_1 \end{array} = \langle\sigma\rangle_a - \langle\sigma\rangle_b. \quad (3.14)$$

Once we substitute (3.11) into (3.9) and take into account that for large R the integral is dominated by $\theta \simeq \theta' \simeq 0$, we can use (3.13) to obtain

$$\langle\sigma(x, y)\rangle_{ab} \simeq \langle\sigma\rangle_a + \frac{|f_{ab}(0)|^2 e^{-mR}}{\mathcal{Z}_{ab}(R)} \int_{\mathbb{R}^2} \frac{d\theta d\theta'}{2\pi 2\pi} \frac{i\Delta\langle\sigma\rangle}{\theta - \theta' - i\epsilon} e^{-[\frac{M_-}{2}\theta^2 + \frac{M_+}{2}(\theta')^2] + imx(\theta - \theta')}, \quad (3.15)$$

where $\Delta\langle\sigma\rangle \equiv \langle\sigma\rangle_a - \langle\sigma\rangle_b$. Defining $\theta_{\pm} = \sqrt{mR/8}(\theta \pm \theta')$,

$$\lambda \equiv \sqrt{R/(2m)}, \quad (3.16)$$

$$\kappa \equiv \sqrt{1 - 4y^2/R^2}, \quad |y| < \frac{R}{2}, \quad (3.17)$$

¹Relativistically invariant quantities depend on rapidity differences.

²Kinematical poles like (3.13) are well known to experts of two-dimensional integrable field theory (see [42, 43] and, for the case of kink excitations of interest here, [44, 45]). While integrability simplify the scattering theory and allows the general determination of residues, kinematical poles exist in any two-dimensional field theory. For the two-leg case (3.14) no scattering is involved and the residue is completely general.

and performing the integral on θ_+ gives

$$\langle \sigma(x, y) \rangle_{ab} = \langle \sigma \rangle_a + \frac{i\Delta \langle \sigma \rangle}{2\pi} \int_{\mathbb{R}} \frac{d\theta_-}{\theta_- - i\epsilon} e^{-\kappa^2 \theta_-^2 + 2ix\theta_-/\lambda}. \quad (3.18)$$

We can now differentiate with respect to x in order to cancel the pole, perform the Gaussian integral over θ_- and integrate back over x with the asymptotic condition $\langle \sigma(+\infty, y) \rangle_{ab} = \langle \sigma \rangle_b$; the result is

$$\langle \sigma(x, y) \rangle_{ab} \simeq \frac{\langle \sigma \rangle_a + \langle \sigma \rangle_b}{2} - \frac{\langle \sigma \rangle_a - \langle \sigma \rangle_b}{2} \operatorname{erf}(\chi), \quad (3.19)$$

where $\operatorname{erf}(x) = (2/\sqrt{\pi}) \int_0^x du e^{-u^2}$ is the error function and

$$\chi \equiv \frac{x}{\lambda \kappa}. \quad (3.20)$$

For the Ising model $\langle \sigma \rangle_a = -\langle \sigma \rangle_b = \langle \sigma \rangle_{\pm}$ and (3.19) reduces to $-\langle \sigma \rangle_{\pm} \operatorname{erf}(\chi)$, which is the scaling limit of the exact lattice result of [46]. The Ising magnetization $\langle \sigma(x, y) \rangle_{-+}$ is shown in Fig.3.2.

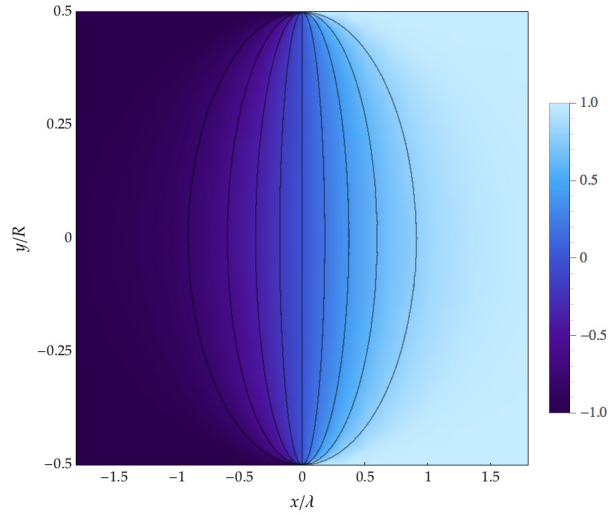


Figure 3.2: Ising magnetization $\langle \sigma(x, y) \rangle_{-+}/\langle \sigma \rangle_+$. The ellipses correspond to constant values of χ , and then to constant values of the magnetization.

3.2.2 Interface structure and passage probability

Subleading terms in the large R expansion of (3.19) can be worked out systematically from the small rapidity expansion of the boundary amplitude $f_{ab}(\theta)$ and of the matrix element $\mathcal{F}_{ab}^\sigma(\theta|\theta')$. If the phases a and b play a symmetric role, we have $f_{ab}(\theta) = f_{ab}(0) + O(\theta^2)$, and the next contribution to (3.19) is easily found to be

$$\frac{\mathcal{C}_{ab}^\sigma}{m} \frac{e^{-x^2}}{\sqrt{\pi \kappa \lambda}}, \quad (3.21)$$

where \mathcal{C}_{ab}^σ is the coefficient c_0 of the expansion $\mathcal{F}_{ab}^\sigma(\theta|\theta') = \sum_{k=-1}^{\infty} c_k(\theta - \theta')^k$, and then depends only on the bulk theory.

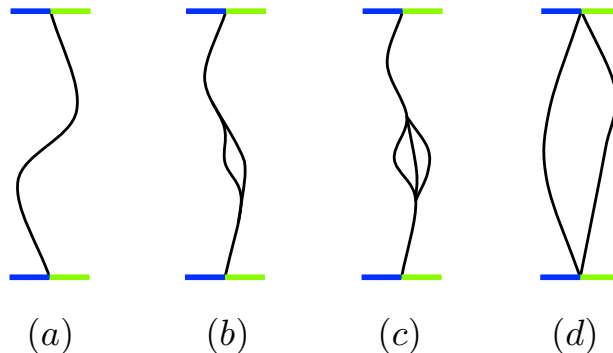


Figure 3.3: Some configurations of a single interface (a,b,c) and the leading large R configuration of a double interface (d).

It is easy to see that the result (3.19) corresponds to the average over the configurations of an interface which intersects only once the lines $y = \text{constant}$ and sharply separates two pure phases a and b (Fig. 3.3a). Indeed, if we call $p(u, y)du$ the probability that such an interface passes in the interval $(u, u + du)$ on the line of constant y on the strip, and¹

$$\sigma_{ab}(x|u) = \theta(u - x)\langle\sigma\rangle_a + \theta(x - u)\langle\sigma\rangle_b \quad (3.22)$$

the magnetization at a point x on this line for the given interface configuration,

¹We denote by $\theta(x)$ the step function which equals 1 if $x > 0$ and 0 if $x < 0$.

the average magnetization

$$\langle \sigma(x, y) \rangle_{ab}^{\text{sharp}} = \int_{\mathbb{R}} du \sigma_{ab}(x|u) p(u, y) \quad (3.23)$$

coincides with (3.19) for¹

$$p(x, y) = \frac{e^{-\chi^2}}{\sqrt{\pi} \kappa \lambda}. \quad (3.24)$$

We also see that (3.21) corresponds to adding to (3.22) the local term $(\mathcal{C}_{ab}^\sigma/m)\delta(x-u)$, which represents a deviation from sharp phase separation and is the first manifestation of an internal structure of the interface. A typical effect contributing to (3.21) is the bifurcation and recombination of the interface depicted in Fig. 3.3b; we see from the factor of λ in the denominator of (3.21) that it is suppressed as $R^{-1/2}$. The formation of such bubbles requires three different phases, and the term (3.21) is indeed absent in the Ising model, in which the magnetization is odd in x by symmetry. The first branching effect in the Ising model (trifurcation, Fig. 3.3c) contributes to the subsequent term of the low energy expansion and is suppressed² as R^{-1} at large R .

The bifurcation of the interface requires the presence in the theory of a three-kink vertex, corresponding to the bound state formation $|K_{ac}(\theta_1)K_{cb}(\theta_2)\rangle \rightarrow |K_{ab}(0)\rangle$ for some resonant value $\theta_1 - \theta_2 = i\gamma$, $\gamma \in (0, \pi)$. Relativistic kinematics yields the relation $m_{ab}^2 = m_{ac}^2 + m_{cb}^2 + 2m_{ac}m_{cb} \cos \gamma$ among the masses of the three kinks. In view of (3.5) this becomes the well known relation among the components of the superficial tensions at each vertex of the bubble [12] (Fig. 3.4). It also follows from (3.1) that energy conservation at the vertex becomes the equilibrium condition

$$\Sigma_{ab} + \Sigma_{ac} \cos \alpha + \Sigma_{cb} \cos \beta = 0. \quad (3.25)$$

¹The Gaussian passage probability density (3.24), with a width shrinking to zero at the boundary condition changing points, gives to the interface the property of a Brownian bridge, which has been rigorously proved for the Ising model [47] and the Potts model [48].

²Within the saddle point evaluation of (3.9) at large R each additional power of rapidity in the product $f_{ab}^*(\theta)f_{ab}(\theta')\mathcal{M}_{ab}^\sigma$ contributes a factor $R^{-1/2}$.

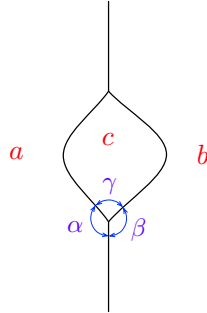


Figure 3.4: A bubble of phase c contributing to the internal structure of the interface between phases a and b .

3.3 Intermediate phases

In systems allowing for a third degenerate phase, the latter can appear in the interfacial region either via the formation of bubbles (or drops, Fig. 3.5a), or because a macroscopic (“wetting”) intermediate layer of phase c forms between phases a and b (Fig. 3.5b). A transition from the first to the second regime induced by the variation of a parameter of the system goes under the name of wetting transition (see e.g. [12]).

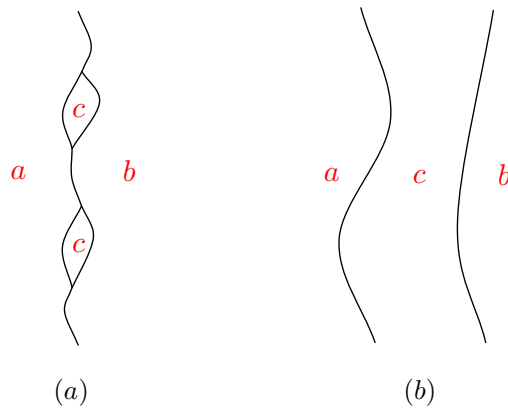


Figure 3.5: Two different regimes of phase separation: a third phase appears in bubbles (a), or through a wetting layer (b).

We now consider the case in which, still starting with the ab boundary conditions of Fig. 3.1, phases a and b are not adjacent. More precisely, we consider

the simplest case of this type, the one in which the minimal path between $|\Omega_a\rangle$ and $|\Omega_b\rangle$ is a two-kink state $|K_{ac}K_{cb}\rangle$ passing through a third vacuum $|\Omega_c\rangle$ (an example of this kind is shown in Fig. 3.6). This means that now the expansion

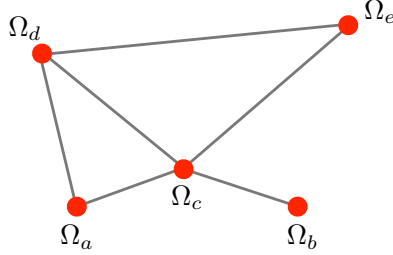


Figure 3.6: A vacuum structure including non-adjacent vacua.

(3.2) of the boundary state is replaced by

$$|B_{ab}(x_0; t)\rangle = e^{-itH+ix_0P} \left[\sum_{c \neq a,b} \int_{\mathbb{R}^2} \frac{d\theta_1}{2\pi} \frac{d\theta_2}{2\pi} f_{acb}(\theta_1, \theta_2) |K_{ac}(\theta_1)K_{cb}(\theta_2)\rangle + \dots \right], \quad (3.26)$$

where the summation over c indicates that, in general, there can be more than one two-kink path interpolating between $|\Omega_a\rangle$ and $|\Omega_b\rangle$. For simplicity we refer to the case in which the lightest state $|K_{ac}K_{cb}\rangle$, is made of two kinks with the same mass m . Then we can stipulate that the sum in (3.26) includes only the states $|K_{ac}K_{cb}\rangle$ with mass $2m$, with the dots including all heavier states and contributing subleading terms in the large R expansion. Plugging (3.26) into (3.3) then gives

$$\mathcal{Z}_{ab}(R) \simeq \sum_{c,d \neq a,b} \int_{\mathbb{R}^4} \frac{d\theta_1 d\theta_2 d\theta_3 d\theta_4}{(2\pi)^4} \mathcal{F}_{ab,cd} \mathcal{M}_{ab,cd} \mathcal{Y}, \quad (3.27)$$

where we defined

$$\begin{aligned} \mathcal{F}_{ab,cd}(\theta_1, \theta_2, \theta_3, \theta_4) &\equiv f_{acb}(\theta_1, \theta_2) f_{adb}^*(\theta_3, \theta_4) \\ \mathcal{M}_{ab,cd}(\theta_1, \theta_2 | \theta_3, \theta_4) &\equiv \langle K_{bd}(\theta_3) K_{da}(\theta_4) | K_{ac}(\theta_1) K_{cb}(\theta_2) \rangle \end{aligned} \quad (3.28)$$

$$\begin{aligned} \mathcal{Y}(\theta_1, \theta_2, \theta_3, \theta_4) &\equiv Y^-(\theta_1) Y^-(\theta_2) Y^+(\theta_3) Y^+(\theta_4) \\ Y^\pm(\theta) &\equiv e^m \left[-\frac{R}{2} \cosh \theta \pm ix \sinh \theta \right]. \end{aligned} \quad (3.29)$$

In our framework, the two-kink states are asymptotic states that can be either incoming or outgoing, the two basis being related by the scattering operator. Since the large R limit we are interested in projects towards small rapidities, scattering processes take place at energies below any particle production threshold, and are then elastic. In particular, two-kink states scatter into two-kink states, and we can write

$$|K_{ac}(\theta_1)K_{cb}(\theta_2)\rangle = \sum_{d \neq a,b} S_{ab}^{cd}(\theta_1 - \theta_2) |K_{ad}(\theta_2)K_{db}(\theta_1)\rangle, \quad (3.30)$$

where

$$S_{ab}^{cd}(\theta_1 - \theta_2) = \begin{array}{c} \text{d} \\ \diagdown \quad \diagup \\ \text{a} \quad \text{b} \\ \diagup \quad \diagdown \\ \text{c} \\ \theta_1 \quad \theta_2 \end{array} \quad (3.31)$$

are the two-kink scattering amplitudes, in which all kinks have mass m and initial and final rapidities coincide by two-dimensional energy-momentum conservation; in (3.30) we also stipulated that $\theta_1 > \theta_2$ and that kinks are ordered according to decreasing (resp. increasing) rapidity for incoming (resp. outgoing) states. The unitarity condition associated to (3.30) then reads

$$\sum_{e \neq a,b} S_{ab}^{ce}(\theta) S_{ab}^{ed}(-\theta) = \delta_{cd}. \quad (3.32)$$

Since the large R limit leads to consider rapidities which tend to zero, the essential information we need from the scattering theory is the threshold value $S_{ab}^{cd}(0)$ of the amplitudes. The models to which we will specialize in the next sections satisfy

$$S_{ab}^{cd}(0) = -\delta_{cd}, \quad (3.33)$$

and this is the case that we consider in the following¹. The use of (3.33) into (3.30) with $\theta_1 = \theta_2$ shows that the states $|K_{ac}(\theta)K_{cb}(\theta)\rangle$ are not allowed. It follows in particular that the amplitudes f_{acb} in (3.26) need to vanish when $\theta_1 = \theta_2$, and can be written as $f_{acb}(\theta_1, \theta_2) \simeq c_{acb} \theta_{12}$ at small rapidities, where we defined

¹It is possible that (3.33) is a necessary condition for the formation of an intermediate phase.

$\theta_{ij} \equiv \theta_i - \theta_j$. As a consequence

$$\mathcal{F}_{ab,cd}(\theta_1, \theta_2, \theta_3, \theta_4) \simeq c_{acb} c_{adb}^* \theta_{12} \theta_{34} \quad (3.34)$$

at small rapidities. Concerning the product (3.28), it is the sum of the two terms¹ depicted in Fig. 3.7, and reads

$$\mathcal{M}_{ab,cd}(\theta_1, \theta_2 | \theta_3, \theta_4) = (2\pi)^2 [\delta(\theta_{14}) \delta(\theta_{23}) \delta_{cd} + \delta(\theta_{13}) \delta(\theta_{24}) S_{ab}^{cd}(\theta_{12})]. \quad (3.35)$$

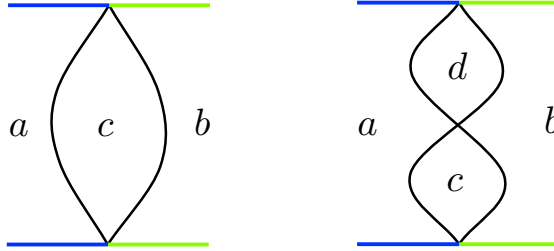


Figure 3.7: The two contributions to (3.35).

With (3.34) and (3.35) we can proceed to the saddle point evaluation of (3.27), obtaining

$$\mathcal{Z}_{ab}(R) \simeq \zeta_{ab} \int_{\mathbb{R}^2} \frac{d\theta_1 d\theta_2}{(2\pi)^2} \theta_{12}^2 e^{-mR(\cosh \theta_1 + \cosh \theta_2)} \simeq \zeta_{ab} \frac{e^{-2mR}}{\pi(mR)^2}, \quad (3.36)$$

with

$$\zeta_{ab} = \sum_{c,d \neq a,b} c_{acb} c_{adb}^* [S_{ab}^{cd}(0) - \delta_{cd}] = -2 \sum_{c \neq a,b} |c_{acb}|^2. \quad (3.37)$$

The interfacial tension (3.4) is now $2m$, as expected for the double interface of Fig. 3.3d.

¹Due to (3.32) terms with more than one bulk crossing reduce to those of Fig. 3.7.

The magnetization (3.6) with the boundary state (3.26) becomes

$$\begin{aligned}
 \langle \sigma(x, y) \rangle_{ab} &\simeq \frac{1}{\mathcal{Z}_{ab}(R)} \sum_{c,d \neq a,b} \int_{\mathbb{R}^4} \frac{d\theta_1 d\theta_2 d\theta_3 d\theta_4}{(2\pi)^4} \mathcal{F}_{ab,cd}(\theta_1, \theta_2, \theta_3, \theta_4) \times \\
 &\times \langle K_{bd}(\theta_3) K_{da}(\theta_4) | e^{-\frac{R}{2}H} \overbrace{e^{ixP+yH} \sigma(0,0) e^{-ixP-yH}}^{\sigma(x,y)} e^{-\frac{R}{2}H} | K_{ac}(\theta_1) K_{cb}(\theta_2) \rangle \\
 &= \frac{1}{\mathcal{Z}_{ab}(R)} \sum_{c,d \neq a,b} \int_{\mathbb{R}^4} \frac{d\theta_1 d\theta_2 d\theta_3 d\theta_4}{(2\pi)^4} \mathcal{F}_{ab,cd}(\theta_1, \theta_2, \theta_3, \theta_4) \mathcal{Y}^*(\theta_1, \theta_2, \theta_3, \theta_4) \\
 &\times \mathcal{M}_{ab,cd}^\sigma(\theta_1, \theta_2 | \theta_3, \theta_4), \tag{3.38}
 \end{aligned}$$

where

$$\mathcal{Y}^*(\theta_1, \dots, \theta_4) \equiv \mathcal{Y}(\theta_1, \dots, \theta_4) e^{my(\cosh \theta_3 + \cosh \theta_4 - \cosh \theta_1 - \cosh \theta_2)}, \tag{3.39}$$

$$\mathcal{M}_{ab,cd}^\sigma(\theta_1, \theta_2 | \theta_3, \theta_4) \equiv \langle K_{bd}(\theta_3) K_{da}(\theta_4) | \sigma(0,0) | K_{ac}(\theta_1) K_{cb}(\theta_2) \rangle. \tag{3.40}$$

Analogously to what discussed in the previous section for the two-leg case, the matrix element (3.40) contains a connected part, that we will denote $\mathcal{M}_{ab,cd}^{\sigma, \text{conn}}$, and a number of disconnected contributions; pictorially

$$\begin{array}{c} \theta_4 \\ \diagdown \\ a \\ \circlearrowleft \sigma \\ \diagup \\ b \\ \theta_3 \end{array} \begin{array}{c} d \\ \diagdown \\ \theta_1 \\ \diagup \\ \theta_2 \\ c \end{array} = \begin{array}{c} \theta_4 \\ \diagdown \\ a \\ \circlearrowleft \sigma \\ \diagup \\ b \\ \theta_3 \end{array} \begin{array}{c} d \\ \diagdown \\ \theta_1 \\ \diagup \\ \theta_2 \\ c \end{array} + \text{disconnected parts}. \tag{3.41}$$

As in the two-leg case, the possibility of performing the decomposition in two different ways, depending on whether the disconnected trajectories pass to the right or to the left of the insertion point of the magnetization operator, leads to kinematical singularities in the connected parts. The residues on these poles are

given by the generalization of (3.14), namely

$$\begin{aligned}
 -i \operatorname{Res}_{\theta_1=\theta_3} & \begin{array}{c} \theta_4 \quad \theta_3 \\ \diagdown \quad \diagup \\ d \\ \sigma \\ \diagup \quad \diagdown \\ a \quad b \\ \diagdown \quad \diagup \\ c \\ \theta_1 \quad \theta_2 \end{array} = \begin{array}{c} \theta_4 \quad \theta_3 \\ \diagdown \quad \diagup \\ d \\ \sigma \\ \diagup \quad \diagdown \\ a \quad b \\ \diagdown \quad \diagup \\ c \\ \theta_1 \quad \theta_2 \end{array} - \begin{array}{c} \theta_4 \quad \theta_3 \\ \diagdown \quad \diagup \\ d \\ \sigma \\ \diagup \quad \diagdown \\ a \quad b \\ \diagdown \quad \diagup \\ c \\ \theta_1 \quad \theta_2 \end{array} \\
 & = S_{ab}^{cd}(0) \begin{array}{c} \theta_4 \\ | \\ \sigma \\ | \\ \theta_2 \end{array} \begin{array}{c} d \\ \sigma \\ c \end{array} - S_{ab}^{cd}(0) \begin{array}{c} \theta_4 \\ | \\ \sigma \\ | \\ \theta_2 \end{array} \begin{array}{c} \theta_4 \\ | \\ \sigma \\ | \\ \theta_2 \end{array} \\
 & \simeq \frac{i S_{ab}^{cd}(0)}{\theta_{24}} \left[\langle \sigma \rangle_a - \langle \sigma \rangle_d - \langle \sigma \rangle_c + \langle \sigma \rangle_b \right], \quad (3.42)
 \end{aligned}$$

where we work directly in the limit $\theta_1, \dots, \theta_4 \rightarrow 0$ and used (3.13) in the last line (we do not need to keep track of the $i\epsilon$ prescriptions here). Similarly,

$$\begin{aligned}
 -i \operatorname{Res}_{\theta_1=\theta_4} & \begin{array}{c} \theta_4 \quad \theta_3 \\ \diagdown \quad \diagup \\ d \\ \sigma \\ \diagup \quad \diagdown \\ a \quad b \\ \diagdown \quad \diagup \\ c \\ \theta_1 \quad \theta_2 \end{array} = \sum_e \begin{array}{c} \theta_4 \quad \theta_3 \\ \diagdown \quad \diagup \\ d \\ \sigma \\ \diagup \quad \diagdown \\ a \quad e \quad b \\ \diagdown \quad \diagup \\ c \\ \theta_1 \quad \theta_2 \end{array} - \delta_{cd} \begin{array}{c} \theta_4 \quad \theta_3 \\ | \quad | \\ a \quad c \\ \sigma \\ | \\ \theta_2 \end{array} \\
 & = \sum_e S_{ab}^{ce}(0) S_{ab}^{ed}(0) \begin{array}{c} \theta_3 \\ | \\ \sigma \\ | \\ \theta_2 \end{array} \begin{array}{c} \theta_3 \\ | \\ \sigma \\ | \\ \theta_2 \end{array} \begin{array}{c} e \\ \sigma \\ b \end{array} - \delta_{cd} \begin{array}{c} \theta_3 \\ | \\ \sigma \\ | \\ \theta_2 \end{array} \begin{array}{c} \theta_3 \\ | \\ \sigma \\ | \\ \theta_2 \end{array} \\
 & \simeq \frac{i}{\theta_{23}} \left[\sum_e S_{ab}^{ce}(0) S_{ab}^{ed}(0) \left[\langle \sigma \rangle_a - \langle \sigma \rangle_e \right] - \delta_{cd} \left[\langle \sigma \rangle_c - \langle \sigma \rangle_b \right] \right] \\
 & = \frac{i}{\theta_{23}} \left[- \sum_e S_{ab}^{ce}(0) S_{ab}^{ed}(0) \langle \sigma \rangle_e - \delta_{cd} \left[\langle \sigma \rangle_c - \langle \sigma \rangle_a - \langle \sigma \rangle_b \right] \right];
 \end{aligned}$$

(3.32) was used in the last line. Analogous results are obtained when the kink with rapidity θ_2 is disconnected, and we have

$$\begin{aligned}
 -\operatorname{Res}_{\theta_1=\theta_3}\mathcal{M}_{ab,cd}^{\sigma,\text{conn}}(\theta_1,\dots,\theta_4) &= \frac{\mathcal{A}_{ab,cd}}{\theta_{24}}, \\
 -\operatorname{Res}_{\theta_1=\theta_4}\mathcal{M}_{ab,cd}^{\sigma,\text{conn}}(\theta_1,\dots,\theta_4) &= \frac{\mathcal{B}_{ab,cd}}{\theta_{23}}, \\
 -\operatorname{Res}_{\theta_2=\theta_4}\mathcal{M}_{ab,cd}^{\sigma,\text{conn}}(\theta_1,\dots,\theta_4) &= \frac{\mathcal{A}_{ab,cd}}{\theta_{13}}, \\
 -\operatorname{Res}_{\theta_2=\theta_3}\mathcal{M}_{ab,cd}^{\sigma,\text{conn}}(\theta_1,\dots,\theta_4) &= \frac{\mathcal{B}_{ab,cd}}{\theta_{14}},
 \end{aligned}$$

with

$$\begin{aligned}
 \mathcal{A}_{ab,cd} &= S_{ab}^{cd}(0)[\langle\sigma\rangle_a + \langle\sigma\rangle_b - \langle\sigma\rangle_c - \langle\sigma\rangle_d], \\
 \mathcal{B}_{ab,cd} &= \delta_{cd}[\langle\sigma\rangle_a + \langle\sigma\rangle_b - \langle\sigma\rangle_c] - \sum_e S_{ab}^{ce}(0)S_{ab}^{ed}(0)\langle\sigma\rangle_e.
 \end{aligned}$$

The condition (3.33) simplifies the result to $\mathcal{A}_{ab,cd} = \delta_{cd}(2\langle\sigma\rangle_c - \langle\sigma\rangle_a - \langle\sigma\rangle_b) = -\mathcal{B}_{ab,cd}$, and we obtain

$$\mathcal{M}_{ab,cc}^{\sigma,\text{conn}}(\theta_1,\theta_2,\theta_3,\theta_4) \simeq [2\langle\sigma\rangle_c - \langle\sigma\rangle_a - \langle\sigma\rangle_b] \frac{\theta_{12}\theta_{34}}{\theta_{13}\theta_{14}\theta_{23}\theta_{24}}, \quad (3.43)$$

$$\mathcal{M}_{ab,cd}^{\sigma,\text{conn}}(\theta_1,\theta_2,\theta_3,\theta_4) \simeq \mathcal{C}_{ab,cd}^{\sigma} \theta_{12}\theta_{34}, \quad c \neq d, \quad (3.44)$$

at small rapidities. As in (3.34), the prefactor $\theta_{12}\theta_{34}$ accounts for the property (3.33), and provides the leading term for $c \neq d$, when all the residues vanish. The value of the constant $\mathcal{C}_{ab,cd}^{\sigma}$ depends on the form of the scattering amplitudes $S_{ab}^{cd}(\theta)$ for $\theta \neq 0$. Notice, however, that the total degree of (3.44) in the rapidity variables exceeds by four units that of (3.43), so that the contribution of (3.44) to the magnetization is subleading¹ at large R with respect to the leading as well as to some of the subleading terms we are omitting in (3.43). This means that (3.44) must be ignored at this level of the calculation. Hence the contribution of

¹Within the saddle point evaluation of (3.38) at large R each additional power of rapidity in the product $\mathcal{F}_{ab,cd}\mathcal{M}_{ab,cd}^{\sigma}$ contributes a factor $1/\sqrt{R}$.

$$\mathcal{D}_{1324}^{(R)} = \text{diagram 1}, \quad \mathcal{D}_{2413}^{(R)} = \text{diagram 2},$$

depending on the left or right passage prescription. In the limit $\theta_1, \dots, \theta_4 \rightarrow 0$, taking into account (3.33) and (3.14), we have¹

$$\mathcal{D}_{ijkl}^{(L)} \simeq (-1)^{i+j} 2\pi \delta_{cd} \delta(\theta_{ij}) i \frac{\langle \sigma \rangle_c - \langle \sigma \rangle_b}{\theta_{kl}}, \quad (3.47)$$

$$\mathcal{D}_{ijkl}^{(R)} \simeq (-1)^{i+j} 2\pi \delta_{cd} \delta(\theta_{ij}) i \frac{\langle \sigma \rangle_a - \langle \sigma \rangle_c}{\theta_{kl}}, \quad (3.48)$$

from which we see that the two prescriptions are inequivalent. The natural idea to take the average

$$\mathcal{D}_{ijkl} \equiv \frac{\mathcal{D}_{ijkl}^{(L)} + \mathcal{D}_{ijkl}^{(R)}}{2} = (-1)^{i+j} \pi \delta_{cd} \delta(\theta_{ij}) i \frac{\langle \sigma \rangle_a - \langle \sigma \rangle_b}{\theta_{kl}} \quad (3.49)$$

is the right one. Indeed, as seen in the previous section, single pole terms of this type generate a difference between the values of the magnetization at $x = -\infty$ and $x = +\infty$ proportional to the residue on the pole; we are going to see that (3.49) produces precisely the required difference² $\langle \sigma \rangle_a - \langle \sigma \rangle_b$. The contribution of \mathcal{D}_{ijkl} to the magnetization (3.38) is $(\langle \sigma \rangle_a - \langle \sigma \rangle_b)/2$ times

$$\begin{aligned} \Delta_{ijkl}(x, y) &= (-1)^{i+j} \sum_{c \neq a, b} \frac{|c_{acb}|^2}{\mathcal{Z}_{ab}(R)} \int_{\mathbb{R}^4} \frac{d\theta_1 d\theta_2 d\theta_3 d\theta_4}{(2\pi)^4} \theta_{12} \theta_{34} \frac{2\pi i \delta(\theta_{ij})}{\theta_{kl}} \times \\ &\times \mathcal{Y}^*(\theta_1, \theta_2, \theta_3, \theta_4), \\ &= \frac{1}{4} \mathcal{L}(\chi) + \text{constant}; \end{aligned} \quad (3.50)$$

¹It is understood that the indices $ijkl$ take only the four combinations given above.

²The connected contribution (3.45) is even in x and does not contribute to the difference between the asymptotic values.

the integral is performed in the appendix and gives

$$\mathcal{L}(\chi) = \frac{\chi}{\sqrt{\pi}} e^{-\chi^2} - \operatorname{erf}(\chi). \quad (3.51)$$

Recalling that there are four choices of $ijkl$, we obtain

$$\langle \sigma(x, y) \rangle_{ab}^{\text{disc}} \simeq \frac{\langle \sigma \rangle_a - \langle \sigma \rangle_b}{2} \mathcal{L}(\chi) + \text{constant} \quad (3.52)$$

for the contribution of the disconnected parts to the magnetization. With (3.45) and (3.52) we can turn to the study of specific models.

3.4 Application to the q -state Potts model

The q -state Potts model is a generalization of the Ising model to the case in which the spin variable takes q values (colors), and is characterized by the invariance of the Hamiltonian under global permutations of the colors [49]. For ferromagnetic interaction in two dimensions it undergoes at a critical temperature T_c a phase transition which is continuous for $q \leq 4$ and first order for $q > 4$ [50] (see [51] for a derivation in the continuum). Hence, for $q \leq 4$ and $T < T_c$ there is a scaling limit corresponding to a field theory with q degenerate vacua and kinks interpolating between each pair of them (see Fig. 3.8.a). Phase separation is necessarily of the type discussed in Section 3.2.

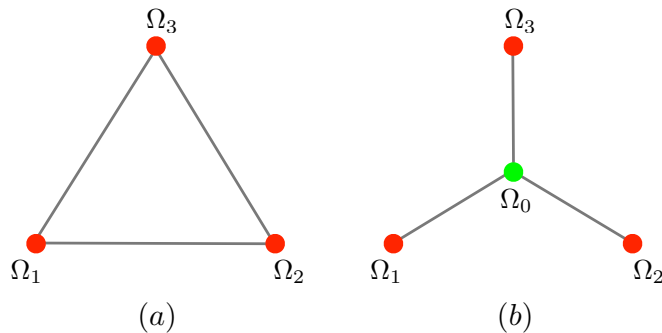


Figure 3.8: Vacuum and kink structure of the three-state Potts model at first order transition points in the pure case (a) and in the dilute case (b).

When annealed vacancies are introduced, the transition for $q < 4$ stays continuous up to a critical value ρ_c of the vacancy density, above which it becomes first order. As q is varied, there is then a tricritical line for $T = T_c(\rho)$, $\rho = \rho_c$, which is known to coalesce with the critical line of the undilute ($\rho = 0$) model at $q = 4$ [49]. On the first order surface $T = T_c(\rho)$, $\rho > \rho_c$ the ferromagnetic vacua $|\Omega_i\rangle$, $i = 1, \dots, q$, are degenerate with the disordered one $|\Omega_0\rangle$. The elementary excitations are the kinks $|K_{0i}\rangle$ running between the disordered vacuum and the ferromagnetic ones (Fig. 3.8.b), as two ferromagnetic vacua will be related by $|K_{i_0}K_{0j}\rangle$. In principle such two-kink configurations could give rise to stable bound state kinks $|K_{ij}\rangle$, that would make the vacua $|\Omega_i\rangle$ and $|\Omega_j\rangle$ adjacent. This, however, is not the case. Indeed, the field theory corresponding to the scaling limit on the first order surface is integrable¹, and the spectrum of excitations and the scattering amplitudes are known exactly [53]. The kinks $|K_{0i}\rangle$ and $|K_{i0}\rangle$ do not form bound states and are the only single-particle excitations of the theory. As a consequence the vacua $|\Omega_i\rangle$ and $|\Omega_j\rangle$ are not adjacent and the strip with boundary conditions i on the left and j on the right will give rise to a double interface containing a bubble of the disordered phase. We now apply to this case the formalism of the previous section.

All kinks have the same mass as a consequence of permutational symmetry of the colors, which is unaffected by dilution. Since the only two-kink state connecting two different ferromagnetic vacua $|\Omega_i\rangle$ and $|\Omega_j\rangle$ is $|K_{i_0}K_{0j}\rangle$, the intermediate index c in (3.26) is fixed to the value 0. Similarly,

$$S_{ij}^{cd}(\theta) = \delta_{c0}\delta_{d0} S_{ij}^{00}(\theta); \quad (3.53)$$

in addition $S_{ij}^{00}(0) = -1$ [53], so that (3.33) is fulfilled. If $s(x, y)$ is the color of a spin at site (x, y) , we define the spin variables

$$\sigma_k(x, y) = \delta_{k,s(x,y)} - \frac{1}{q}, \quad k = 1, \dots, q, \quad (3.54)$$

and use the same notation $\sigma_k(x, y)$ for the corresponding components of the magnetization operator in the continuum; they satisfy $\sum_{k=1}^q \sigma_k(x, y) = 0$. The sym-

¹The scaling limit without dilution is also integrable [52].

metry gives

$$\langle \sigma_k \rangle_j = \frac{q\delta_{kj} - 1}{q - 1} M \quad (3.55)$$

in the pure ferromagnetic phases, and

$$\langle \sigma_k \rangle_0 = 0 \quad (3.56)$$

in the pure disordered phase. Taking all this into account (3.45) gives

$$\langle \sigma_k(x, y) \rangle_{ij}^{\text{conn}} \simeq \frac{\langle \sigma_k \rangle_i + \langle \sigma_k \rangle_j}{4} \left[\mathcal{G}(\chi) - 1 \right]. \quad (3.57)$$

Adding the disconnected contribution (3.52) and fixing the additive constant by the condition $\langle \sigma_k(+\infty, y) \rangle_{ij} = \langle \sigma_k \rangle_j$ we finally obtain

$$\langle \sigma_k(x, y) \rangle_{ij} \simeq \frac{\langle \sigma_k \rangle_i + \langle \sigma_k \rangle_j}{4} \left[1 + \mathcal{G}(\chi) \right] + \frac{\langle \sigma_k \rangle_i - \langle \sigma_k \rangle_j}{2} \mathcal{L}(\chi). \quad (3.58)$$

For $q = 2$ this becomes $\langle \sigma_k(x, y) \rangle_{ij} = (-1)^{\delta_{kj}} M \mathcal{L}(\chi)$, from which we see that, with respect to the pure Ising case (3.19), the effect of dilution and of the formation of the intermediate wetting phase is the appearance of the first term of (3.51) (see Fig. 3.9). The results (3.58) are shown in Figs. 3.10 and 3.11 for $q = 3$.

As for the case of single interface of Section 3.2, the results (3.58) admit a probabilistic interpretation in terms of average over configurations of interfaces sharply separating pure phases. Suppose indeed that two such interfaces intersect at $x = u_1$ and $x = u_2$ the horizontal axis of constant y inside the strip with ab boundary conditions, and that they can contain a single phase c in between them. The magnetization corresponding to such a configuration on the line of constant y can then be written as

$$\sigma_{acb}(x|u_1, u_2) = \sigma_{acb}^*(x|u_1, u_2) \theta(u_2 - u_1) + \sigma_{acb}^*(x|u_2, u_1) \theta(u_1 - u_2), \quad (3.59)$$

with

$$\sigma_{acb}^*(x|u_1, u_2) = \langle \sigma \rangle_a \theta(u_1 - x) + \langle \sigma \rangle_b \theta(x - u_2) + \langle \sigma \rangle_c (\theta(x - u_1) - \theta(x - u_2)). \quad (3.60)$$

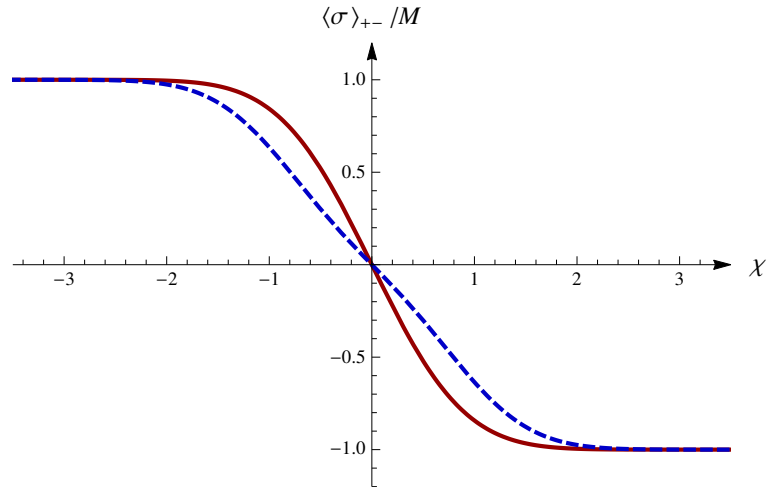


Figure 3.9: Ising magnetization profile $\langle \sigma \rangle_{+-} / M$ at the first order transition in the pure model (continuous curve), and in the dilute model (dashed curve). The presence of an intermediate disordered phase in the dilute case flattens the profile.

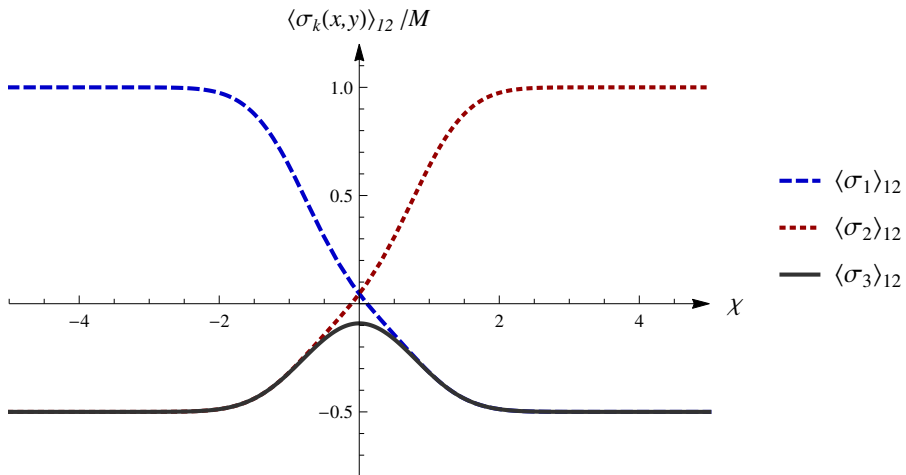


Figure 3.10: Magnetization profiles (3.58) for $q = 3$.

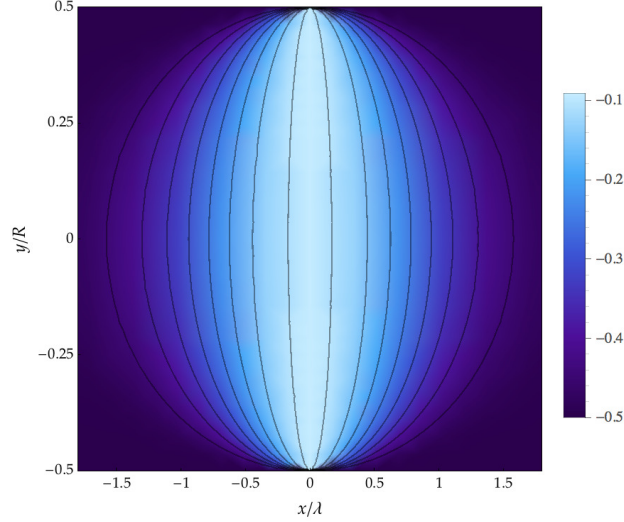


Figure 3.11: The magnetization $\langle \sigma_3(x, y) \rangle_{12}/M$ for $q = 3$. The curves are the ellipses $\frac{x^2}{\lambda^2 C^2} + \frac{4y^2}{R^2} = 1$, corresponding to $\chi = C$, and then to constant magnetization.

The magnetization is obtained averaging over the interface positions,

$$\langle \sigma(x, y) \rangle_{ab,c}^{\text{sharp}} = \int_{\mathbb{R}^2} du_1 du_2 \sigma_{acb}(x|u_1, u_2) p(u_1, u_2; y), \quad (3.61)$$

with $p(u_1, u_2; y)$ the probability density for intersections at u_1 and u_2 . It is not difficult to check that, for $\langle \sigma \rangle_c = 0$, the result (3.58) is precisely reproduced by the probability density

$$p(x_1, x_2; y) = \left(\frac{x_1 - x_2}{\lambda \kappa} \right)^2 p(x_1, y) p(x_2, y) = \frac{(\chi_1 - \chi_2)^2}{\pi \lambda^2 \kappa^2} e^{-(\chi_1^2 + \chi_2^2)}, \quad (3.62)$$

which correctly satisfies $\int_{\mathbb{R}^2} du_1 du_2 p(u_1, u_2; y) = 1$. Hence we see that the probability density $p(x_1, y) p(x_2, y)$ for non-interacting interfaces gets corrected by the factor $(\chi_1 - \chi_2)^2$, whose origin must be traced back to the property (3.33). For a generic $\langle \sigma \rangle_c$ (3.62) gives

$$\langle \sigma(x, y) \rangle_{ab,c}^{\text{sharp}} = \frac{\langle \sigma \rangle_a + \langle \sigma \rangle_b - 2\langle \sigma \rangle_c}{4} \mathcal{G}(\chi) + \frac{\langle \sigma \rangle_a - \langle \sigma \rangle_b}{2} \mathcal{L}(\chi) + \frac{\langle \sigma \rangle_a + \langle \sigma \rangle_b + 2\langle \sigma \rangle_c}{4}. \quad (3.63)$$

In Fig. 3.12 we show $\langle \sigma_3 \rangle_{12}$ from (3.58) and for the undilute $T < T_c$ three-

state Potts model, for which the leading non-constant term is provided by (3.21) with $\mathcal{C}_{12}^{\sigma_3} = M/(2\sqrt{3})$ [1]. This latter term accounts for the formation of bubbles of third color depicted in Fig. 3.4 and corresponding to the vertex $K_{ac}K_{cb} \sim K_{ab}$ which is indeed present in the pure model [52]; since all kinks have the same mass, the angles in Fig. 3.4 are $\alpha = \beta = \gamma = 2\pi/3$. Hence Fig. 3.12 makes clear the quantitative difference between the effect of the formation of an intermediate disordered phase in the dilute case ($T = T_c, \rho > \rho_c$) and that due to the appearance of color 3 via branching and recombination of the single interface in the undilute case. The maximum of (3.21) decreases as $(mR)^{-1/2}$; for the models we discuss in this and the next section, the correlation length defined by the exponential decay of bulk spin-spin correlations is

$$\xi = \frac{1}{2m}. \quad (3.64)$$

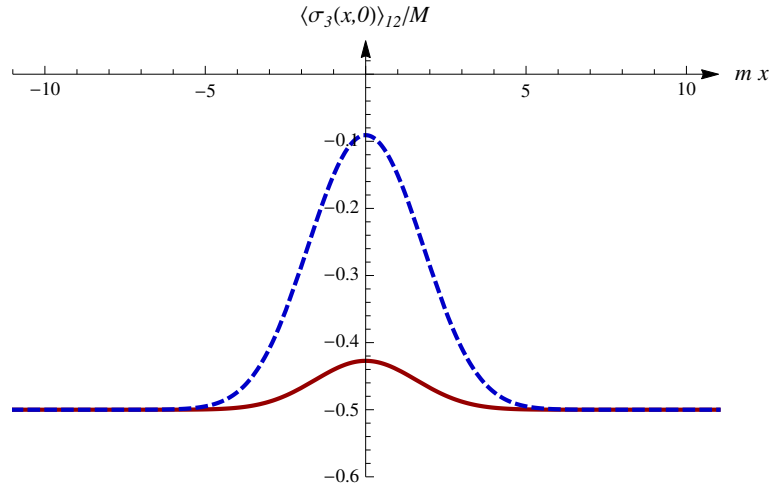


Figure 3.12: Magnetization profile $\langle \sigma_3(x, 0) \rangle_{12}/M$ in the three-state Potts model at the first order transition for $mR = 10$. For the undilute case (continuous curve) the bump is produced by the branching of the single interface and is suppressed as $R^{-1/2}$. For the dilute case (dashed curve) the bump is due to the disordered intermediate phase and its height persists asymptotically at large R .

We derived the results (3.58), (3.62) for the dilute Potts model on the first order surface $T = T_c, \rho > \rho_c, q < 4$. For the undilute model with $q > 4$ the phase

transition becomes first order and the same vacuum structure considered above (q ferromagnetic vacua degenerate with the disordered vacuum) is present at T_c . Strictly speaking, the scaling limit at T_c is only defined in the limit¹ $q \rightarrow 4^+$, and the exact solution of the associated field theory was studied in [55]. The vacuum adjacency structure and the property (3.33) are unchanged with respect to the dilute $q < 4$ case, and so is the result for the magnetization profiles. It was also shown in [55] that the field theoretical description remains quantitatively accurate as long as the correlation length ξ is much larger than lattice spacing. We then expect that (3.58) and (3.62) are essentially exact in the $q > 4$ critical pure model up to values such as $q = 10$, where $\xi \approx 10$.

It is interesting to notice that the function (3.43) originally appeared in [56] within an exact lattice computation of asymptotics of three-point spin correlators in the Ising model below T_c . In the language of this chapter, the coincidence is made possible by the fact that the leading non-constant contribution to this asymptotic correlator comes from a two-kink intermediate state. Later on this fact was exploited in [57] to propose that $\mathcal{G}(\chi)$ gives the magnetization profile across a bubble of down spins surrounded by up spins in the Ising model. It was shown in [58] by lattice computations that this is indeed the case provided that the pinning points of the interfaces are taken a fixed number of lattice spacings apart on the edges of the strip, and that the configurations with interfaces starting and ending on the same edge are removed by hand, before taking the scaling limit which makes the pinning points on the same edge coalesce. This is a technical way around the basic problem that the Ising model does not possess the three different phases necessary to generate two interfaces with the boundary conditions of Fig. 3.1.

3.5 Exact interfacial wetting transition: Ashkin-Teller model

The two-dimensional Ashkin-Teller model is defined on the lattice placing at each site $r = (x, y)$ two Ising spins $\sigma_1(r), \sigma_2(r) = \pm 1$, whose interaction is specified by

¹It is well known that the Potts model can be continued to real values of q [54].

the Hamiltonian

$$\mathcal{H}_{AT} = - \sum_{\langle r_1, r_2 \rangle} \{ J[\sigma_1(r_1)\sigma_1(r_2) + \sigma_2(r_1)\sigma_2(r_2)] + J_4 \sigma_1(r_1)\sigma_1(r_2)\sigma_2(r_1)\sigma_2(r_2) \}, \quad (3.65)$$

where the sum is taken over nearest neighbors; we consider the ferromagnetic case $J > 0$. The Hamiltonian is invariant under the exchange

$$E : \sigma_1 \leftrightarrow \sigma_2, \quad (3.66)$$

as well as under separate spin reversals

$$I_i : \sigma_i \rightarrow -\sigma_i. \quad (3.67)$$

The second order phase transition occurring for $J_4 = 0$, when the two Ising models are decoupled, is known to extend to $J_4 \neq 0$ (see e.g. [59] and references therein). There is then a second order critical line $J_c(J_4)$, and the scaling limit around it is described by the sine-Gordon field theory with Euclidean action

$$\mathcal{A}_{SG}[\varphi] = \int d^2x \left[\frac{1}{2} (\partial\varphi)^2 - \tau \cos \beta\varphi \right], \quad (3.68)$$

where τ measures the deviation of J from J_c , and β is the coordinate along the critical line. On the square lattice the relation between β and J_4 is [60]

$$\frac{4\pi}{\beta^2} = 1 - \frac{2}{\pi} \arcsin \left(\frac{\tanh 2J_4}{\tanh 2J_4 - 1} \right). \quad (3.69)$$

For $J > J_c$ the spin reversal symmetries are both spontaneously broken and the theory possesses four degenerate vacua $\Omega_{\alpha_1, \alpha_2}$, $\alpha_i = \pm 1$, corresponding to the breaking of I_i in the direction α_i . These vacua are connected as shown in Fig. 3.13 by elementary excitations A_1 and A_2 , which are kinks with respect to σ_1 and σ_2 , respectively¹, and have the same mass m . For $J_4 > 0$ these kinks form bound states [61] with mass $2m \sin(\pi\beta^2/2(8\pi - \beta^2))$ which run along the diagonals of Fig. 3.13 and make all vacua adjacent. For $J_4 \leq 0$, on the other hand, there are

¹Sine-Gordon soliton and anti-soliton correspond to $A_1 \pm iA_2$.

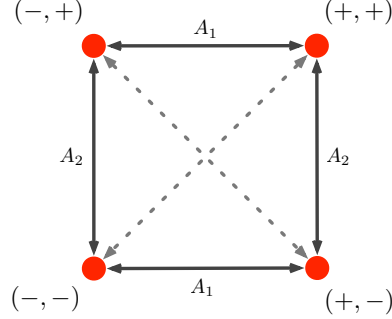


Figure 3.13: Vacuum connectivity in the Ashkin-Teller model. The diagonal kinks are present only for $J_4 > 0$.

no bound states, and the pairs of vacua $\Omega_{\alpha_1, \alpha_2}$ and $\Omega_{-\alpha_1, -\alpha_2}$ are non-adjacent. This is the case we now analyze.

To be definite, in the following we consider ab boundary conditions on the strip, with $a = ++$ and $b = --$. It follows from the adjacency structure of Fig. 3.13 for $J_4 \leq 0$ that these boundary conditions correspond to a boundary state of the form (3.26), with c taking the values $+ -$ and $- +$; in addition, exchange symmetry implies that the amplitudes $f_{acb}(\theta_1, \theta_2)$ coincide for the two values of c . Sine-Gordon field theory is integrable and all the scattering amplitudes are known [61]. For our purposes it is sufficient to know that (see [59])

$$S_{++,-}^{+-}(\theta) = S_{++,-}^{-+}(\theta) = \frac{S(\theta) + S_-(\theta)}{2}, \quad (3.70)$$

$$S_{++,-}^{+-}(\theta) = S_{++,-}^{-+}(\theta) = \frac{S(\theta) - S_-(\theta)}{2}, \quad (3.71)$$

where the notation is that of (3.31),

$$S_-(\theta) = -\frac{\cosh \frac{\pi}{2\xi}(\theta + i\pi)}{\cosh \frac{\pi}{2\xi}(\theta - i\pi)} S(\theta), \quad \xi = \frac{\pi\beta^2}{8\pi - \beta^2}, \quad (3.72)$$

and $S(\theta)$ satisfies $S(0) = -1$ for any ξ . The decoupling point $J_4 = 0$ corresponds to $\beta^2 = 4\pi$, namely to $\xi = \pi$, and $J_4 < 0$ corresponds to $\xi > \pi$. For $J_4 < 0$ we have $S_{++,-}^{cd}(0) = -\delta_{cd}$, so that (3.33) is fulfilled.

We consider the magnetization operators $\sigma_1(x, y)$, $\sigma_2(x, y)$ and $\sigma_1\sigma_2(x, y)$. The

symmetries imply that their expectation values in the four pure phases can be written as

$$\langle \sigma_i \rangle_{(\alpha_1, \alpha_2)} = \alpha_i M, \quad \langle \sigma_1 \sigma_2 \rangle_{(\alpha_1, \alpha_2)} = \alpha_1 \alpha_2 \tilde{M}. \quad (3.73)$$

Concerning the magnetization profiles on the strip with ab boundary conditions, since c_{acb} in (3.45) does not depend on the allowed values of c , (3.73) leads to $\langle \sigma_i(x, y) \rangle_{++,-}^{\text{conn}} = 0$ and $\langle \sigma_1 \sigma_2(x, y) \rangle_{++,-}^{\text{conn}} \simeq \tilde{M}(\mathcal{G}(\chi) - 1)$. Adding the disconnected contribution (3.52) and fixing the constant at infinity finally gives

$$\langle \sigma_i(x, y) \rangle_{++,-} \simeq M \mathcal{L}(\chi), \quad (3.74)$$

$$\langle \sigma_1 \sigma_2(x, y) \rangle_{++,-} \simeq \tilde{M} \mathcal{G}(\chi). \quad (3.75)$$

It is straightforward to see that these results correspond to the passage probability density (3.62) for the two interfaces. Indeed, it is sufficient to sum (3.63) over the two allowed values of c , and to consider that each intermediate phase occurs with probability $1/2$.

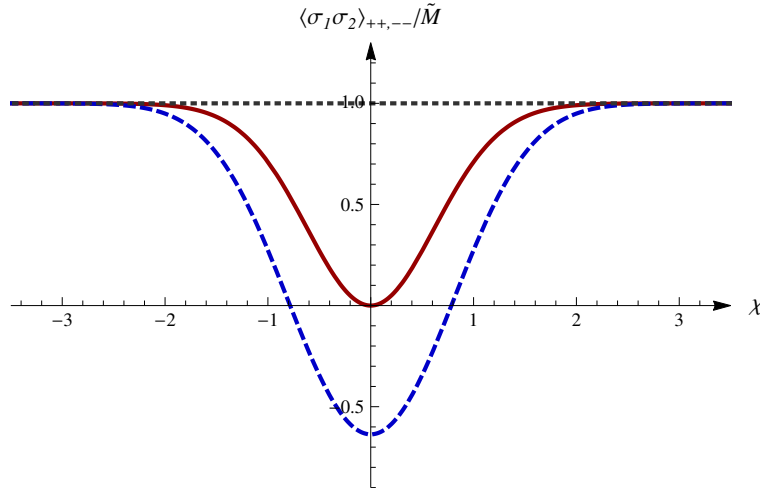


Figure 3.14: Asymptotic magnetization $\langle \sigma_1 \sigma_2 \rangle_{++,-} / \tilde{M}$ in the Ashkin-Teller model for $J_4 < 0$ (dashed curve), $J_4 = 0$ (continuous curve) and $J_4 > 0$ (dotted curve).

The results (3.74), (3.75) have been obtained for $J_4 < 0$, but do not depend on J_4 , namely on the interaction between two Ising spins. This corresponds to the fact that the leading large R behavior is entirely determined by the non-

crossing condition for the interfaces induced by (3.33). Consistency then requires that (3.33) is violated at the decoupling point $J_4 = 0$, where profiles corresponding to single interfaces must be recovered. Indeed, it follows from (3.70)-(3.72) that precisely at $\xi = \pi$ the threshold value of the amplitudes switches discontinuously to $S_{++,-}^{cd}(0) = \delta_{cd} - 1$. A first consequence is that the boundary amplitudes $f_{++,-}(0)$ no longer vanish, because the state $|K_{++,-}(\theta)K_{c,-}(\theta)\rangle$ no longer scatters into minus itself; the partition function then becomes the square of (3.3), as it should. In a similar way, one can adapt to this $J_4 = 0$ case the rest of the analysis of Section 3.3 and formally recover the single interface results $-M \operatorname{erf}(\chi)$ instead of (3.74), and $(M \operatorname{erf}(\chi))^2$ instead of (3.75) (Fig. 3.14). Hence, we see how an arbitrarily small $J_4 < 0$ is sufficient to induce in a discontinuous way the appearance of the intermediate phase, and a switch in passage probability density from $p(x_1, y)p(x_2, y)$ to (3.62).

Also the passage to $J_4 > 0$ is discontinuous, since in this regime the vacua $++$ and $--$ become adjacent and the asymptotic profiles are given by (3.19) (Fig. 3.14). We then have an exact description of the wetting transition occurring at $J_4 = 0$ and associated to the interfacial tension

$$\Sigma_{++,-} = \begin{cases} 2m, & J_4 \leq 0, \\ 2m \sin(\xi/2), & J_4 > 0. \end{cases} \quad (3.76)$$

For $J_4 > 0$ there is formation of interfacial bubbles as in Fig. 3.4 with $a = ++$, $b = --$, $c = +- \text{ or } -+$, $\alpha = \beta$ and $\gamma = \pi - \xi$. These bubbles contribute to the term (3.21) with coefficients which can be deduced¹ from the results of [62, 59]. Actually, only $\mathcal{C}_{++,-}^{\sigma_1 \sigma_2}$ does not vanish, since $\langle \sigma_i(x, y) \rangle_{++,-}$ is odd in x by symmetry and cannot include the even term (3.21); this is consistent with the fact that the contributions of the bubbles $+-$ and $-+$ to the profile of σ_i have opposite sign and cancel each other.

¹In doing this one has to take into account that [62, 59] use the language of the high temperature phase, so that the operators σ_i have to be replaced with their duals μ_i .

3.6 Summary

In this chapter we showed how field theory yields the exact asymptotic description of phase separation in the scaling limit of two-dimensional statistical systems at a first order phase transition point. The derivation is performed within the scattering formalism, in which the interfaces eventually correspond to the trajectories of kink excitations propagating in imaginary time. While this peculiarity of the two-dimensional case is intuitively clear, the technical way it enters the derivation is more subtle. In any dimension the matrix elements of local operators contain disconnected parts corresponding to particles propagating without coupling to the operator. Only in two-dimensional space-time, however, the trajectory of a disconnected particle cannot be taken around the point where the local operator is inserted; it will pass either to the left or to the right of this point, a circumstance resulting into the presence of pole singularities in the connected part of the matrix element. These singularities determine the jumps in the order parameter across an interface which are the signature of phase separation.

We derived in particular the following properties. Whether the third phase is wetting or not is determined by the spectrum of kinks of the field theory. The interfacial tension between two phases coincides with the mass of the lightest kink connecting these two phases, and the equilibrium condition among the three interfacial tensions at the vertex of a bubble coincides with energy conservation for the relativistic particles at a bound state vertex. The transverse fluctuations of the interface in the non-wetting regime of Fig. 3.5a are Gaussian with a width increasing as $R^{1/2}$, where R is the size of the system in the direction parallel to the interface; the size in the transverse direction is assumed infinite, while R is taken much larger than the correlation length in the pure phases, which in turn is inversely proportional to the mass scale. The effect on the order parameter of the bubbles of Fig. 3.5a vanishes as $R^{-1/2}$ to leave a sharp separation between phases a and b in the asymptotic large R limit. For systems in which the external phases are exchanged by a symmetry, the coefficient of this bubble term depends only on the bulk theory and can also be determined exactly in many cases. The subsequent term in the large R expansion corresponds to trifurcations rather than bifurcations in Fig. 3.5a and is suppressed as R^{-1} ; in two-phase, Ising-like sys-

tems this provides the first correction to sharp separation. In the wetting regime of Fig. 3.5b the order parameter profile does not approach at large R that corresponding to sharp separation between phases a and b . Its exact determination leads to a combined passage probability which differs from that of two independent interfaces by a factor of the square of the distance between the interfaces, which are then mutually avoiding. The transition from the first to the second regime of Fig. 3.5 corresponds to the unbinding of a bound state and we exhibit the Ashkin-Teller model as a first exactly solved example of such a bulk wetting transition.

We remark that the analysis was performed exploiting general properties of two-dimensional field theory at low energies. The information needed for specialization to models concerns the existence of bound states and the threshold values of kink-kink scattering amplitudes. The main models, however, are integrable in the scaling limit in two dimensions, and this information is available. In this way we were able, in particular, to establish the formation of an intermediate disordered phase in the dilute q -state Potts model, and to show how the Ashkin-Teller model yields an example of exactly solved bulk wetting transition. In all cases we determined the exact magnetization profiles and deduced from them the interface properties.

The analysis of this chapter can be extended to cases in which, with the boundary conditions of Fig. 3.1, the interfacial region consists of more than two interfaces. This is possible, for example, in the regime III of the RSOS models [63], in which the degenerate vacua and the kinks connecting them form a chain in order parameter space. Scattering amplitudes [64] and matrix elements [65] of the bulk theory are available, but a detailed study is beyond our present scope.

3.7 Appendix A: computation of integrals

This appendix is devoted to the derivation of the results

$$F(x, y) \equiv \frac{1}{\zeta(R)} \int_{\mathbb{R}^4} \frac{d\theta_1 d\theta_2 d\theta_3 d\theta_4}{(2\pi)^4} \frac{\theta_{12}^2 \theta_{34}^2}{\theta_{13} \theta_{14} \theta_{23} \theta_{24}} \tilde{\mathcal{Y}}^*(\theta_1, \theta_2, \theta_3, \theta_4) = \frac{\mathcal{G}(\chi) - 1}{2}, \quad (3.77)$$

$$\Delta(x, y) \equiv \frac{i}{2\zeta(R)} \int_{\mathbb{R}^4} \frac{d\theta_1 d\theta_2 d\theta_3}{(2\pi)^3} \frac{\theta_{12} \theta_{13}}{\theta_{32}} \tilde{\mathcal{Y}}^*(\theta_1, \theta_2, \theta_3, \theta_1) = \frac{\mathcal{L}(\chi)}{4} + \text{const}, \quad (3.78)$$

where $\zeta(R) \equiv \frac{e^{-2mR}}{\pi(mR)^2}$, \mathcal{G} and \mathcal{L} were given in (3.46) and (3.51), and

$$\tilde{\mathcal{Y}}^*(\theta_1, \theta_2, \theta_3, \theta_4) = e^{-2mR} e^{-\frac{mR}{4} [\theta_1^2 + \theta_2^2 + \theta_3^2 + \theta_4^2] + imx [\theta_3 + \theta_4 - \theta_1 - \theta_2]} e^{\frac{my}{2} [\theta_3^2 + \theta_4^2 - \theta_1^2 - \theta_2^2]} \quad (3.79)$$

is (3.39) evaluated at small rapidities. In the derivation we will use the Dawson function [66]

$$\mathcal{F}_D(x) \equiv e^{-x^2} \int_0^x dt e^{t^2}, \quad (3.80)$$

and the functions

$$\omega_n(\lambda; a) = \int_{\mathbb{R}} dx \frac{x^{2n}}{x^2 - a^2} e^{-\lambda x^2}, \quad (3.81)$$

with n a non-negative integer. Let us evaluate (3.81). Using

$$\lim_{\epsilon \rightarrow 0} \frac{1}{x - a \mp i\epsilon} = \pm \pi i \delta(x - a) + \mathcal{P} \frac{1}{x - a}, \quad (3.82)$$

we have

$$\omega_0(\lambda; a) = \mathcal{P} \int_{\mathbb{R}} \frac{dx}{x^2 - a^2} e^{-\lambda x^2} = \frac{1}{2a} \mathcal{P} \int_{\mathbb{R}} \frac{dx}{x - a} e^{-\lambda x^2} - \frac{1}{2a} \mathcal{P} \int_{\mathbb{R}} \frac{dx}{x + a} e^{-\lambda x^2}. \quad (3.83)$$

Defining

$$\nu(\lambda, a) = \mathcal{P} \int_{\mathbb{R}} \frac{dx}{x - a} e^{-\lambda x^2}, \quad (3.84)$$

and using $x = u + a$ we have

$$\partial_a \left[\nu(\lambda, a) e^{\lambda a^2} \right] = -2\lambda \int_{\mathbb{R}} du e^{-\lambda(u^2 + 2au)} = -2\sqrt{\pi\lambda} e^{\lambda a^2}; \quad (3.85)$$

integrating with respect to a and using $\nu(\lambda, 0) = 0$, we have

$$\nu(\lambda, a) = -\pi \operatorname{erfi}(\sqrt{\lambda}a) e^{-\lambda a^2} = -2\sqrt{\pi} \mathcal{F}_D(\sqrt{\lambda}a), \quad (3.86)$$

where $\operatorname{erfi}(z) = -i \operatorname{erf}(iz)$ and $\mathcal{F}_D(z) = (\sqrt{\pi}/2) \operatorname{erfi}(z) e^{-z^2}$ [66]. It follows from (3.86) that

$$\omega_0(\lambda; a) = -2\sqrt{\pi} \frac{\mathcal{F}_D(\sqrt{\lambda}a)}{a}, \quad (3.87)$$

while for arbitrary n we can use $\omega_n(\lambda; a) = (-\partial_\lambda)^n \omega_0(\lambda; a)$; in particular

$$\omega_1(\lambda; a) = \mathcal{P} \int_{\mathbb{R}} dx \frac{x^2}{x^2 - a^2} e^{-\lambda x^2} = \sqrt{\pi} \left[\frac{1}{\sqrt{\lambda}} - 2a \mathcal{F}_D(\sqrt{\lambda}a) \right]. \quad (3.88)$$

We will also need the result

$$\Xi(\ell) \equiv \int_{\mathbb{R}} du \frac{\mathcal{F}_D(u)}{u} e^{-u^2 - i\ell u} = \frac{\pi^{3/2}}{4} \left[1 - \operatorname{erf}^2 \left(\frac{\ell}{\sqrt{8}} \right) \right], \quad (3.89)$$

which can be derived as follows. Using the integral representation of the Dawson function

$$\mathcal{F}_D(x) = \int_0^\infty du e^{-u^2} \sin(2ux), \quad (3.90)$$

we can write $\Xi(\ell)$ in the form

$$\Xi(\ell) = \int_0^\infty du Q(\ell, u) e^{-u^2}, \quad Q(\ell, u) = \int_{\mathbb{R}} dx \frac{\sin(2ux)}{x} e^{-x^2 - i\ell x}. \quad (3.91)$$

Taking the first derivative with respect to ℓ and carrying out the Gaussian integrations we find¹

$$\Xi(\ell) = \frac{\pi}{2} \int_0^\infty du e^{-u^2} \left[\operatorname{erf} \left(u - \frac{\ell}{2} \right) + \operatorname{erf} \left(u + \frac{\ell}{2} \right) \right], \quad (3.92)$$

and with the aid of

$$\int_0^\infty du e^{-u^2} \operatorname{erf}(u + a) = \frac{\sqrt{\pi}}{4} \left[2 - \operatorname{erfc}^2(a/\sqrt{2}) \right], \quad (3.93)$$

¹Using the identity $\int_{\mathbb{R}} dx \frac{\sin(2ux)}{x} e^{-x^2} = \pi \operatorname{erf}(u)$, we found that the integration constant is zero.

we obtain (3.89).

Consider now (3.77). Introducing the variables $x_{\pm} = \theta_1 \pm \theta_3$, $y_{\pm} = \theta_2 \pm \theta_4$, and then $u_{\mp} = x_{\pm} \mp y_{\pm}$, $v_{\mp} = x_{\mp} \mp y_{\mp}$, we have $\left| \det \frac{\partial(\theta_1, \theta_2, \theta_3, \theta_4)}{\partial(u_-, u_+, v_-, v_+)} \right| = \frac{1}{16}$, $d\theta_1 d\theta_2 d\theta_3 d\theta_4 = 16^{-1} du_+ du_- dv_+ dv_-$, and

$$\tilde{\mathcal{Y}}^*(\theta_1, \theta_2, \theta_3, \theta_4) = e^{-2mR} e^{-\frac{mR}{16} [u_+^2 + u_-^2 + v_+^2 + v_-^2]} e^{-imxv_+} e^{-\frac{my}{4} [u_+v_+ + u_-v_-]}.$$

Rescaling the variables as $u_{\pm} \rightarrow (4/\sqrt{mR})u_{\pm}$ and $v_{\pm} \rightarrow (4/\sqrt{mR})v_{\pm}$, we have $F(x, y) = \pi^{-3}E(h, \epsilon)$, where

$$\begin{aligned} E(h, \epsilon) &\equiv \int_{\mathbb{R}^4} du_+ du_- dv_+ dv_- \frac{(u_-^2 - v_-^2)^2}{(v_+^2 - u_+^2)(v_+^2 - v_-^2)} \times \\ &\times e^{-(u_+^2 + u_-^2 + v_+^2 + v_-^2) - ihv_+ - 2\epsilon(u_+v_+ + u_-v_-)}, \end{aligned} \quad (3.94)$$

with $h = 4mx/\sqrt{mR}$ and $\epsilon = 2y/R$. We write

$$\begin{aligned} E(h, \epsilon) &= \int_{\mathbb{R}^2} du_+ dv_+ e^{-u_+^2} e^{-v_+^2 - ihv_+ - 2\epsilon u_+ v_+} f(v_+, \epsilon) \\ &= \sqrt{\pi} \int_{\mathbb{R}} dv_+ e^{-\kappa^2 v_+^2 - ihv_+} f(v_+, \epsilon), \end{aligned} \quad (3.95)$$

where we have used the parameter $\kappa^2 = 1 - \epsilon^2$ and the function

$$\begin{aligned} f(\alpha, \epsilon) &\equiv \int_{\mathbb{R}^2} dx dy \frac{(x^2 - y^2)^2}{(x^2 - \alpha^2)(y^2 - \alpha^2)} e^{-x^2 - y^2 - 2\epsilon xy} \\ &= \int_{\mathbb{R}^2} dx dy \frac{[(x^2 - \alpha^2) - (y^2 - \alpha^2)]^2}{(x^2 - \alpha^2)(y^2 - \alpha^2)} e^{-x^2 - y^2 - 2\epsilon xy} \\ &= 2 \int_{\mathbb{R}^2} dx dy \left[\frac{x^2 - \alpha^2}{y^2 - \alpha^2} - 1 \right] e^{-x^2 - y^2 - 2\epsilon xy} = \sqrt{\pi} \int_{\mathbb{R}} dy \frac{1 - 2\kappa^2 y^2}{y^2 - \alpha^2} e^{-\kappa^2 y^2}; \end{aligned} \quad (3.96)$$

the integration over y can be performed using the functions (3.81), thus

$$f(\alpha, \epsilon) = \sqrt{\pi} \left[\omega_0(\kappa^2, \alpha) - 2\kappa^2 \omega_1(\kappa^2, \alpha) \right], \quad (3.97)$$

and

$$E(h, \epsilon) = 2\pi^{3/2}\kappa \int_{\mathbb{R}} du e^{-\kappa^2 u^2 - ihu} \left[2\kappa u \mathcal{F}_D(\kappa u) - \frac{\mathcal{F}_D(\kappa u)}{\kappa u} - 1 \right]. \quad (3.98)$$

The function (3.98) satisfies $E(h, \epsilon) = E(h/\sqrt{1-\epsilon^2}, 0)$, as one can easily verify with the rescaling $\kappa u \rightarrow u$. We recall that $h/\kappa = \sqrt{8}\chi$, therefore (3.98) becomes

$$E(h/\kappa, 0) = 2\pi^{3/2} \int_{\mathbb{R}} du e^{-u^2 - i\sqrt{8}\chi u} \left[2u \mathcal{F}_D(u) - \frac{\mathcal{F}_D(u)}{u} - 1 \right]. \quad (3.99)$$

It follows from (3.80) that $\mathcal{F}'_D(x) = 1 - 2x \mathcal{F}_D(x)$; using this property, an integration by parts of (3.99) and recalling (3.89) we can show that (3.99) can be written in the form

$$E(h/\kappa, 0) = 2\pi^{3/2} \left[\frac{1}{4} \partial_\chi^2 + \chi \partial_\chi - 1 \right] \Xi(\sqrt{8}\chi) = \frac{\pi^3}{2} \left[\mathcal{G}(\chi) - 1 \right], \quad (3.100)$$

which amounts to (3.77).

We now turn to (3.78). We rescale the integration variables as $\theta_i \rightarrow \sqrt{2/mR} \theta_i$, perform the Gaussian integral over θ_1 and for the remaining integration rapidities adopt the change of variables $\theta_\pm = \theta_3 \pm \theta_2$; obtaining

$$\Delta(x, y) = \frac{i}{32\pi^{3/2}} \int_{\mathbb{R}^2} d\theta_+ d\theta_- \left[\frac{2 + \theta_+^2 - \theta_-^2}{\theta_-} \right] e^{-\frac{\theta_+^2 + \theta_-^2}{4} + \frac{\epsilon}{2} \theta_+ \theta_- + i(x/\lambda) \theta_-}; \quad (3.101)$$

Gaussian integration gives

$$\Delta(x, y) = \frac{i}{16\pi} \int_{\mathbb{R}} \frac{d\theta_-}{\theta_-} (4 - \theta_-^2) e^{-\frac{\theta_-^2}{4} + i\chi \theta_-}, \quad (3.102)$$

and then

$$\partial_\chi \Delta(x, y) = -\frac{1}{4\sqrt{\pi}} (1 + 2\chi^2) e^{-\chi^2}. \quad (3.103)$$

Integrating back we obtain (3.78).

3.8 Appendix B: Critical interfaces

Phase coexistence arises at first-order transition points. The interfaces we find in this regime separate two non-critical phases and thus we term these *off-critical interfaces*. A notion of interface, however, can be introduced also for systems at a second order phase transition point defined on a lattice; we can refer to these interfaces as *critical interfaces*.

Such a curve can be defined for the planar Ising model on a triangular lattice. Consider the system on the upper half-plane \mathbb{H} . Boundary conditions $+/-$ on the right/left side of the edge will lead to a path (on the dual hexagonal lattice) with negative spins on its left and positive spins on its right, as in Fig.3.15. The

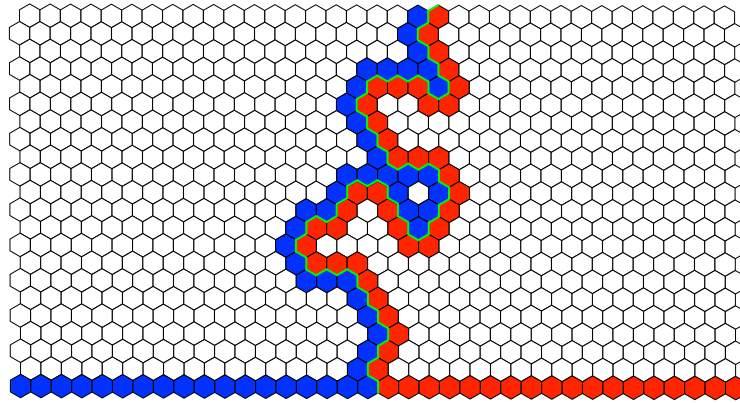


Figure 3.15: Exploration process for the Ising model. The interface is represented with colored bonds.

curve starts exactly at the boundary condition changing point and its evolution in the bulk can be defined rigorously as an *exploration process*. The analogous process in the continuum limit is described by *Loewner's evolution* ([67] and [68] for a review).

In the continuum version the curve may touch itself forming closed regions. At time t the *hull* K_t is defined as the union of such a regions with the curve γ . Using Riemann theorem we can map the complement of the hull, $\mathbb{H} - K_t$, in the upper half plane. At a fixed time such a mapping can be uniquely determined using some asymptotic restrictions. Loewner's equation determines the time evolution of such a mapping.

A critical curve however is not a deterministic process but rather a random one. Consider a domain $\mathbb{D} \subset \mathbb{H}$ and a curve γ that connects the points z_1 and z_2 on the boundary of \mathbb{D} . It is possible to define a measure $\mu(\gamma; \mathbb{D}, z_1, z_2)$ on such an ensemble of random curves requiring the following properties:

- *Domain Markov property.* Let z^* be a point on γ , γ_1 the portion of γ with endpoints z_1, z^* and γ_2 the portion of γ with endpoints z^*, z_2 . The conditional measure obeys to $\mu(\gamma_2 | \gamma_1; \mathbb{D}, z_1, z_2) = \mu(\gamma_2 | \mathbb{D} \setminus \gamma_1; z^*, z_2)$.
- *Conformal Invariance.* Let Φ be a conformal transformation that maps the interior of \mathbb{D} onto the interior of a domain \mathbb{D}' . The boundary points z_k are thus mapped into z'_k . The conformal mapping induces a measure $\Phi * \mu$ on the curves mapped through Φ . Conformal invariance states the equality of these measures: $(\Phi * \mu)(\gamma; \mathbb{D}, z_1, z_2) = \mu(\Phi(\gamma); \mathbb{D}', z'_1, z'_2)$.

The above properties jointly with Loewner's evolution defines the continuum limit of critical curves on the lattice. Such a process goes under the name of *Schramm-Loewner Evolution* (SLE) [67]. Passage probabilities can be defined also for critical curves and exact computations have been carried out [67]. The same results for passage probabilities have been obtained by means conformal field theory techniques; see [68], [69]. Establishing a link between these critical interfaces and the off-critical ones we study directly in the continuum in this thesis appears as an interesting subject for future research.

Chapter 4

Interfaces and wetting on the half plane

In this chapter we will develop the field theory of phase separation in presence of a flat boundary. For the case of adjacent phases we will examine the drop configuration in which the interface has endpoints pinned on the boundary. Then we will analyze the unbound regime corresponding to the wetting of a flat substrate. Lastly we will consider phase separation in presence of intermediate phases.

4.1 Introduction

Interfacial phenomena at boundaries are a subject of relevant interest for both theory and applications. On the theoretical side - the one this thesis is concerned with - the effects of the boundary on an interface separating different phases of a statistical system have been extensively studied using phenomenological, mean field, renormalization group and other methods ([15], [31], [12], [14], [13], [17], [70], [16] is a certainly incomplete list of review articles). The only exact result that has been available concerns the Ising model on the half plane [71, 40], a circumstance that, while confirming a specificity of the two-dimensional case, raises the question about the role of Ising solvability in these exact findings.

We show in this chapter that exact results, including those of [40] as a particular case, are obtained quite generally for any two-dimensional model exhibiting

a continuous phase transition. This is done extending to the half plane the non-perturbative field theoretical approach used in the previous chapter. As in that case, general exact results emerge because, when its end-to-end distance R is much larger than the correlation length, the interface is described by a single particle (domain wall) state, in a low-energy limit leading to a general solution. In this way, the fluctuations of the interface turn out to be ruled by the low-energy singularity of the matrix element of the order parameter field (as for the strip), with the fields pinning the interface endpoints to the boundary producing boundary reflection and an average midpoint distance from the boundary of order \sqrt{R} .

The result changes qualitatively if boundary and domain wall excitation admit a stable bound state, which becomes dominant in the spectral sum at low energies and bounds the interface to the boundary. The contact angle and the spreading coefficient of the phenomenological theory of wetting then emerge in a completely natural way within the field theoretical formalism.

4.2 Single interface

Consider a ferromagnetic spin model of two-dimensional classical statistical mechanics in which spins take discrete values labelled by an index $a = 1, 2, \dots, n$. The energy of the system is invariant under global transformations of the spins according to a symmetry whose spontaneous breaking below a critical temperature T_c is responsible for the presence on the infinite plane of n translation invariant pure phases; we denote by $\langle \dots \rangle_a$ statistical averages in the phase a .

Assuming a continuous transition, we consider the scaling limit below T_c , corresponding to a Euclidean field theory defined on the plane with coordinates (x, y) , which can be seen as the analytic continuation to imaginary time of a (1+1)-dimensional relativistic field theory with space coordinate x and time coordinate $t = iy$. If H and P are the Hamiltonian and momentum operators and Φ a field of the theory, translation invariance on the plane yields the relation

$$\Phi(x, y) = e^{ixP+yH} \Phi(0, 0) e^{-ixP-yH} . \quad (4.1)$$

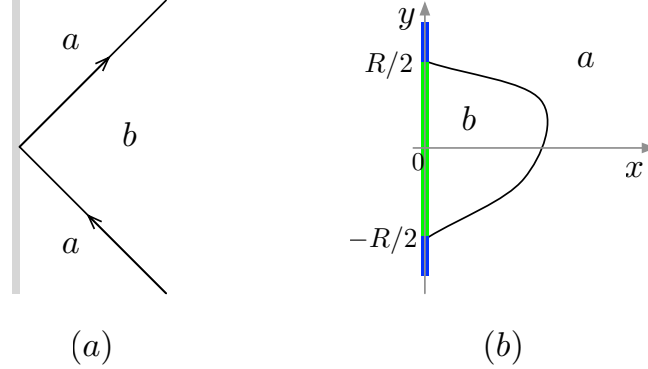


Figure 4.1: Elastic scattering (reflection) of a kink off the boundary (a), and interface pinned at the boundary (b).

The (1+1)-dimensional theory possesses degenerate vacua $|0\rangle_a$ associated with the pure phases of the system. The elementary excitations correspond to stable kink states $|K_{ab}(\theta)\rangle$ interpolating between different vacua $|0\rangle_a$ and $|0\rangle_b$. We introduced the rapidity variable θ , which conveniently parameterizes the energy and momentum of the kinks as $(E, p) = (m \cosh \theta, m \sinh \theta)$, m being the kink mass or inverse correlation length. The trajectory of the kink on the Euclidean plane corresponds to a domain wall between the phases a and b . Multi-kink excitations take the form $|K_{aa_1}(\theta_1)K_{a_1a_2}(\theta_2) \dots K_{a_{n-1}b}(\theta_n)\rangle$. Within the scattering framework [36] we consider, these are asymptotic states, incoming if considered long before the collisions among the kinks, outgoing if considered long after, and their energy is simply $\sum_{i=1}^n m \cosh \theta_i$.

Consider now the system on the half-plane $x \geq 0$. We denote by B_a a boundary condition at $x = 0$ which is y -independent and breaks the symmetry of the bulk in the direction a in order parameter space; this can be realized applying a constant boundary magnetic field pointing in the direction a . We denote by $\langle \dots \rangle_{B_a}$ statistical averages in the presence of the boundary condition B_a . Preservation of translation invariance in the y direction yields energy conservation in the (1 + 1)-dimensional picture. The bulk excitations are still the kink states described for the full plane case, but now they are restricted to $x > 0$; we indicate this restriction by a subscript B_a . Hence $|0\rangle_{B_a}$ denotes the vacuum (no

excitations in the bulk) on the half plane with the boundary condition B_a . If σ is the spin field, the magnetization $\langle \sigma(x, y) \rangle_{B_a} = {}_{B_a} \langle 0 | \sigma(x, y) | 0 \rangle_{B_a}$ points in the direction a and depends only on the distance x from the boundary; in particular

$$\lim_{x \rightarrow \infty} \langle \sigma(x, y) \rangle_{B_a} = \langle \sigma \rangle_a, \quad (4.2)$$

where $\langle \sigma \rangle_a$ is the constant magnetization in phase a on the full plane. The state $|0\rangle_{B_a}$ is an eigenstate of the Hamiltonian H_{B_a} of the system on the half line. We consider the case in which boundary conditions B_a and B_b are related by the symmetry, so that $|0\rangle_{B_a}$ and $|0\rangle_{B_b}$ have the same energy E_B .

The asymptotic scattering state $|K_{ba}(\theta)\rangle_{B_a}$ corresponds to an incoming kink (travelling towards the boundary) if its momentum is negative, i.e. if $\theta < 0$. If its energy is lower than the energy $2m$ needed to produce two kinks upon interaction with the boundary, it will simply be reflected into an outgoing kink¹ with rapidity $-\theta$ (Fig. 1a). The state $|K_{ba}(\theta)\rangle_{B_a}$ is an eigenstate of H_{B_a} with eigenvalue $E_B + m \cosh \theta$.

We are now ready to set up the configuration we want to study, namely a boundary condition which is of type B_a if $|y| > R/2$ and of type B_b if $|y| < R/2$. The interest of such a boundary condition, which we denote B_{aba} , is easily understood by observing that the limit for $x \rightarrow \infty$ of the magnetization profile $\langle \sigma(x, 0) \rangle_{B_{aba}}$ has to tend to $\langle \sigma \rangle_a$ if R is finite, and to $\langle \sigma \rangle_b$ if R is infinite. The natural way to account for this situation is to expect the formation of an interface pinned at $R/2$ and $-R/2$ on the boundary, separating an inner phase b from an outer phase a (Fig. 1b), and whose average distance from the boundary at $y = 0$ diverges with R . The remainder of this section is devoted to seeing how such a picture indeed emerges within our general field theoretical framework.

Technically the change from the boundary condition B_a to B_b at a point y is realized starting with B_a and inserting on the boundary a field $\mu_{ab}(0, y)$, which acting on the vacuum $|0\rangle_{B_a}$ creates kink states interpolating between phase a and phase b . Hence the simplest non-vanishing matrix element of the boundary field

¹As emphasized in [38], the analogies between bulk and boundary scattering become evident thinking of the boundary as the propagation of an infinitely heavy particle sitting at $x = 0$.

μ_{ab} is

$${}_{B_a}\langle 0|\mu_{ab}(0, y)|K_{ba}(\theta)\rangle_{B_a} = e^{-ym \cosh \theta} {}_{B_a}\langle 0|\mu_{ab}(0, 0)|K_{ba}(\theta)\rangle_{B_a} \equiv e^{-ym \cosh \theta} \mathcal{F}_\mu(\theta). \quad (4.3)$$

The partition function of the system with boundary condition B_{aba} reads

$$Z = {}_{B_a}\langle 0|\mu_{ab}(0, R/2)\mu_{ba}(0, -R/2)|0\rangle_{B_a} = \int_0^\infty \frac{d\theta}{2\pi} |\mathcal{F}_\mu(\theta)|^2 e^{-mR \cosh \theta} + O(e^{-2mR}), \quad (4.4)$$

where the last expression is obtained by expanding over an intermediate set of outgoing kink states and retaining only the lightest (single kink) contribution which is leading in the large mR limit we will consider from now on. Since the above integral is dominated by small rapidities and \mathcal{F}_μ is expected to behave as¹

$$\mathcal{F}_\mu(\theta) = a\theta + O(\theta^2), \quad (4.5)$$

the partition function becomes

$$Z \sim |a|^2 \int_0^\infty \frac{d\theta}{2\pi} \theta^2 e^{-mR(1+\theta^2/2)} = \frac{|a|^2 e^{-mR}}{2\sqrt{2\pi} (mR)^{3/2}}. \quad (4.6)$$

The magnetization profile along the x axis is given by

$$\begin{aligned} \langle \sigma(x, 0) \rangle_{B_{aba}} &= \frac{1}{Z} {}_{B_a}\langle 0|\mu_{ab}(0, R/2)\sigma(x, 0)\mu_{ba}(0, -R/2)|0\rangle_{B_a} \\ &\sim \frac{1}{Z} \int_{-\infty}^{+\infty} \frac{d\theta_1}{2\pi} \frac{d\theta_2}{2\pi} \mathcal{F}_\mu(\theta_1) \langle K_{ab}(\theta_1)|\sigma(0, 0)|K_{ba}(\theta_2)\rangle \mathcal{F}_\mu^*(\theta_2) \times \\ &\times e^{m[i(\sinh \theta_1 - \sinh \theta_2)x - (\cosh \theta_1 + \cosh \theta_2)\frac{R}{2}]}, \end{aligned} \quad (4.7)$$

where in the last line we have taken $mR \gg 1$ to project on the one-kink intermediate states, but also $mx \gg 1$ to be able to treat $\sigma(x, 0)$ as a bulk field which satisfies (4.1) and is evaluated on bulk-kink states (whose rapidities take both positive and negative values). In other words, for mx large the only effect of the boundary on the magnetization comes from the boundary changing fields

¹Linear behavior of matrix elements at small rapidities in two-dimensional theories is well known. Within the framework of integrable boundary field theory [38] exact examples can be found in [72]. More generally, see [43] about matrix elements in integrable theories.

at $(0, \pm R/2)$; in their absence one would simply observe the constant value $\langle \sigma \rangle_a$. The bulk matrix element of the spin field between one-kink states is related by the crossing relation¹

$$\langle K_{ab}(\theta_1) | \sigma(0, 0) | K_{ba}(\theta_2) \rangle = F_\sigma(\theta_1 + i\pi - \theta_2) + 2\pi\delta(\theta_1 - \theta_2)\langle \sigma \rangle_a, \quad (4.8)$$

to the form factor

$$F_\sigma(\theta_1 - \theta_2) \equiv {}_a\langle 0 | \sigma(0, 0) | K_{ab}(\theta_1) K_{ba}(\theta_2) \rangle. \quad (4.9)$$

As already observed in Chapter 3 for the case of phase separation in the strip, it is crucial that quite generally, due to non-locality of the kinks with respect to the spin field, $F_\sigma(\theta)$ possesses an annihilation pole at $\theta = i\pi$ with residue [44]

$$-i \operatorname{Res}_{\theta=i\pi} F_\sigma(\theta) = \langle \sigma \rangle_a - \langle \sigma \rangle_b \equiv \Delta\langle \sigma \rangle. \quad (4.10)$$

Since mR is large, (4.7) is dominated by small rapidities and (4.5), (4.8) and (4.10) lead to

$$\langle \sigma(x, 0) \rangle_{B_{aba}} \sim 2\langle \sigma \rangle_a + i\Delta\langle \sigma \rangle \frac{|a|^2}{Z} e^{-mR} \int_{-\infty}^{+\infty} \frac{d\theta_1}{2\pi} \frac{d\theta_2}{2\pi} \frac{\theta_1\theta_2}{\theta_1 - \theta_2} e^{m[i(\theta_1 - \theta_2)x - (\theta_1^2 + \theta_2^2)\frac{R}{4}]}. \quad (4.11)$$

Differentiation removes the singularity of the integrand and gives

$$\begin{aligned} \partial_{mx} \langle \sigma(x, 0) \rangle_{B_{aba}} &\sim -\Delta\langle \sigma \rangle \frac{|a|^2 e^{-mR}}{(2\pi)^2 Z} g(x)g(-x) \\ &= \Delta\langle \sigma \rangle \frac{4\sqrt{2}}{\sqrt{\pi mR}} z^2 e^{-z^2}, \quad z \equiv \sqrt{\frac{2m}{R}} x \end{aligned} \quad (4.12)$$

where we used (4.6) and

$$g(x) = \int_{-\infty}^{+\infty} d\theta \theta e^{-mR\theta^2/4 + imx\theta} = \frac{2i\sqrt{2\pi}}{mR} z e^{-z^2/2}. \quad (4.13)$$

¹Crossing a particle from the initial to the final state (or vice versa) involves reversing the sign of its energy and momentum [36], namely an $i\pi$ rapidity shift. The delta function term in (4.8) is a disconnected part arising from annihilation of the two kinks.

Integrating (4.12) with the asymptotic condition $\langle \sigma(\infty, 0) \rangle_{B_{aba}} = \langle \sigma \rangle_a$ gives

$$\langle \sigma(x, 0) \rangle_{B_{aba}} \sim \langle \sigma \rangle_b - \frac{2}{\sqrt{\pi}} \Delta \langle \sigma \rangle \left(z e^{-z^2} - \int_0^z du e^{-u^2} \right), \quad mx \gg 1. \quad (4.14)$$

From this result we can compute exactly $\lim_{R \rightarrow \infty} \langle \sigma((\alpha/m)(mR)^\delta, 0) \rangle_{B_{aba}}$, obtaining $\langle \sigma \rangle_b$ for $0 < \delta < 1/2$, $\langle \sigma \rangle_a$ for $\delta > 1/2$, and the rhs of (4.14) with $z = \alpha\sqrt{2}$ for $\delta = 1/2$. For $\langle \sigma \rangle_a = -\langle \sigma \rangle_b = \langle \sigma \rangle_+$ these are precisely the limits obtained from the lattice in [73, 71] for the Ising model on the half plane with boundary spins fixed to be positive for $|y| > R/2$ and negative for $|y| < R/2$.

The derivative (4.12) of the magnetization profile is peaked around $z = 1$, confirming the presence of an interface whose average distance from the boundary increases as $\sqrt{R/m}$. It is also easy to see that the result for the magnetization profile is consistent with a simple probabilistic interpretation. Since we are computing the magnetization on a scale R much larger than the correlation length and far away from the boundary, we can think of the interface as a sharp separation between pure phases¹, and write

$$\langle \sigma(x, 0) \rangle_{B_{aba}} \sim \langle \sigma \rangle_a \int_0^x du p(u) + \langle \sigma \rangle_b \int_x^\infty du p(u), \quad mx \gg 1, \quad (4.15)$$

where $p(u)du$ is the probability that the interface intersects the x -axis in the interval $(u, u + du)$, so that the two integrals are the left and right passage probabilities with respect to x . Differentiating and comparing with (4.12) gives the passage probability density

$$p(x) = 4\sqrt{\frac{2m}{\pi R}} z^2 e^{-z^2}, \quad (4.16)$$

which correctly satisfies $\int_0^\infty dx p(x) = 1$.

¹It has been shown in Section 3.2 how the internal structure of the interface arises from subleading terms in the large mR expansion.

4.3 Wetting transition

The results of the previous section are modified if the kink-boundary system associated to the asymptotic state $|K_{ab}(\theta)\rangle_{B_b}$ admits a stable bound state $|0\rangle_{B'_a}$, corresponding to the binding of the kink K_{ab} on the boundary B_b . As usual for stable bound states [36], such a binding will correspond to a “virtual” value θ_0 of the kink rapidity, leading to a bound state energy $E_B + m \cosh \theta_0$ real and smaller than the unbinding energy $E_B + m$. This amounts to taking $\theta_0 = iu$ with $0 < u < \pi$, so that

$$E_{B'} = E_B + m \cos u. \quad (4.17)$$

The existence of the bound state manifests in particular through a simple pole in the elastic scattering amplitude of the kink off the boundary, which reads $\mathcal{R}(\theta) \sim ig^2/(\theta - iu)$ for $\theta \rightarrow iu$, with g a kink-boundary coupling constant (Fig. 2a). This pole is inherited by the matrix element (4.3), for which we have¹ (Fig. 2b)

$$\mathcal{F}_\mu(\theta) = {}_{B_a}\langle 0|\mu_{ab}(0,0)|K_{ba}(\theta)\rangle_{B_a} \sim \frac{ig}{\theta - iu} {}_{B_a}\langle 0|\mu_{ab}(0,0)|0\rangle_{B'_a}, \quad \theta \rightarrow iu. \quad (4.18)$$

The boundary bound state affects the results of the previous section for the boundary condition B_{aba} because the leading low-energy contribution in the expansion over intermediate states now comes from $|0\rangle_{B'_a}$ rather than from $|K_{ba}(\theta)\rangle_{B_a}$. So the partition function becomes

$$\begin{aligned} Z &= {}_{B_a}\langle 0|\mu_{ab}(0, R/2)\mu_{ba}(0, -R/2)|0\rangle_{B_a}, \\ &= \left| {}_{B_a}\langle 0|\mu_{ab}(0,0)|0\rangle_{B'_a} \right|^2 e^{-mR \cos u} + O(e^{-mR}), \end{aligned} \quad (4.19)$$

and the magnetization profile

$$\begin{aligned} \langle \sigma(x,0) \rangle_{B_{aba}} &\sim \frac{1}{Z} {}_{B_a}\langle 0|\mu_{ab}(0, R/2)|0\rangle_{B'_a} {}_{B'_a}\langle 0|\sigma(x,0)|0\rangle_{B'_a} {}_{B'_a}\langle 0|\mu_{ba}(0, -R/2)|0\rangle_{B_a} \\ &= \langle \sigma(x,0) \rangle_{B'_a}. \end{aligned} \quad (4.20)$$

¹Exact solutions exhibiting boundary bound states poles can be found in [38] for scattering amplitudes and in [72] for matrix elements.

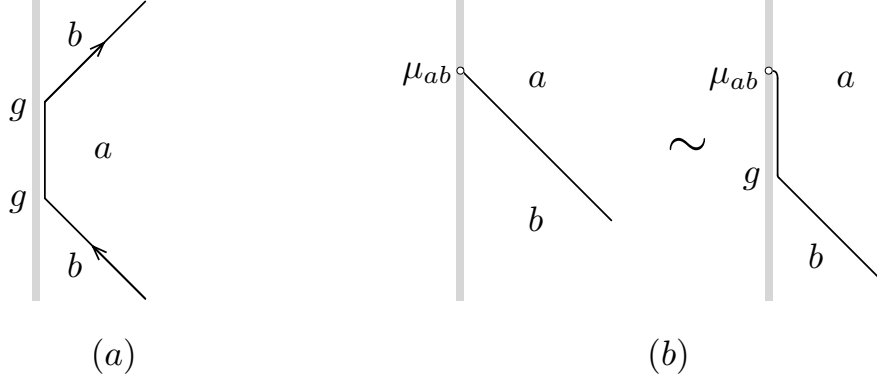


Figure 4.2: The boundary bound state (double line) originating in kink-boundary scattering (a), and a pictorial representation of equation (4.18) (b).

We see then that, as a consequence of (4.2), the magnetization profile now tends to $\langle\sigma\rangle_a$ at large mx , in contrast to what was obtained in the previous section, where it tended to $\langle\sigma\rangle_b$ for R large enough. This corresponds to the fact that now the asymptotic behavior is determined by the state in which the interface, and then the phase b , are bound to the boundary, while before the dominant state was that in which phase b extended to an average midpoint distance of order \sqrt{R} from the boundary.

Consistency of the asymptotic expansion requires that the corrections to (4.20) vanish as $R \rightarrow \infty$. For mx large, the first of these corrections is that due to the $|K_{ba}(\theta)\rangle$ intermediate states given in (4.7). The Z in the denominator, however, is now (4.19) rather than (4.6), so that the correction behaves as $e^{mR(\cos u - 1)}$ at large R . Hence, if u approaches 0, i.e. if the interface approaches the unbinding point, consistency requires that R diverges faster than $1/u^2$. If we adopt a vocabulary within which b is a liquid phase and a a vapor phase, we can say that as $u \rightarrow 0$ a thin layer of the liquid phase spreads all over the boundary.

The relationship with the usual characterization of interfacial phenomena at boundaries becomes more transparent if we consider the situation usually referred to as “partial wetting”, corresponding to a drop of liquid surrounded by a thin layer of liquid adsorbed on the rest of the boundary (see e.g. [16]). In our formalism this amounts to splitting and recombination of the boundary bound

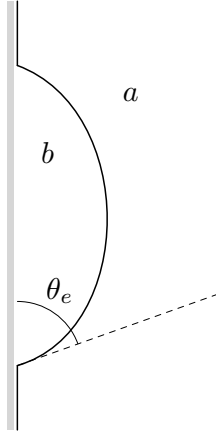


Figure 4.3: Splitting and recombination of the boundary bound state B'_a corresponds to “partial wetting”, in which a drop of phase b makes an equilibrium contact angle θ_e with the boundary. Equation (4.17) with $u = \theta_e$ gives the surface tension balance condition at the contact points.

state B'_a (Fig. 3). Considering that the kink mass m is the surface tension of the interface (see Chapter 3), that E_B is the surface tension between the boundary and the drop, and that $E_{B'}$ is the surface tension between the boundary away from the drop and phase a , we recognize in (4.17) the Young equilibrium condition at contact points (see e.g. [15] and references therein), with u playing the role of the equilibrium contact angle θ_e (Fig. 3). In addition, the combination $m(\cos u - 1)$ encountered a moment ago is recognized as the so called “equilibrium spreading coefficient” (see [16]). We also see that interface unbinding at $u = 0$ corresponds to vanishing of the contact angle, namely to the usual characterization of the wetting transition point (passage from partial to complete wetting).

The boundary bound state is a property of the theory with translationally invariant boundary condition B_b . Parameters of this theory are the temperature, related to the kink mass as $m \propto (T_c - T)^\nu$, and a coupling λ entering the boundary term $\lambda \int dy \phi(0, y)$ of the classical reduced Hamiltonian. If X is the scaling dimension¹ of the boundary field $\phi(0, y)$, u is function of the dimensionless combination λ/m^{1-X} . If λ is kept fixed, the condition $u = 0$ determines a wetting

¹The exponents ν and X are known exactly from bulk [74] and boundary [75] conformal field theory, respectively.

transition temperature $T_w(\lambda) < T_c$.

The results (4.6), (4.19) and (4.20) account for those reported in [71, 40] for the particular case of an Ising model with boundary condition B_{+-+} and coupling between the boundary spins and their nearest neighbors different from the coupling within the rest of the lattice; this modified coupling corresponds to the boundary parameter λ in this case. The generality of our results also explains why approximated treatments of other models resulted in findings similar to the Ising ones (see [40] and references therein).

4.4 Intermediate phases

In this section we consider the case in which the phases associated to the vacua $|0\rangle_a$ and $|0\rangle_b$ are not adjacent. This scenario occurs for a model with vacuum structure as the one of Fig.3.6. The calculation that we are going to show for the half-plane retraces only partially the one carried out in Chapter 3 for the strip. We will point out the technical differences along the way. Anticipating some results, we will argue in Chapter 5 that the results of this section can be obtained in a simpler way. More precisely, we will show that the two-leg disconnected diagrams of the expansion (3.41) are enough to reconstruct the whole profile. In this section, instead, we will compute the magnetization profile summing all the contributions analogous to (3.47) for the half-plane geometry.

The simplest excitation that interpolates among the two vacua is now a two-kink state $|K_{ac}K_{cb}\rangle$ passing through a third vacuum $|0\rangle_c$. In this situation the emission amplitude of a single-kink vanishes ($a = 0$ in (4.5)) and the leading contribution in the expansion of $\mathcal{Z}_{B_{bab}}$ starts with a double-kink excitation, thus (4.4) is replaced by

$$\begin{aligned} \mathcal{Z}_{B_{bab}}(R) &\simeq \sum_{c,d \neq a,b} \int_{\mathbb{R}_+^4} \frac{d\theta_1 d\theta_2 d\theta_3 d\theta_4}{(2\pi)^4} f_{adb}^\mu(\theta_4, \theta_3) \mathcal{M}_{ab,cd}(\theta_1, \theta_2 | \theta_3, \theta_4) \overline{f_{acb}^\mu}(\theta_1, \theta_2) \times \\ &\times e^{-\frac{mR}{2}(\cosh \theta_1 + \cosh \theta_2 + \cosh \theta_3 + \cosh \theta_4)} + \dots \end{aligned} \quad (4.21)$$

The summation in (4.21) takes into account double-kink states $|K_{ac}K_{cb}\rangle$ with total mass $2m$, where m is the single-kink mass. The ellipses stand for heavier

states with total mass $M > 2m$ which contributes as subleading corrections in the large R expansion. The product of states for the half-plane coincides with the one of the strip, hence

$$\begin{aligned} \mathcal{M}_{ab,cd}(\theta_1, \theta_2 | \theta_3, \theta_4) &= {}_b\langle 0 | K_{bd}(\theta_3) K_{da}(\theta_4) | K_{ac}(\theta_1) K_{cb}(\theta_2) | 0 \rangle_b, \\ &= (2\pi)^2 \left[\delta(\theta_{14}) \delta(\theta_{23}) \delta_{cd} + \delta(\theta_{13}) \delta(\theta_{24}) S_{ab}^{cd}(\theta_{12}) \right], \end{aligned} \quad (4.22)$$

and the information about the geometry is entirely codified by the boundary amplitudes

$$f_{acb}^\mu(\theta_1, \theta_2) = {}_{B_b}\langle 0 | \mu_{ba}(0, 0) | K_{ac}(\theta_1) K_{cb}(\theta_2) \rangle_{B_b}. \quad (4.23)$$

The matrix element (4.23) is discussed in detail in Chapter 5, here we borrow its expression in the low-energy limit,

$$f_{acb}^\mu(\theta_1, \theta_2) \simeq c_{acb} \theta_1 \theta_2 (\theta_1^2 - \theta_2^2). \quad (4.24)$$

The computation of the partition function for the large separation regimes is now a straightforward computation. Using (4.22) and (4.24) we can evaluate the large mR behavior of (4.21) by means of a saddle-point approximation which give us

$$\mathcal{Z}_{B_{bab}}(R) \simeq \zeta_{ab} \int_{\mathbb{R}_+^2} \frac{d\theta_1 d\theta_2}{(2\pi)^2} \theta_1^2 \theta_2^2 (\theta_1^2 - \theta_2^2)^2 e^{-mR(\cosh \theta_1 + \cosh \theta_2)} \simeq \frac{3\zeta_{ab}}{2\pi} \frac{e^{-2mR}}{(mR)^5}, \quad (4.25)$$

where

$$\zeta_{ab} = \sum_{c,d \neq a,b} c_{adb} \overline{c_{acb}} [\delta_{cd} - S_{ab}^{cd}(0)] = 2 \sum_{c \neq a,b} |c_{acb}|^2, \quad (4.26)$$

in the last equality we used (3.33). The exponential decay at large distances of (4.25) is related to the interfacial tension of the double interface, $\Sigma_{ab} = 2m$, which is twice the interfacial tension of a single interface. Consistently, this last property is shared by strip and half-plane geometries.

We consider now the statistical average of the spin field with the boundary

condition B_{bab}

$$\langle \sigma(x, y) \rangle_{B_{bab}} = \frac{{}_{B_b} \langle 0 | \mu_{ba}(0, R/2) \sigma(x, y) \mu_{ab}(0, -R/2) | 0 \rangle_{B_b}}{\mathcal{Z}_{B_{bab}}(R)}. \quad (4.27)$$

Following the steps already outlined for the evaluation of the partition function, we insert a resolution of the identity between the operators $\mu_{ba}\sigma$ and $\sigma\mu_{ab}$. Then we truncate the expansion at leading order and we obtain

$$\begin{aligned} \langle \sigma(x, y) \rangle_{B_{bab}} &\simeq \frac{1}{\mathcal{Z}_{B_{bab}}} \sum_{c,d \neq a,b} \int_{\mathbb{R}^4} \frac{d\theta_1 d\theta_2 d\theta_3 d\theta_4}{(2\pi)^4} f_{adb}^\mu(\theta_4, \theta_3) \mathcal{M}_{ab,cd}^\sigma(\theta_1, \theta_2 | \theta_3, \theta_4) \times \\ &\times \overline{f_{acb}^\mu}(\theta_1, \theta_2) \mathcal{Y}^*(\theta_1, \theta_2, \theta_3, \theta_4), \end{aligned} \quad (4.28)$$

the symbol \simeq stands for the omission of the subleading contributions we discussed one moment ago. The matrix element of the spin field coincides with the one used for the strip geometry, (3.40). In the same way, the function \mathcal{Y}^* is the one defined in (3.39). In analogy with the strip geometry, the four-leg matrix element appearing in (4.28) admits a decomposition into connected and disconnected components similar to (3.41). The connected part is the same for both the geometries. As we shall see, the only difference is that for the half-plane we consider only a subclass of disconnected diagrams.

Let us consider the contribution to the magnetization profile originated by the connected component of such an expansion. The non relativistic limit of the matrix element entering (4.28) follows from Chapter 3; for completeness we write its expression

$$\mathcal{M}_{ab,cc}^{\sigma, \text{conn}}(\theta_1, \theta_2, \theta_3, \theta_4) \simeq [2\langle \sigma \rangle_c - \langle \sigma \rangle_a - \langle \sigma \rangle_b] \frac{\theta_{12}\theta_{34}}{\theta_{13}\theta_{14}\theta_{23}\theta_{24}}, \quad (4.29)$$

in which we used the condition $c = d$, otherwise it becomes

$$\mathcal{M}_{ab,cd}^{\sigma, \text{conn}}(\theta_1, \theta_2, \theta_3, \theta_4) \simeq \mathcal{C}_{ab}^\sigma \theta_{12}\theta_{34}, \quad (4.30)$$

with \mathcal{C}_{ab}^σ a model-dependent constant which depends on the scattering dynamics at $\theta \neq 0$. We will consider restrict ourselves to models with a unique intermediate phase, thus fixing $c = d$ the contribution of the magnetization profile originated

by the connected part reads

$$\langle \sigma(x, y) \rangle_{B_{bab}}^{\text{connected}} = \varsigma_{ab} \int_{\mathbb{R}^4} \frac{d\theta_1 d\theta_2 d\theta_3 d\theta_4}{(2\pi)^4 \mathcal{Z}_{B_{bab}}} \mathcal{M}^{\sigma, \text{conn.}} \theta_1 \theta_2 \theta_3 \theta_4 (\theta_1^2 - \theta_2^2) (\theta_3^2 - \theta_4^2) \mathcal{Y}^*, \quad (4.31)$$

with a factor

$$\varsigma_{ab} \equiv \frac{\sum_{c \neq a, b} |c_{acb}|^2 [\langle \sigma \rangle_a + \langle \sigma \rangle_b - 2\langle \sigma \rangle_c]}{\sum_{c \neq a, b} |c_{acb}|^2}. \quad (4.32)$$

The integrals in (4.31) can be carried out using the results of Appendix 4.6; thus we find

$$\langle \sigma(x, y) \rangle_{B_{bab}}^{\text{conn.}} = \varsigma_{ab} [\mathcal{A}(\chi) - 1], \quad (4.33)$$

with a scaling function

$$\mathcal{A}(\chi) = -\frac{4}{3\pi} \chi^2 (\chi^2 - 3) e^{-2\chi^2} + \frac{2}{3\sqrt{\pi}} \chi (-2\chi^4 + \chi^2 - 6) e^{-\chi^2} \text{erf}(\chi) + \text{erf}(\chi)^2. \quad (4.34)$$

Let us consider now the disconnected diagrams entering the decomposition of the matrix element of the spin operator. The disconnected graphs are listed below

$$\begin{aligned} \mathcal{D}_{23,14}^{(R)} &= \begin{array}{c} \theta_4 \quad \theta_3 \\ | \quad | \\ \sigma \\ | \quad | \\ \theta_1 \quad \theta_2 \end{array} \quad , \quad \mathcal{D}_{14,23}^{(R)} = \sum_{e \neq a, b} \begin{array}{c} \theta_4 \quad \theta_3 \\ \quad \quad \quad d \\ \quad \quad \quad | \\ \sigma \\ \quad \quad \quad | \\ \theta_1 \quad \theta_2 \end{array} \quad , \\ \mathcal{D}_{24,13}^{(R)} &= \begin{array}{c} \theta_4 \quad \theta_3 \\ \quad \quad \quad d \\ \quad \quad \quad | \\ \sigma \\ \quad \quad \quad | \\ \theta_1 \quad \theta_2 \end{array} \quad , \quad \mathcal{D}_{13,24}^{(R)} = \begin{array}{c} \theta_4 \quad \theta_3 \\ \quad \quad \quad d \\ \quad \quad \quad | \\ \sigma \\ \quad \quad \quad | \\ \theta_1 \quad \theta_2 \end{array} \quad . \end{aligned}$$

These diagrams are constructed passing aside right of the spin operator. The analytic expression of the disconnected graphs in the low-rapidity regime coin-

cides with (3.47), as done for the strip. Therefore the generic contribution of a disconnected diagram with two legs has the form

$$\frac{|c_{acb}|^2}{\mathcal{Z}_{\mathcal{B}_{bab}}} \int_{\mathbb{R}^4} \frac{d\theta_1 d\theta_2 d\theta_3 d\theta_4}{(2\pi)^4} \theta_1 \theta_2 \theta_3 \theta_4 (\theta_1^2 - \theta_2^2) (\theta_3^2 - \theta_4^2) \frac{2\pi i \delta(\theta_{ij})}{\theta_{kl}} \mathcal{Y}^*(\theta_1, \theta_2, \theta_3, \theta_4). \quad (4.35)$$

It has been shown in Chapter 2 that for the strip geometry we need to take into account also the diagrams formed passing aside left of the spin operator. In that case the (total) disconnected contribution can be obtained taking the arithmetic average of left and right ones, Eq. (3.49). On the other hand, for the case of our interest we are allowed to construct only half of the diagrams, thus we simply divide by a factor 2 the sum of the pass-right graphs. The explicit computation of (4.35) is carried out in Appendix 4.6. Collecting the connected and disconnected contributions as discussed we arrive at

$$\langle \sigma(x, y) \rangle_{\mathcal{B}_{bab}} = [\langle \sigma \rangle_a + \langle \sigma \rangle_b - 2\langle \sigma \rangle_c] \mathcal{A}(\chi) + 2[\langle \sigma \rangle_c - \langle \sigma \rangle_a] \mathcal{B}(\chi) + \langle \sigma \rangle_a, \quad (4.36)$$

with

$$\mathcal{B}(\chi) = \frac{1}{3\sqrt{\pi}} \chi (-6 + \chi^2 - 2\chi^4) e^{-\chi^2} + \operatorname{erf}(\chi). \quad (4.37)$$

It is simple to check that (4.36) interpolates between the boundary and bulk values $\langle \sigma \rangle_a$ and $\langle \sigma \rangle_b$, respectively for $x = 0$ and $x \rightarrow \infty$. The scaling functions entering (4.36) will be derived in the next chapter with a different technique that avoids the computation of the connected part. We postpone to Chapter 5 the discussion of specific models and the derivation of the passage probability in the presence of intermediate phases.

To conclude, we recall that \mathcal{A} and \mathcal{B} are universal scaling functions in the sense that they enter in the magnetization profile for a generic model that admits an intermediate phase in presence of a repulsive boundary¹. The specific choice of the aforementioned scaling functions follows from the connected and disconnected diagrams. Nonetheless, there is no reason to prefer them in favor of a different pair of scaling functions obtained as two linearly independent combinations of \mathcal{A}

¹With boundary repulsion we refer to the fermionic behavior $R(0) = -1$.

and \mathcal{B} . We notice that with the choice of scaling functions

$$\tilde{\mathcal{G}}(\chi) \equiv 4\mathcal{A}(\chi) - 4\mathcal{B}(\chi) + 1, \quad (4.38)$$

$$\tilde{\mathcal{L}}(\chi) \equiv 2\mathcal{B}(\chi) - 1, \quad (4.39)$$

the magnetization profiles (4.36) becomes

$$\langle \sigma(x, y) \rangle_{B_{bab}} = \frac{\langle \sigma \rangle_a + \langle \sigma \rangle_b - 2\langle \sigma \rangle_c}{4} \tilde{\mathcal{G}}(\chi) + \frac{\langle \sigma \rangle_b - \langle \sigma \rangle_a}{2} \tilde{\mathcal{L}}(\chi) + \frac{\langle \sigma \rangle_a + \langle \sigma \rangle_b + 2\langle \sigma \rangle_c}{4}. \quad (4.40)$$

At the formal level, the structure of (4.40) coincides with the scaling profile obtained in the strip geometry, the difference is the explicit form of the scaling functions. The magnetization profile (4.40) enlighten the meaning of the scaling function $\tilde{\mathcal{G}}(\chi)$. In fact, $\mathcal{G}(\chi)$ and $\tilde{\mathcal{G}}(\chi)$ are proportional to the bubble-like magnetization profiles of the dilute q -Potts model, respectively for the strip (Fig.3.11) and half-plane (Fig.5.7).

4.5 Summary

In this chapter we studied the scaling limit of a generic ferromagnetic system with a continuous phase transition, below criticality and on the half plane, with boundary conditions favoring one of the phases along an interval of length R , and a different phase outside this interval. We used field theory to determine exact large R asymptotics of the magnetization profile perpendicular to the boundary at the middle of the interval. We showed that, generically, the large R asymptotic behavior corresponds to the presence of an interface pinned at the boundary condition changing points, with an average midpoint distance from the boundary which grows as \sqrt{R} . The passage probability density of the interface has the Gaussian form found in Section 3.2 for the strip, modified by a quadratic factor which accounts for the presence of the boundary. These results are modified if the scattering on the boundary admits a stable bound state, which then becomes leading at low energies and corresponds to the binding of the interface to the boundary. In this case we showed how field theory accounts at a fundamental level for the contact angle and spreading coefficient of the phenomenological wetting

theory. In particular, the contact angle coincides with the parameter $u \in (0, \pi)$ determining the binding energy as $m(1 - \cos u)$, with m the kink mass. For fixed boundary parameters, u is a function of the temperature and the unbinding condition $u = 0$ determines the wetting temperature T_w .

These results follow from general low-energy properties of two-dimensional field theory. In particular, the annihilation singularity of the spin field matrix element on one-kink states and the boundary-kink bound state pole play a key role in determining the asymptotics of the magnetization profile in the unbound and bound regimes, respectively.

Additional interfacial properties, such as the internal structure arising from subleading terms of the large R expansion or double interfaces appearing in some models for particular choices of boundary conditions, can be analyzed in the same way as was done in the previous chapter.

4.6 Appendix A: computation of integrals

In this section we will compute the following integrals

$$\begin{aligned}
 F(x, y) &= \frac{1}{\zeta(R)} \int_{\mathbb{R}^4} \frac{d\theta_1 d\theta_2 d\theta_3 d\theta_4}{(2\pi)^4} \frac{\theta_{12}\theta_{34}}{\theta_{13}\theta_{14}\theta_{23}\theta_{24}} \theta_1 \theta_2 \theta_3 \theta_4 (\theta_1^2 - \theta_2^2) (\theta_3^2 - \theta_4^2) \times \\
 &\times \widetilde{\mathcal{Y}}^*(\theta_1, \theta_2, \theta_3, \theta_4) \\
 &= \mathcal{A}(\chi) - 1,
 \end{aligned} \tag{4.41}$$

$$\begin{aligned}
 G(x, y) &= \frac{i}{\zeta(R)} \int_{\mathbb{R}^3} \frac{d\theta_1 d\theta_2 d\theta_3}{(2\pi)^3} \frac{\theta_1^2 \theta_2 \theta_3 (\theta_1^2 - \theta_2^2) (\theta_1^2 - \theta_3^2)}{\theta_{23}} \widetilde{\mathcal{Y}}^*(\theta_1, \theta_2, \theta_3, \theta_1) \\
 &= \mathcal{B}(\chi) + \text{const},
 \end{aligned} \tag{4.42}$$

where $\zeta(R) = \frac{3}{\pi} \frac{e^{-2mR}}{(mR)^5}$, while the function $\widetilde{\mathcal{Y}}^*$ corresponds to \mathcal{Y}^* expanded at small θ_j ,

$$\begin{aligned} \mathcal{Y}^* &= \exp \left\{ -\frac{mR}{2} \left[\cosh \theta_1 + \cosh \theta_2 + \cosh \theta_3 + \cosh \theta_4 \right] + \right. & (4.43) \\ &+ imx \left[\sinh \theta_3 + \sinh \theta_4 - \sinh \theta_1 - \sinh \theta_2 \right] + \\ &+ my \left[\cosh \theta_3 + \cosh \theta_4 - \cosh \theta_1 - \cosh \theta_2 \right] \left. \right\} \\ &\simeq e^{-2mR} e^{\left[-\frac{mR}{4} (\theta_1^2 + \theta_2^2 + \theta_3^2 + \theta_4^2) + \frac{my}{2} (\theta_1^2 + \theta_2^2 - \theta_3^2 - \theta_4^2) + imx(\theta_{13} + \theta_{24}) \right]} = \widetilde{\mathcal{Y}}^*. \end{aligned}$$

We will need to use the following preliminaries; the Dawson function [66]

$$\mathcal{D}(x) = e^{-x^2} \int_0^x ds e^{s^2}, \quad (4.44)$$

and

$$\omega_n(\lambda; a) = \int_0^{+\infty} dx \frac{x^{2n}}{x^2 - a^2} e^{-\lambda x^2}, \quad (4.45)$$

this latter function can be computed for arbitrary integer n thanks to $\omega_n(\lambda; a) = (-\partial_\lambda)^n \omega_0(\lambda; a)$, where

$$\omega_0(\lambda; a) = -2\sqrt{\pi} \frac{\mathcal{D}(\sqrt{\lambda}a)}{a}, \quad (4.46)$$

this result can be established after the usual regularization of the poles present in (4.45), we refer to Appendix 3.7 for the details. Let us consider the computation of the function $F(x, y)$. We perform two changes of variables, the first one $x_\pm = \theta_1 \pm \theta_3$, $y_\pm = \theta_2 \pm \theta_4$ and then $u_\mp = x_+ \mp y_+$, $v_\mp = x_- \mp y_-$, in these new variables

$$\begin{aligned} \frac{\theta_{12}\theta_{34}}{\theta_{13}\theta_{14}\theta_{23}\theta_{24}} \theta_1 \theta_2 \theta_3 \theta_4 (\theta_1^2 - \theta_2^2) (\theta_3^2 - \theta_4^2) &= \frac{1}{1024} \frac{(u_-^2 - v_-^2)^2 (u_+^2 - v_+^2)}{(v_+^2 - u_-^2) (v_-^2 - u_+^2)} \times \\ &\times \Phi(u_+, v_+, u_-, v_-), \end{aligned} \quad (4.47)$$

with

$$\Phi(\alpha, \beta, x, y) = (\alpha^2 - \beta^2 + x^2 - y^2)^2 - 4(\alpha x - \beta y)^2, \quad (4.48)$$

and

$$\widetilde{\mathcal{Y}}^* = e^{-2mR} e^{-\frac{mR}{16} [u_+^2 + u_-^2 + v_+^2 + v_-^2]} - imxv_+ e^{-\frac{my}{4} [u_+v_+ + u_-v_-]}, \quad (4.49)$$

while the Jacobian matrix for the composition of the mappings is

$$\left| \det \frac{\partial (\theta_1, \theta_2, \theta_3, \theta_4)}{\partial (u_-, u_+, v_-, v_+)} \right| = \frac{1}{16}, \quad (4.50)$$

thus $d\theta_1 d\theta_2 d\theta_3 d\theta_4 = 16^{-1} du_+ du_- dv_+ dv_-$. After these manipulation we can write the function F in the form

$$F(x, y) = \frac{4}{3\pi^3} \int_{\mathbb{R}^2} d\alpha d\beta f(\alpha, \beta, \epsilon) e^{-\alpha^2 - \beta^2 - 2\epsilon\alpha\beta - ih\beta}, \quad (4.51)$$

with

$$f(\alpha, \beta, \epsilon) = (\alpha^2 - \beta^2) \int_{\mathbb{R}^2} dx dy \frac{(x^2 - y^2)^2}{(x^2 - \beta^2)(y^2 - \beta^2)} \Phi(\alpha, \beta, x, y) e^{-x^2 - y^2 - 2\epsilon xy}. \quad (4.52)$$

The function f can be written in the form

$$f(\alpha, \beta, \epsilon) = (\alpha^2 - \beta^2) \int_{\mathbb{R}^2} dx dy \frac{L(\alpha, \beta, x, y)}{y^2 - \beta^2} e^{-x^2 - y^2 - 2\epsilon xy}, \quad (4.53)$$

with

$$L(\alpha, \beta, x, y) = (x^2 - \beta^2) [\Phi(\alpha, \beta, x, y) + \Phi(\beta, \alpha, x, y)] - 2(y^2 - \beta^2) \Phi(\alpha, \beta, x, y). \quad (4.54)$$

We proceed with the integrations starting from the variable x , the computation is carried out through the auxiliary function

$$\Lambda(\alpha, \beta, \epsilon, y) = \frac{e^{-\epsilon^2 y^2}}{\sqrt{\pi}} \int_{\mathbb{R}} dx L(\alpha, \beta, x, y) e^{-x^2 - 2\epsilon xy}, \quad (4.55)$$

the exponential factor in y is introduced to make $\Lambda(\alpha, \beta, \epsilon, y)$ a polynomial in y , hence we can write

$$\Lambda(\alpha, \beta, \epsilon, y) = \sum_{n=0}^3 \lambda_{2n}(\alpha, \beta, \epsilon) y^{2n}, \quad (4.56)$$

the coefficients $\lambda_{2n}(\alpha, \beta, \epsilon)$ are quite long expressions, so we will not write them. Then we integrate over y using the functions ω_n and we find

$$f(\alpha, \beta, \epsilon) = \sqrt{\pi} (\alpha^2 - \beta^2) \sum_{n=0}^3 \lambda_{2n}(\alpha, \beta, \epsilon) \omega_n(\kappa^2, \beta), \quad (4.57)$$

with $\kappa = \sqrt{1 - \epsilon^2}$. Now we turn back to the function F , the integration over α is immediate since α enters only through the polynomials $\lambda(\alpha, \beta, \epsilon)$ and an exponential factor. The result of this integration is congenitally expressed through the polynomials

$$K_{2n}(\beta\kappa) = \frac{e^{-\epsilon^2\beta^2}}{\sqrt{\pi}} \int_{\mathbb{R}} d\alpha (\alpha^2 - \beta^2) \lambda_{2n}(\alpha, \beta, \epsilon) e^{-\alpha^2 - 2\epsilon\alpha\beta}, \quad (4.58)$$

and finally we are left with the integration over β

$$F(x, y) = \frac{4}{3\pi^2} \sum_{n=0}^3 \int_{\mathbb{R}} d\beta \left[K_{2n}(\beta\kappa) \omega_n(\kappa^2, \beta) \right] e^{-\kappa^2\beta^2 - ih\beta}, \quad (4.59)$$

the summation in the integrand can be considerably simplified, after some manipulations it reads

$$\begin{aligned} & \frac{1}{\sqrt{\pi\kappa}} \sum_{n=0}^3 K_n(\beta, \epsilon) \omega_n(\kappa^2, \beta) = \\ & = \left(-\frac{9}{2} + 13t^2 - 8t^4 + (-3 + 24t^2 - 36t^4 + 16t^6) \frac{\mathcal{D}(\kappa\beta)}{\kappa\beta} \right) \Big|_{t=\kappa\beta}. \end{aligned} \quad (4.60)$$

Then we use the identity

$$\int_{\mathbb{R}} dt t^{n-1} e^{-t^2 - i\chi t} \mathcal{D}(t) = \frac{\pi^{3/2}}{4} (i\partial_\chi)^n \left[1 - \operatorname{erf}^2(\chi/\sqrt{8}) \right], \quad (4.61)$$

and the Gaussian integral

$$\int_{\mathbb{R}} dt t^n e^{-t^2 - i\chi t} = \sqrt{\pi} (i\partial_\chi)^n e^{-\frac{\chi^2}{4}}, \quad (4.62)$$

to express $F(x, y)$ as a combination of derivatives acting on e^{-x^2} and $\operatorname{erf}^2(\chi)$ as follows

$$F(x, y) = -\frac{1}{6\pi} (36 + 13\partial_\chi^2 + \partial_\chi^4) e^{-2\chi^2} + \left[1 + \partial_\chi^2 + \frac{3}{16}\partial_\chi^4 + \frac{1}{96}\partial_\chi^6 \right] (\operatorname{erf}^2(\chi) - 1), \quad (4.63)$$

the explicit computation of this unwieldy expression gives finally

$$1 + F(x, y) = \frac{4}{3\pi} \chi^2 (3 - \chi^2) e^{-2\chi^2} + \frac{2}{3\sqrt{\pi}} \chi (-2\chi^4 + \chi^2 - 6) e^{-\chi^2} \operatorname{erf}(\chi) + \operatorname{erf}^2(\chi), \quad (4.64)$$

the RHS of the above expression is the function $\mathcal{A}(\chi)$. The computation of the function $G(x, y)$ retraces the same arguments already used of the function $F(x, y)$; after a rescaling of the integration variables we have

$$G(x, y) = \frac{4i}{3\pi^2} \int_{\mathbb{R}^3} d\theta_1 d\theta_2 d\theta_3 \frac{\theta_1^2 \theta_2 \theta_3 (\theta_1^2 - \theta_2^2) (\theta_1^2 - \theta_3^2)}{\theta_{23}} e^{-\theta_1^2 - \frac{1-\epsilon}{2}\theta_2^2 - \frac{1+\epsilon}{2}\theta_3^2 - i\eta\theta_{23}}, \quad (4.65)$$

we regularize the singularity according to the usual prescription and then we get rid of the pole by taking the first derivative with respect to η . The term originated by the Dirac delta $\delta(\theta_{23})$ does not depend on η and we are left with

$$\partial_\eta G(x, y) = \frac{4}{3\pi^2} \int_{\mathbb{R}^3} d\theta_1 d\theta_2 d\theta_3 \theta_1^2 \theta_2 \theta_3 (\theta_1^2 - \theta_2^2) (\theta_1^2 - \theta_3^2) e^{-\theta_1^2 - \frac{1-\epsilon}{2}\theta_2^2 - \frac{1+\epsilon}{2}\theta_3^2 - i\eta\theta_{23}}, \quad (4.66)$$

the resulting gaussian integrations are quite tedious but nonetheless simple, we find

$$\partial_\eta G(x, y) = \frac{\chi^2 (15 - 12\chi^2 + 4\chi^4)}{3\sqrt{\pi}\kappa} e^{-\chi^2}, \quad (4.67)$$

integrating back we find the function $G(x, y)$

$$G(x, y) = \frac{1}{3\sqrt{\pi}} (-6 + \chi^2 - 2\chi^4) e^{-\chi^2} + \operatorname{erf}(\chi) + \operatorname{const.}, \quad (4.68)$$

which coincides, up to an additive constant, with the function $\mathcal{B}(\chi)$.

Chapter 5

Phase separation and filling transition in a wedge

Interfacial phenomena strongly depend on the geometry in which they occur. In this chapter we illustrate how the planar substrate studied in the last chapter can be continuously deformed into a wedge-shaped one. We will show the corresponding field-theoretical meaning of this operation both for adjacent phases and for the case in which a third phase appears.

5.1 Introduction

Interfacial phenomena at boundaries are a subject of both experimental and theoretical relevance which has received continuous and extensive interest in the last decades [15, 12, 14, 16]. An aspect particularly important for applications is that the structure and geometry of the substrate can alter the adsorption characteristics of a fluid in an important way (see [76] for a review). Adsorption measurements can then be used, for example, to characterize fractally rough surfaces [77], or the connectivity of porous substrates [78]. The basic case of a wedge-shaped substrate [79] acquired special interest since phenomenological and thermodynamic arguments [80] indicated a specific relation with the adsorption properties of a completely flat surface: the wedge wetting (or filling) transition occurs at the temperature for which the contact angle of a fluid drop on a flat

substrate equals the tilt angle ψ of the wedge, a circumstance that allows us to regulate the transition temperature adjusting ψ . The connections between adsorption characteristics for different opening angles are known as properties of *wedge covariance* [81, 82, 83] and are experimentally testable [84].

It is clearly important to pass from a macroscopic to a fundamental statistical mechanical description. In two dimensions the essential role of fluctuations was established by the exact lattice results for the Ising model on the half plane [85, 86, 87, 71, 40, 88], which provided essential support for heuristic statistical descriptions of the wetting of a flat boundary [41]. For the wedge geometry the existence of the filling transition was established for the Ising model on a planar lattice forming a right-angle corner [89, 90] (see also [91] for a 60° opening angle on the triangular lattice), but otherwise the theoretical investigations in two and three dimensions have been based on effective interfacial Hamiltonian models [81, 82, 83, 92, 93, 94] or density functional methods [95].

In this chapter, we derive general exact results for phase separation in a two-dimensional wedge. This is achieved by exploiting low energy properties of bulk two-dimensional field theory (see Chapter 3) together with a characterization of the operators responsible for the departure of an interface from a point on a boundary. For a shallow wedge we determine the exact passage probability of interfaces with endpoints on the boundary. The theory provides a fundamental meaning to the contact angle and, for generic ψ , yields the filling transition condition. More generally, wedge covariance is shown to originate from the properties of the boundary condition changing operators in momentum space.

5.2 Two phases in a wedge

We start with the characterization of the statistical system in absence of boundaries, i.e. on the infinite plane. The system is considered at a first order phase transition point, where different phases, that we label by an index $a = 1, 2, \dots, n$, have the same free energy and can coexist at equilibrium. At the same time the system is supposed to be close to a second order transition point¹, in such

¹As an example, for the Ising ferromagnet these specifications amount to consider a temperature slightly below the critical value T_c , in absence of external field.

a way that the correlation length is much larger than microscopic scales and a continuous description is allowed. For homogeneous and isotropic systems this continuous description is provided by a Euclidean field theory with coordinates (x, y) identifying a point on the plane. This field theory in turn corresponds to the continuation to imaginary time $t = iy$ of a quantum field theory in one space dimension with coordinate x . The degenerate phases of the statistical system are in one-to-one correspondence with degenerate vacua $|0_a\rangle$ of the associated quantum theory. We denote by $\sigma(x, y)$ the order parameter field, and by $\langle\sigma\rangle_a = \langle 0_a | \sigma(x, y) | 0_a \rangle$ the value of the order parameter in phase a . For a generic field Φ we have

$$\Phi(x, y) = e^{yH - ixP} \Phi(0, 0) e^{-yH + ixP}, \quad (5.1)$$

with the Hamiltonian H and momentum operator P of the quantum system acting as generators of time and space translations, respectively; the vacuum states carry zero energy and momentum.

As usual in presence of degenerate vacua in (1+1) dimensions (see [96]), the elementary excitations correspond to kinks $|K_{ab}(\theta)\rangle$ which interpolate between two different vacua $|0_a\rangle$ and $|0_b\rangle$, and whose energy and momentum satisfy the relativistic dispersion relation

$$(e, p) = (m_{ab} \cosh \theta, m_{ab} \sinh \theta), \quad (5.2)$$

where m_{ab} is the kink mass (inversely proportional to the bulk correlation length) and θ is known as rapidity. Two vacua $|0_a\rangle$ and $|0_b\rangle$ (as well as the corresponding phases) are said to be adjacent if they can be connected by an elementary kink; when the connection requires a state $|K_{ac_1}(\theta_1) K_{c_1 c_2}(\theta_2) \dots K_{c_{n-1} b}(\theta_n)\rangle$, with n necessarily larger than one, the two vacua are said to be non-adjacent.

As a further step towards the study of the wedge problem, we consider this statistical system on the half plane $x \geq 0$. We call boundary condition of type a a uniform (i.e. y -independent) boundary condition at $x = 0$ favoring phase a in the bulk¹, in such a way that the order parameter approaches $\langle\sigma\rangle_a$ as $x \rightarrow +\infty$. We will use the notation $|0_a\rangle_0$ for the vacuum state of the quantum system on the half line with this boundary condition; more generally, the subscript 0 will

¹In a ferromagnet this is achieved applying a magnetic field on the boundary.

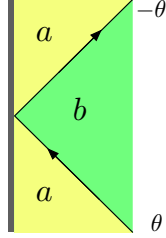


Figure 5.1: A uniform boundary reflects a low energy kink.

be used to indicate the presence of the vertical boundary.

Phase separation can be induced through a change of boundary conditions. Within the field theoretical description, the change of boundary conditions from type a to type b at a point y on the boundary is realized by the insertion of a field $\mu_{ab}(0, y)$, with non-zero matrix elements on states interpolating between $|0_a\rangle_0$ and $|0_b\rangle_0$. When these two vacua are adjacent, which is the case we consider in this section, the simplest matrix element of μ_{ab} is¹

$${}_0\langle 0_a | \mu_{ab}(0, y) | K_{ba}(\theta) \rangle_0 = e^{-my \cosh \theta} f_0(\theta), \quad (5.3)$$

where $f_0(\theta)$ gives the amplitude for the emission/absorption of a kink from the boundary condition changing point. The kink travels towards the boundary for $\theta < 0$ (in-state), and away from it for $\theta > 0$ (out-state). In- and out-states are related by the scattering operator [36]. As we are going to see, our computations involve low energy particles, whose scattering with the boundary is necessarily elastic, i.e. conserves the number of particles. Moreover, the field μ_{ab} acts on a uniform vertical boundary, which preserves the energy. For these reasons the low energy scattering of a particle on the boundary is a pure reflection (Fig. 5.1), and the relation between the in- and out-state for (5.3) takes for small momenta the simple form $f_0(\theta) = \pm f_0(-\theta)$. On the other hand, only the choice

$$f_0(\theta) = -f_0(-\theta), \quad \theta \rightarrow 0 \quad (5.4)$$

implies the property $f_0(0) = 0$ which will eventually be responsible for the im-

¹Here and below, in order to simplify the notation, we drop the indices on the kink mass.

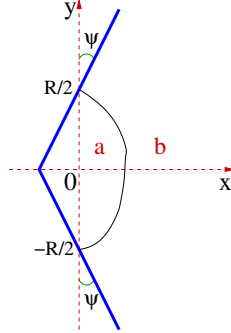


Figure 5.2: Wedge geometry with boundary condition changing points at $(0, \pm R/2)$ and an interface running between them.

penetrability of the wall. Generically, we will then have $f_0(\theta) = c_1 \theta + O(\theta^2)$, with c_1 a constant.

Passing from a vertical boundary to one forming an angle ψ with the vertical involves a rotation in Euclidean space, and then a relativistic transformation for the associated quantum field theory. Recalling (5.2), this transformation shifts rapidities by $i\psi$, so that the kink emission amplitude in the rotated frame, that we denote by f_ψ , is related to that in the original frame as

$$f_\psi(\theta) = f_0(\theta + i\psi); \quad (5.5)$$

our considerations on f_0 then yield

$$f_\psi(\theta) \simeq c_1(\theta + i\psi), \quad |\theta|, |\psi| \ll 1. \quad (5.6)$$

At this point we are able to consider, instead of the half plane, the more general wedge geometry of Fig. 5.2. The points $(0, \pm R/2)$ are boundary condition changing points, such that phase b (resp. a) is favored for $|y| > R/2$ (resp. $|y| < R/2$) on the wedge. For mR large, i.e. when the system is observed on a scale much larger than the bulk fluctuations, one then expects an interface running between the points $(0, \pm R/2)$, separating an inner phase a from an outer phase b . These expectations emerge from the theory in the following way. For $|y| < R/2$ the order parameter in the wedge, that we denote by $\langle \sigma(x, y) \rangle_{W_{bab}}$,

reads

$$\langle \sigma(x, y) \rangle_{W_{bab}} = \frac{\psi \langle 0_b | \mu_{ba}(0, \frac{R}{2}) \sigma(x, y) \mu_{ab}(0, -\frac{R}{2}) | 0_b \rangle_{-\psi}}{Z_{W_{bab}}}, \quad (5.7)$$

where the subscripts $\pm\psi$ indicate the different rotations performed for positive and negative y , and

$$\begin{aligned} Z_{W_{bab}} &= \psi \langle 0_b | \mu_{ba}(0, R/2) \mu_{ab}(0, -R/2) | 0_b \rangle_{-\psi} \\ &\sim \int_0^\infty \frac{d\theta}{2\pi} f_\psi(\theta) f_{-\psi}(\theta) e^{-mR(1+\frac{\theta^2}{2})} \sim \frac{c_1^2 e^{-mR}}{2\sqrt{2\pi}(mR)^{3/2}} (1 + mR\psi^2) \end{aligned} \quad (5.8)$$

This result is obtained inserting a complete set of particle states in between the two fields, taking the limit mR large which projects on the lightest (single-kink) intermediate state and to small rapidities, and considering ψ small in order to use (5.6); here and in the following the symbol \sim indicates omission of terms subleading for mR large. In a similar way we obtain

$$\begin{aligned} \langle \sigma(x, y) \rangle_{W_{bab}} &\sim \frac{e^{-mR}}{Z_{W_{bab}}} \int_{-\infty}^{+\infty} \frac{d\theta_1 d\theta_2}{(2\pi)^2} e^{-\frac{m}{2}[(\frac{R}{2}-y)\theta_1^2 + (\frac{R}{2}+y)\theta_2^2] - imx(\theta_1 - \theta_2)} \\ &\times f_\psi(\theta_1) \langle K_{ba}(\theta_1) | \sigma(0, 0) | K_{ab}(\theta_2) \rangle f_{-\psi}(\theta_2), \end{aligned} \quad (5.9)$$

where we evaluate the order parameter field on bulk states, implying that the boundary condition changing fields account for the leading boundary effects at large R . The matrix element in (5.9) contains a disconnected part proportional to $\delta(\theta_1 - \theta_2)$ which yields a constant after integration, and then does not contribute to the derivative with respect to x we are going to take in a moment; the behavior of the connected part in the relevant region $\theta_1, \theta_2 \rightarrow 0$, is instead determined by the ‘kinematical’ pole (see [96] and references therein)

$$\langle K_{ba}(\theta_1) | \sigma(0, 0) | K_{ab}(\theta_2) \rangle_{\text{connected}} \simeq i \frac{\langle \sigma \rangle_b - \langle \sigma \rangle_a}{\theta_1 - \theta_2}, \quad \theta_1 \simeq \theta_2. \quad (5.10)$$

With this information we obtain

$$\frac{\partial_x \langle \sigma(x, y) \rangle_{W_{bab}}}{\langle \sigma \rangle_b - \langle \sigma \rangle_a} \sim 8\sqrt{2} \left(\frac{m}{R}\right)^{\frac{3}{2}} \frac{(x + \frac{R\psi}{2})^2 - (\psi y)^2}{\sqrt{\pi} \kappa^3 (1 + mR\psi^2)} e^{-\chi^2}, \quad (5.11)$$

where

$$\kappa = \sqrt{1 - \epsilon^2}, \quad \epsilon = \frac{2y}{R}, \quad \chi = \sqrt{\frac{2m}{R}} \frac{x}{\kappa}, \quad (5.12)$$

and, integrating back over x with the condition $\langle \sigma(+\infty, y) \rangle_{W_{bab}} = \langle \sigma \rangle_b$,

$$\langle \sigma(x, y) \rangle_{W_{bab}} \sim \langle \sigma \rangle_a + [\langle \sigma \rangle_b - \langle \sigma \rangle_a] \left[\operatorname{erf}(\chi) - \frac{2}{\sqrt{\pi}} \frac{\chi + \sqrt{2mR} \frac{\psi}{\kappa}}{1 + mR\psi^2} e^{-\chi^2} \right]; \quad (5.13)$$

for $\psi = y = 0$ and $\langle \sigma \rangle_a = -\langle \sigma \rangle_b$ this result coincides with that obtained in [71] from the lattice solution of the Ising model on the half plane.

It was shown in Chapter 3 that the leading large R contribution to the order parameter profile, i.e. the one associated to the pole in (5.10), corresponds to a sharp phase separation between pure phases. In the present case of adjacent phases, there will be a single interface, with a probability $P_1^{(\psi)}(x; y)$ to intersect the line of constant ordinate y in the interval $(x, x + dx)$. It follows that the leading large R expression of the order parameter can be written as

$$\langle \sigma(x, y) \rangle_{W_{bab}} \sim \langle \sigma \rangle_b \int_{\tilde{x}}^x du P_1^{(\psi)}(u; y) + \langle \sigma \rangle_a \int_x^\infty du P_1^{(\psi)}(u; y), \quad (5.14)$$

where $\tilde{x}(y)$ is the abscissa of the point on the wedge with ordinate y ; this expression shows that $P_1^{(\psi)}(x; y)$ actually coincides with (5.11). Also for later use we introduce the additional notations

$$\lambda = \sqrt{\frac{R}{2m}}, \quad \eta = \frac{x}{\lambda}, \quad \hat{\psi} = \sqrt{\frac{mR}{2}} \psi, \quad (5.15)$$

and rewrite this result as

$$P_1^{(\psi)}(x; y) \sim \frac{4}{\sqrt{\pi} \kappa^3 \lambda (1 + 2\hat{\psi}^2)} [(\eta + \hat{\psi})^2 - (\epsilon \hat{\psi})^2] e^{-\chi^2}. \quad (5.16)$$

The requirement $\int_{\tilde{x}}^\infty dx P_1^{(\psi)}(x; y) \approx 1$ is satisfied as long as $\sqrt{mR} \psi \ll 1$. Notice that (5.11) or (5.16) show that $P_1^{(\psi)}(x; y)$ vanishes for $|y| = \frac{x}{\psi} + \frac{R}{2}$, which for the present case of small ψ are the coordinates of the wedge ($x \geq -R\psi/2$); hence, the properties (5.5), (5.6) that we identified in momentum space indeed lead to an impenetrable wedge in coordinate space. A plot of $P_1^{(\psi)}(x; y)$ is shown in Fig. 5.3.

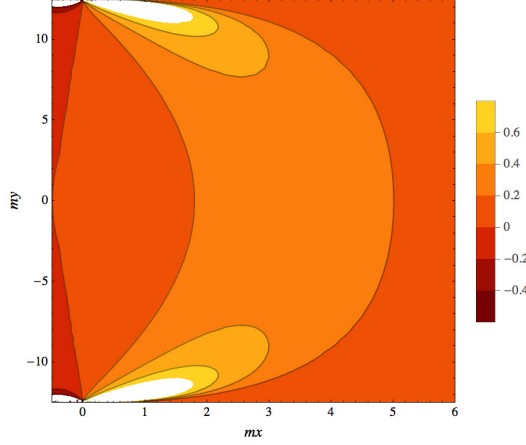


Figure 5.3: Contour plot of the passage probability density $P_1^{(\psi)}(x; y)/m$ for $mR = 25$, $\psi = 0.04$. The leftmost contour line corresponds to $P_1^{(\psi)}(x; y) = 0$, and then to the wedge.

5.3 Filling transition

The results, Eqs. (5.11) and (5.13), apply to values of temperature (i.e., of bulk correlation length $m^{-1} \propto (T_c - T)^{-\nu}$) for which the kink state is the lightest one entering the spectral decomposition of Eq. (5.7). To discuss the situation in which this is not the case we start again from $\psi = 0$. For temperatures below a certain threshold $T_0 < T_c$ the kink $K_{ba}(\theta)$ may form with the boundary a bound state $|\Omega'_a\rangle_0$ with energy E'_0 , in which the phase b forms a thin layer adsorbed on the boundary. As usual for stable bound states, this corresponds to a purely imaginary rapidity $\theta = i\theta_0$ of the kink, leading to a binding energy

$$E'_0 - E_0 = m \cos \theta_0 \quad (5.17)$$

smaller than m . This boundary bound state is now the lightest state contributing to (5.7) and produces an order parameter equal to $\langle \sigma \rangle_a$ for $mx \gg 1$, no matter how large R is (see Chapter 4). Since m is the interfacial tension between the phases a and b (see Chapter 3), and E_0 (respectively E'_0) corresponds to the tension between the boundary and phase b (respectively a), Eq. (5.17) identifies θ_0 as the contact angle of the phenomenological wetting theory. The usual relation $\theta_0(T_0) = 0$ characterizing the wetting transition temperature T_0 corresponds to

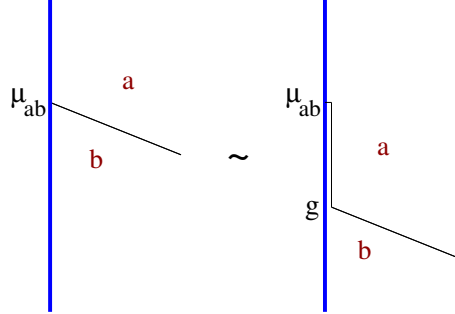


Figure 5.4: Illustration of equation (5.18). The kink emission amplitude exhibits a bound state pole corresponding to adsorption of phase b on the boundary.

the unbinding threshold for the kink.

Bound states manifest in matrix elements as poles in the physical region of kinematical variables [36]. For the matrix element, Eq. (5.3), this physical region corresponds to the strip $\text{Im}\theta \in (0, \pi)$, and the pole induced by the boundary bound state takes the form (see Fig. 5.4)

$$\begin{aligned} \mathcal{F}_0^\mu(\theta) &= {}_0\langle \Omega_a | \mu_{ab}(0, 0) | K_{ba}(\theta) \rangle_0 \\ &\sim \frac{ig}{\theta - i\theta_0} {}_0\langle \Omega_a | \mu_{ab}(0, 0) | \Omega'_a \rangle_0, \quad \theta \sim i\theta_0 \end{aligned} \quad (5.18)$$

with g a coupling measuring the strength of the bound state. It then follows from Eq. (5.5) that the pole of $\mathcal{F}_\psi^\mu(\theta)$ is located at $\theta = i(\theta_0 - \psi)$. Since the kink energy is always $m \cosh \theta$ and the unbinding threshold remains at $\theta = 0$, the filling transition temperature T_ψ is determined by the condition

$$\theta_0(T_\psi) = \psi. \quad (5.19)$$

For $\theta_0 < \psi$ the pole is located at $\text{Im}\theta < 0$, namely outside the physical strip allowed for bound states; in such a case the kink is unbounded and phase b fills the wedge. The condition, Eq.(5.19), is that obtained in the macroscopic framework [80], and follows here from the exact statistical theory. Notice that while Eqs. (5.11) and (5.13) rely on Eq. (5.6), and then on small ψ , Eqs. (5.5) and Eq. (5.19) are general. Equation (5.5), in particular, encodes the essence of wedge covariance.

For the scaling Ising model on the half plane with a boundary magnetic field h , the scattering amplitude off the boundary is known exactly [38], and exhibits a boundary bound state pole corresponding to $1 - \sin \theta_0 = \frac{h^2}{2m} = \frac{T_c - T_0(h)}{T_c - T}$; the last equality follows from $\nu_{\text{Ising}} = 1$ and holds in the scaling limit (see, e.g., [97] for boundary bound states in the lattice formalism).

5.4 Third phase and double interface

In this section we still consider the wedge geometry of Fig. 5.2 with the same boundary conditions bab of the previous section, but now we study the case in which the phases a and b are not adjacent. More precisely, we consider the case in which the lightest state connecting $|0_a\rangle$ and $|0_b\rangle$ is the two-kink state $|K_{ac}(\theta_1)K_{cb}(\theta_2)\rangle$, with a unique choice of the intermediate vacuum $|0_c\rangle$. This situation arises, in particular, in the (dilute) q -state Potts model at first order transition that we discussed in the introduction. Indeed, the model is exactly solvable (integrable) in the scaling limit, and it is known that there are no kinks directly connecting two ferromagnetic vacua at the first order transition [53, 55]. The lightest state connecting two such vacua $|0_a\rangle$ and $|0_b\rangle$ is the two-kink state $|K_{a0}K_{0b}\rangle$ passing by the disordered vacuum $|0_0\rangle$; the symmetry under permutations of the q ferromagnetic phases which characterizes the Potts model [49] ensures that the elementary kinks K_{a0}, K_{0a} ($a = 1, \dots, q$) all have the same mass m .

Technically, the difference with respect to the previous section is that now the large R expansion of (5.7) is dominated by the contribution of the two-kink state. In particular, the relevant matrix element for the boundary condition changing fields is no longer (5.3) but

$${}_0\langle 0_a | \mu_{ab}(0, y) | K_{bc}(\theta_1) K_{ca}(\theta_2) \rangle_0 = e^{-my(\cosh \theta_1 + \cosh \theta_2)} f_0(\theta_1, \theta_2). \quad (5.20)$$

As before, the low energy scattering properties of the kinks on a vertical wall can be used to infer properties of the amplitude $f_0(\theta_1, \theta_2)$, but now we will also exploit the integrability of the scaling (dilute) Potts model at the first order transition. Integrability ensures that the interaction of the two kinks on the wall

can be regarded as consisting of two independent processes (factorization of the scattering [38]), and this in turn allows us to write a relation like (5.4) for each particle, i.e.

$$f_0(\theta_1, \theta_2) = -f_0(-\theta_1, \theta_2) = -f_0(\theta_1, -\theta_2), \quad \theta_1, \theta_2 \rightarrow 0. \quad (5.21)$$

Integrability also yields the exact bulk scattering matrix of the scaling (dilute) Potts model at the first order transition [53, 55]. From this one reads, in particular, that at low energy the state $|K_{b_0}(\theta_1)K_{0a}(\theta_2)\rangle$ scatters in the bulk into the state $-|K_{b_0}(\theta_2)K_{0a}(\theta_1)\rangle$, so that we have the additional relation

$$f_0(\theta_1, \theta_2) = -f_0(\theta_2, \theta_1), \quad \theta_1, \theta_2 \rightarrow 0. \quad (5.22)$$

Equations (5.21) and (5.22) lead to

$$f_0(\theta_1, \theta_2) \simeq c_2 \theta_1 \theta_2 (\theta_1^2 - \theta_2^2), \quad \theta_1, \theta_2 \ll 1. \quad (5.23)$$

As before, the passage from the vertical boundary to that rotated by an angle ψ involves a rapidity shift,

$$f_\psi(\theta_1, \theta_2) = f_0(\theta_1 + i\psi, \theta_2 + i\psi), \quad (5.24)$$

and the leading large mR expression for the order parameter in the wedge can be written as¹

$$\langle \sigma(x, y) \rangle_{W_{bab}} \sim \frac{1}{Z_{W_{bab}}} \int_{\mathbb{R}^4} \frac{d\theta_1 d\theta_2 d\theta_3 d\theta_4}{(2\pi)^4} f_\psi(\theta_4, \theta_3) \langle K_{bc}(\theta_3) K_{ca}(\theta_4) | \sigma(0, 0) | K_{ac}(\theta_1) K_{cb}(\theta_2) \rangle f_{-\psi}(\theta_1, \theta_2) \mathcal{Y}(\theta_1, \theta_2, \theta_3, \theta_4; x, y), \quad (5.25)$$

where

$$\mathcal{Y}(\theta_1, \theta_2, \theta_3, \theta_4; x, y) = U^-(\theta_1; x, y) U^-(\theta_2; x, y) U^+(\theta_3; x, y) U^+(\theta_4; x, y), \quad (5.26)$$

¹Generically, we keep the notation c for the third phase; $c = 0$ for the Potts case.

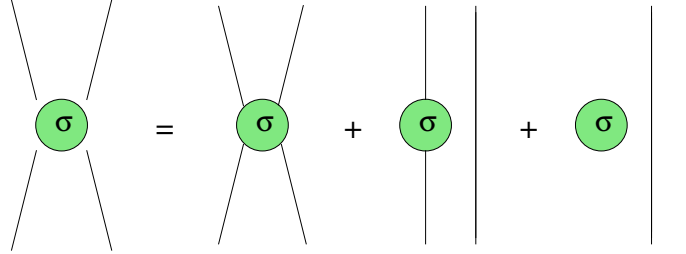


Figure 5.5: The four-leg matrix element of the order parameter field σ decomposes into the sum of the connected and disconnected parts in the r.h.s.

$$U^\pm(\theta; x, y) = e^{m(-\frac{R}{2} \pm y) \cosh \theta \mp imx \sinh \theta}, \quad (5.27)$$

$$\begin{aligned} Z_{W_{bab}} &\sim \int_{\mathbb{R}_+^2} \frac{d\theta_1 d\theta_2}{(2\pi)^2} f_\psi(\theta_2, \theta_1) f_{-\psi}(\theta_1, \theta_2) e^{-\frac{mR}{2}(\cosh \theta_1 + \cosh \theta_2)} \\ &\sim \frac{3c_2^2}{\pi} \frac{e^{-2mR}}{(mR)^5} \left[1 + \left(8 - \frac{32}{3\pi} \right) \hat{\psi}^2 + O(\hat{\psi}^4) \right]. \end{aligned} \quad (5.28)$$

The matrix element of the field σ on two-kink states entering (5.25) contains three types of contributions, depending on the number of annihilations that arise when particles on the left and on the right have the same rapidity. The three contributions are schematically depicted in Fig. 5.5 and correspond to a connected part (no annihilations), a partially disconnected part (one annihilation) and a totally disconnected part (two annihilations). The complete computation of the order parameter taking into account all these contributions has been performed in Chapter 3 for the case of the strip geometry and in Chapter 4 for the case of the half plane ($\psi = 0$). As expected from the fact that the two-kink state yields the leading contribution, the results correspond to the presence of two interfaces separating the intermediate phase c from the phases a and b . For the case of the wedge the complete calculation becomes cumbersome, and it is particularly interesting that we can still obtain the complete results in a relatively simple way through the following procedure, whose exactness we explicitly checked for the strip and the half plane.

Generalizing what seen in the previous section, the probability $P_2^{(\psi)}(x_1, x_2; y)$ that one interface intersects the line of constant ordinate y in the interval $(x_1, x_1 +$

dx), and that the other interface intersects the same line in the interval $(x_2, x_2 + dx)$ is related to the order parameter as

$$\langle \sigma(x, y) \rangle_{W_{bab}} = \int_{\tilde{x}}^{+\infty} dx_1 \int_{\tilde{x}}^{+\infty} dx_2 P_2^{(\psi)}(x_1, x_2; y) \sigma(x|x_1, x_2), \quad (5.29)$$

where

$$\sigma(x|x_1, x_2) = \begin{cases} \langle \sigma \rangle_a, & \tilde{x} < x < \min(x_1, x_2), \\ \langle \sigma \rangle_c, & \min(x_1, x_2) < x < \max(x_1, x_2), \\ \langle \sigma \rangle_b, & x > \max(x_1, x_2), \end{cases}$$

and $\tilde{x}(y)$ is the abscissa of the wedge. On the other hand

$$P_{1,2}^{(\psi)}(x_1; y) = \int_{\tilde{x}}^{\infty} dx_2 P_2^{(\psi)}(x_1, x_2; y) \quad (5.30)$$

is the probability that one of the two interfaces passes in the interval $(x_1, x_1 + dx)$ at ordinate y , irrespectively of the other. Since it is the field σ which ‘detects’ the interfaces, it is natural to expect, and we checked explicitly that this is the case for the strip and the half plane, that $P_{1,2}^{(\psi)}(x; y)$ is determined by the second term in the r.h.s. of Fig. 5.5, proportional to¹

$$\langle K_{ba}(\theta_3) | \sigma(0, 0) | K_{ab}(\theta_1) \rangle_{\text{connected}} \delta(\theta_2 - \theta_4), \quad (5.31)$$

and to which we refer as the two-leg term, from the number of particles connected to the field σ . Up to the factor $\delta(\theta_2 - \theta_4)$, corresponding to the undetected interface, this two-leg term is the same we studied in the previous section for the single interface. Plugging (5.31) into (5.25) we obtain

$$\begin{aligned} \langle \sigma(x, y) \rangle_{W_{bab}}^{\text{two-leg}} &\propto \int_{\mathbb{R}^4} d\theta_1 d\theta_2 d\theta_3 d\theta_4 f_{\psi}(\theta_4, \theta_3) \frac{\delta(\theta_2 - \theta_4)}{\theta_1 - \theta_3} f_{-\psi}(\theta_1, \theta_2) \\ &\times e^{-m \left[\frac{R}{4} \sum_{k=1}^4 \theta_k^2 + \frac{y}{2} (\theta_1^2 + \theta_2^2 - \theta_3^2 - \theta_4^2) - ix(\theta_1 + \theta_2 - \theta_3 - \theta_4) \right]}, \end{aligned} \quad (5.32)$$

where, as usual, we took into account that small rapidities dominate at large R and we used (5.10); as in the previous section, a derivative with respect to x

¹Of course there are analogous terms with different pairings of rapidities, all giving the same contribution to (5.25).

cancels the pole. On the other hand, we can also write $\langle \sigma(x, y) \rangle_{W_{bab}}^{\text{two-leg}}$ in a way analogous to (5.14), with $P_{1,2}^{(\psi)}$ replacing $P_1^{(\psi)}$, and $\langle \sigma \rangle_c$ replacing $\langle \sigma \rangle_a$ or $\langle \sigma \rangle_b$. It follows that $P_{1,2}^{(\psi)}(x; y) \propto \partial_x \langle \sigma(x, y) \rangle_{W_{bab}}^{\text{two-leg}}$, i.e.

$$P_{1,2}^{(\psi)}(x_1; y) \propto \int dx_2 \int_{\mathbb{R}^4} d\theta_1 d\theta_2 d\theta_3 d\theta_4 f_\psi(\theta_4, \theta_3) f_{-\psi}(\theta_1, \theta_2) \times e^{-m \left[\frac{R}{4} \sum_{k=1}^4 \theta_k^2 + \frac{y}{2} (\theta_1^2 + \theta_2^2 - \theta_3^2 - \theta_4^2) + ix_1 (\theta_1 - \theta_3) - ix_2 (\theta_2 - \theta_4) \right]}, \quad (5.33)$$

where we used $\delta(z) \propto \int ds e^{isz}$. Comparison with (5.30) shows that the integrand of the integral in x_2 in (5.33) is proportional to $P_2^{(\psi)}$. Since the identity

$$\int_{\mathbb{R}^2} d\beta_1 d\beta_2 f_\psi(\beta_1, \beta_2) e^{-\frac{\beta_1^2 + \beta_2^2}{2} + iq_1 \beta_1 + iq_2 \beta_2} = 2\pi f_{-i\psi}(q_1, q_2) e^{-\frac{q_1^2 + q_2^2}{2}}, \quad (5.34)$$

holds for the function defined by (5.23) and (5.24), we finally obtain

$$P_2^{(\psi)}(x_1, x_2; y) = \frac{N_{\hat{\psi}}}{\lambda^2 \kappa^{10}} f_{-i(1+\epsilon)\hat{\psi}}(\eta_1, \eta_2) f_{-i(1-\epsilon)\hat{\psi}}(\eta_1, \eta_2) e^{-\chi_1^2 - \chi_2^2} \quad (5.35)$$

$$= \frac{N_{\hat{\psi}}}{\lambda^2 \kappa^{10}} f_0(\eta_1 + (1 + \epsilon)\hat{\psi}, \eta_2 + (1 + \epsilon)\hat{\psi}) \times \\ \times f_0(\eta_1 + (1 - \epsilon)\hat{\psi}, \eta_2 + (1 - \epsilon)\hat{\psi}) e^{-\chi_1^2 - \chi_2^2}, \quad (5.36)$$

where we are using the notations (5.12) and (5.15) with η_i and χ_i corresponding to x_i , and $N_{\hat{\psi}}$ is dimensionless and determined by the condition $\int_{\tilde{x}}^\infty dx P_{1,2}(x; y) = 1$.

Recalling the form (5.23) of the function f_0 , we see that the joint passage probability density (5.35) factors the terms $(\eta_1 - \eta_2)^2$ and $\pm\epsilon = 1 + \eta_i/\hat{\psi}$ (i.e. $\pm y = \frac{R}{2} + \frac{x_i}{\psi}$). It follows that the considerations in momentum space that led us to the result (5.24) for the function $f_\psi(\theta_1, \theta_2)$ produce in coordinate space a mutual repulsion among the interfaces ($P_2^{(\psi)}(x, x; y) = 0$), as well as the presence of an impenetrable wedge along which the passage probability density vanishes. A plot of $P_{1,2}^{(\psi)}(x; y)$ is shown in Fig. 5.6.

For $\psi = 0$ (5.35) reduces to

$$P_2^{(0)}(x_1, x_2; y) = \frac{16}{3\pi} \frac{\chi_1^2 \chi_2^2 (\chi_1^2 - \chi_2^2)^2}{\kappa^2 \lambda^2} e^{-\chi_1^2 - \chi_2^2}, \quad (5.37)$$

a result which is known [98] to correspond to the so-called ‘‘vicious’’ walkers [41]

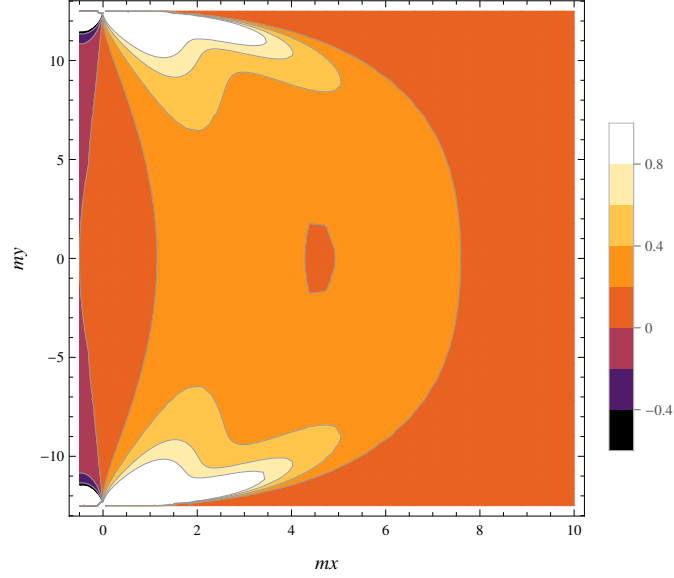


Figure 5.6: Contour plot of the passage probability density $m^{-1}P_{1,2}^{(\psi)}(x; y)$ for $mR = 25$ and $\psi = 0.04$. The leftmost contour corresponds to $P_{1,2}^{(\psi)} = 0$, and then to the wedge.

on the half line $x \geq 0$: the walkers start at $x = 0$, move randomly with the constraint of avoiding each other and the boundary, and return to $x = 0$ after a time R . Hence, our result (5.35) yields the exact joint passage probability density of two vicious walkers in the wedge.

The order parameter can be determined from $P_2^{(\psi)}$ through (5.29). We quote here the explicit result in the case of the half plane, for which the expressions simplify. For the Potts model the order parameter field has components σ_k ($\sum_{k=1}^q \sigma_k = 0$), with $\langle \sigma_k \rangle_0 = 0$ in the disordered phase, and we obtain¹

$$\langle \sigma_k(x, y) \rangle_{W_{bab}}^{\psi=0} = [\langle \sigma_k \rangle_b + \langle \sigma_k \rangle_a] \mathcal{A}(\chi) - 2\langle \sigma_k \rangle_a \mathcal{B}(\chi) + \langle \sigma_k \rangle_a, \quad (5.38)$$

with

$$\langle \sigma_k \rangle_a = \frac{q\delta_{ka} - 1}{q - 1} M, \quad a, k = 1, \dots, q, \quad (5.39)$$

¹These results coincide with those derived in Chapter 4 by direct summation of all terms in Fig. 5.5.

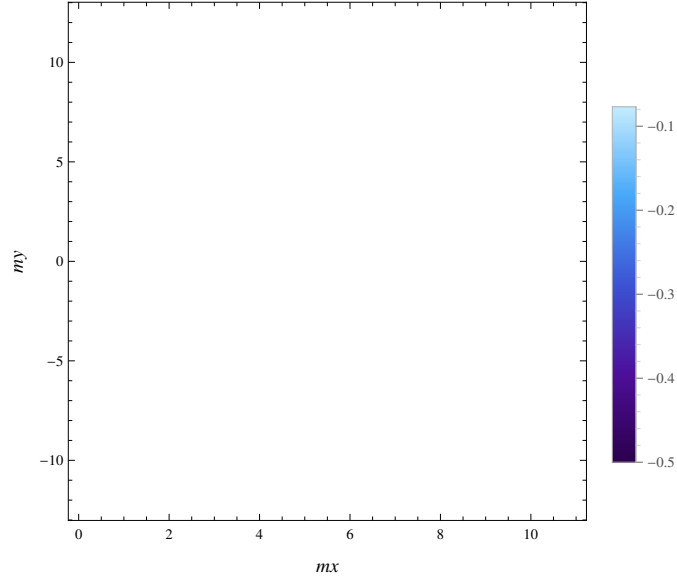


Figure 5.7: Order parameter $M^{-1}\langle\sigma_3(x,y)\rangle_{W_{121}}^{\psi=0}$ and contour lines for the dilute three-state Potts model at first order transition. Due to permutational symmetry, σ_3 does not distinguish between phases 1 and 2, and the intermediate bubble of the disorder phase is clearly visible.

$$\mathcal{A}(\chi) = -\frac{4}{3\pi}\chi^2(\chi^2 - 3)e^{-2\chi^2} + \frac{2}{3\sqrt{\pi}}\chi(-2\chi^4 + \chi^2 - 6)e^{-\chi^2}\text{erf}(\chi) + \text{erf}(\chi)^2, \quad (5.40)$$

$$\mathcal{B}(\chi) = \frac{\chi}{3\sqrt{\pi}}(-6 + \chi^2 - 2\chi^4)e^{-\chi^2} + \text{erf}(\chi). \quad (5.41)$$

A plot is shown in Fig. 5.7 for $q = 3$; for $q = 2$ (Ising) Fig. 5.8 compares the order parameter profile in the dilute case with the undilute result of Chapter 3.

5.5 Summary

In summary, we constructed the exact theory of phase separation in a two-dimensional wedge and derived from it the filling transition condition and the origin of wedge covariance. This has been achieved directly in the continuum and for arbitrary opening angles, while previous exact results concerned only the

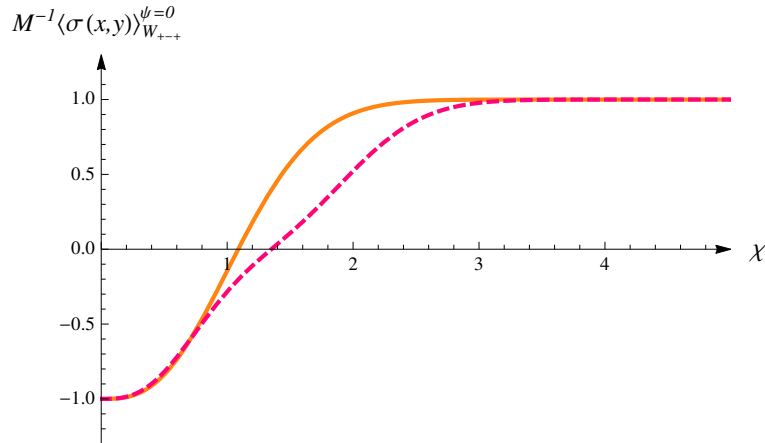


Figure 5.8: Order parameter $M^{-1}\langle\sigma(x,y)\rangle_{W_{+-+}}^{\psi=0}$ for the Ising model in the undilute (continuous) and dilute (dashed) cases; in the dilute case the intermediate disordered bubble smoothens the profile.

lattice Ising model and were limited to a right-angle corner. In particular, our derivation makes transparent the relation of wedge covariance with the relativistic nature of the kink excitations, and explains why this property has been difficult to establish in general within nonrelativistically covariant effective interfacial models. The passage probability for an interface with endpoints on the wedge has also been determined for small tilt angles in the unbound regime.

Moreover we developed the theory of phase separation in a planar wedge for the case in which a macroscopic bubble of a third phase forms in between the two phases favored by the boundary conditions. We discussed the q -state Potts model (dilute for $q < 4$) at its first order transition as an example to which the theory applies. In principle the full field theoretical calculation is much more complicated than that performed for the case of a single interface. However, we found that, isolating a specific contribution to the order parameter which corresponds to the detection of a single interface, the formalism allows to reconstruct the complete result. This finding, that we checked explicitly against the full calculations for the cases of the strip and of the half plane, appears promising for further developments.

For the case of the wedge, it is worth stressing that the very fact that the final result exhibits a wedge-shaped path along which the passage probability for

the interfaces vanishes provides a non-trivial consistency check for the theory. Indeed, the calculation starts from considerations in momentum space, in which the presence of a boundary is codified in properties of matrix elements of boundary condition changing fields. Moreover, the boundary is initially flat, and the information about the wedge is introduced through relativistic transformations performed on the matrix elements, always in momentum space. While in principle these are the same logic steps performed for the separation of two phases, in practice the case with a third phase is much more structured and leads to the specific form (5.23), (5.24) for the matrix element $f_\psi(\theta_1, \theta_2)$ of the boundary condition changing field. It is then remarkable to realize going on with the computation that the wedge in real space emerges because $f_\psi(\theta_1, \theta_2)$ turns out to fulfill the self-Fourier transform property (5.34). In this way, the mechanism which eventually accounts for wedge covariance acquires surprising mathematical implications in presence of a third phase.

This appears to have also additional implications. Indeed, we arrived at (5.23) exploiting also the integrability of the scaling Potts model, which in turn ensures factorization of the scattering and equation (5.21). On the other hand, since (5.21) is necessary to arrive at (5.23), and the latter is necessary for the appearance of the wedge in real space through (5.34), we are led to conclude that factorization of the scattering *at low energies* is required in systems allowing for the appearance of a bubble of a third phase. Notice that this is a weaker property than integrability, which implies factorization of the scattering at all energies.

We determined the joint passage probability for the interfaces separating the three phases and found that, in the case of a flat boundary (tilt angle $\psi = 0$ for the wedge), it coincides with the known probability for vicious walkers in the half plane. Hence for $\psi \neq 0$ our result provides the passage probability for vicious walkers in a wedge. The name vicious walkers is used in the literature for random walkers subject to the constraint of avoiding each other and the boundary. In our framework the properties of random propagation and avoidance for the interfaces emerge from the limit of large separation R between the boundary condition changing points on the boundary (pinning points for the interfaces), which is needed to observe phase separation. This limit projects the dynamics of the particles to low energies, where it turns out to reduce to fermionic statistics and

becomes universal. Consistently, the average distances between the interfaces and between the interfaces and the boundary grow as $\sqrt{R/m}$, and are much larger than the range $1/m$ of the particle-particle and particle-boundary interactions, whose details then affect only subleading orders in the large mR expansion.

Chapter 6

Decay of the thermodynamic Casimir force: bulk and boundary effects

The key idea underlying this thesis is the use of field theory for the description of near-critical interfacial phenomena. We showed how field theory provides a unified framework for the systematic study of phase separation and interfaces on the plane for the various universality classes. As a further application of these techniques we consider the so called thermal Casimir effect, which arises from the spatial confinement of critical fluctuations of a statistical system.

6.1 Introduction

The quantum-electrodynamical Casimir force [99] is known to possess a thermodynamical analogue induced by the spatial confinement of the thermal fluctuations of a medium close to a second-order transition point [100]. Such a thermodynamic (very often also called *critical*) Casimir force is observed experimentally [101, 102, 103, 104, 105, 106, 107] and is important for a variety of applications to microdevices. Despite their relevance, on the other hand, theoretical characterizations have proved to be quite challenging, complicated as they are by the need to deal with interacting theories and by an essential dependence on bound-

ary conditions. For the simplest geometry, a D -dimensional slab whose infinite boundary planes are separated by a distance R , and assigned uniform boundary conditions, it follows on general scaling grounds that the force (in temperature units $k_B T$ and per unit cross-sectional area) is R^{-D} times a scaling function $\vartheta(R/\xi)$, where ξ is the bulk correlation length¹. This function is universal, in the sense that it only depends on the symmetry of the order parameter, on D and on the boundary conditions, but otherwise little is known in general about it, to the point that even the sign of the force represents a non-trivial problem. Indeed, while reflection positivity ensures that mirror symmetric boundaries with identical boundary conditions attract [108, 109], the force is found to be repulsive in main instances of different conditions on the two boundaries (see *e.g.* [102, 110] for experimental and numerical data, respectively, for the three-dimensional Ising universality class). On the other hand, it was pointed out in [111] that for different boundary conditions a tuning of boundary parameters can lead to the reversal of the force as R/ξ varies, a circumstance neatly illustrated in [112] through exact computations for the Ising model in a strip.

In such an intricate situation, a general investigation of the function $\vartheta(R/\xi)$ can only start from asymptotics. For $R/\xi \rightarrow 0$ the force behaves as $\vartheta(0)/R^D$, and all the information about the boundary conditions is contained in the amplitude. Since this is a scale invariant limit for the bulk, boundary conformal field theory [113] allowed the exact determination of critical Casimir amplitudes in $D = 2$ for several universality classes and scale invariant boundary conditions [114, 115]. In this chapter we consider the opposite limit $R/\xi \gg 1$. In the case $D = 2$, that we study in detail, we show that the force decays differently for $R \gg \xi$ depending on the symmetry properties of the boundary conditions on the edges of the strip. Then, in principle, measuring the force in this limit provides a way to distinguish classes of boundary conditions realized in the physical system. Moreover, we show that the effect on the decay of symmetry-breaking and symmetry-preserving boundary conditions is interchanged when exchanging spontaneously broken with disordered phases. In recent years two-dimensional near critical behavior has been identified even in biological systems, such as cellular membranes [116], and the role of the thermodynamic Casimir force in this context has been investigated in

¹We refer to phases with finite correlation length.

[117]. At the end of the chapter we discuss to which extent our arguments extend to higher dimensions.

We begin our analysis considering a two-dimensional statistical system confined on a strip of vertical width R and length $L \rightarrow \infty$, with boundary conditions that we denote by u on the upper edge and d on the lower edge. The Casimir force per unit length between the two edges is given by

$$\mathcal{F}_{ud} = \frac{1}{L} \partial_R \ln Z_{ud} = \frac{1}{L} \frac{\partial_R Z_{ud}}{Z_{ud}}, \quad (6.1)$$

where $-\ln Z_{ud}$ is the contribution to the free energy due to the interaction between the edges. The system is close to a second-order phase transition point, so that its scaling limit corresponds to a Euclidean field theory, which in turn can be regarded as the analytic continuation to imaginary time of a relativistic quantum field theory in one spatial dimension. If H denotes the Hamiltonian of this quantum theory, the partition function Z_{ud} can be written as

$$Z_{ud} = \langle B_u | e^{-HR} | B_d \rangle, \quad (6.2)$$

where $|B_d\rangle$ and $|B_u\rangle$ are boundary states specifying the initial and final conditions of the imaginary time evolution; they can be expanded over the complete basis of asymptotic particle states of the bulk ($R = \infty$) theory, which are eigenstates of the Hamiltonian H .

We consider uniform, *i.e.* translation invariant, boundary conditions. The use of translation invariant boundary states¹ in the off-critical case was illustrated in [38] and exploited for free energy calculations on the strip in [118] in the context of integrable field theories. A study of the leading finite size effects was then performed in [119, 120], with particular attention for the precise relation between boundary state amplitudes and scattering amplitudes in the “crossed channel”. In the present chapter we are interested in the way the symmetry properties of the boundary conditions affect the finite size dependence in the different phases of the system and for the different universality classes, a subject whose systematic study was initiated in [121] in the context of crossing probabilities in percolation;

¹See Chapter 3 for the non-translation-invariant case.

but for Eq. (6.11), that we borrow from [38], our derivations are self-contained.

6.2 Below the critical temperature

The nature of bulk excitations differs above and below the critical temperature T_c associated to the spontaneous breaking of the symmetry (corresponding to a group G) characterizing the universality class; we discuss first the case $T < T_c$. Then, in two dimensions, the system possesses discrete degenerate ground states, corresponding to degenerate vacua of the associated quantum theory, that we denote by $|\Omega_a\rangle$, $a = 1, \dots, n$. For topological reasons, the elementary excitations are kinks $|K_{ab}(\theta)\rangle$ interpolating between different vacua $|\Omega_a\rangle$ and $|\Omega_b\rangle$; the rapidity θ parameterizes the energy and momentum of these relativistic particles as $(e, p) = (m \cosh \theta, m \sinh \theta)$, where m is the kink mass. In general the kink mass depends on the indices a and b ; here, however, we will be interested only in the leading large distance behavior of the Casimir force, which is determined by the particles with the lowest mass, and for this reason we will keep track only of the lightest kinks. Similarly, among the bound states that kinks may form, we will be interested in those arising in the topologically neutral channels $|K_{ab}(\theta_1)K_{ba}(\theta_2)\rangle$, and will denote by $|B_a(\theta)\rangle$ the lightest among them, with mass $m_B < 2m$. Throughout the chapter we call “exponential” correlation length and denote by ξ the correlation length defined by the large distance decay $r^{-\alpha}e^{-r/\xi}$ of the order parameter two-point function in the bulk theory. Since the order parameter operator is topologically neutral, ξ is $1/2m$ in the absence of neutral bound states, and $1/m_B$ otherwise.

6.2.1 Identical boundary conditions

The boundary conditions on the edges of the strip can be either symmetry preserving (*i.e.* left invariant by the action of the group G) or symmetry breaking. In the latter case we consider symmetry breaking (by a boundary field h) in favor of one of the degenerate vacua $|\Omega_a\rangle$, and denote by $|\mathcal{B}_a(h)\rangle$ the corresponding boundary state. The expansion over bulk states of one such boundary state, say

$|\mathcal{B}_1(h)\rangle$, will be of the form

$$\begin{aligned} |\mathcal{B}_1(h)\rangle &= |\Omega_1\rangle + g(h)|B_1(0)\rangle \\ &+ \sum_{b \neq 1} \int \frac{d\theta}{2\pi} f_b(\theta, h) |K_{1b}(-\theta)K_{b1}(\theta)\rangle + \dots, \end{aligned} \quad (6.3)$$

where the bulk states start and end on the vacuum $|\Omega_1\rangle$, and have zero total momentum as a consequence of translation invariance of the boundary condition; the dots stay for states with higher total mass¹ whose contribution to the large distance expansion of the Casimir force is subleading. Turning to the symmetry-preserving boundary states, we will denote them by $|\mathcal{B}_0(u)\rangle$, with u collectively denoting boundary parameters. These states expand in the form

$$\begin{aligned} |\mathcal{B}_0(u)\rangle &= \sum_a \{v_a(u)|\Omega_a\rangle + g_a(u)|B_a(0)\rangle \\ &+ \sum_{b \neq a} \int \frac{d\theta}{2\pi} f_{aba}(\theta, u) |K_{ab}(-\theta)K_{ba}(\theta)\rangle \\ &+ \sum_{c \neq a} [g_{ac}(u)|K_{ac}(0)\rangle \\ &+ \sum_{b \neq a, c} \int \frac{d\theta}{2\pi} f_{abc}(\theta, u) |K_{ab}(-\theta)K_{bc}(\theta)\rangle] \} + \dots, \end{aligned} \quad (6.4)$$

with the different vacua treated on the same footing.

We can now consider the large R asymptotics of the Casimir force for the different combinations of boundary conditions (6.3) and (6.4). For symmetry-preserving, or *free*, boundary conditions on both edges the leading contribution comes from the single-kink state in (6.4), and we have

$$\begin{aligned} Z_{00} &= \langle \mathcal{B}_0(u) | e^{-HR} | \mathcal{B}_0(u') \rangle \\ &\sim \sum_a \left[v_a^*(u) v_a(u') + mL \sum_{c \neq a} g_{ac}^*(u) g_{ac}(u') e^{-mR} \right], \end{aligned} \quad (6.5)$$

where we used $\langle \Omega_a | \Omega_b \rangle = \delta_{ab}$, $\langle K_{ab}(\theta) | K_{ac}(\theta') \rangle = 2\pi \delta(\theta - \theta') \delta_{bc}$ and $2\pi \delta(0) = mL$.

¹To be definite, we discuss the case $m_B > m$.

Equation (6.1) then gives

$$\mathcal{F}_{00} \sim -A_{00} m^2 e^{-mR}, \quad (6.6)$$

with $A_{00} = \sum_{a,c \neq a} g_{ac}^*(u) g_{ac}(u') / \sum_a v_a^*(u) v_a(u')$.

For boundary conditions $\mathcal{B}_1(h)$ on the upper edge and $\mathcal{B}_1(h')$ on the lower edge, the two-kink state gives the leading contribution to the force in absence of neutral bound states ($g = 0$ in (6.3)). The eigenvalue of e^{-HR} on the two-kink state is $e^{-2mR \cosh \theta}$, so that the limit of large mR is determined by the behavior of the excitations at small rapidities, which is a property of the bulk theory. With few exceptions, interacting particles in 1+1 dimensions behave at low energies as free fermions, and here we will discuss this generic case. Then for the product of states entering (6.2) we have in this limit

$$\begin{aligned} & \langle K_{1c}(\theta') K_{c1}(-\theta') | K_{1b}(-\theta) K_{b1}(\theta) \rangle \\ & \sim \delta_{bc} (2\pi)^2 \{ [\delta(\theta - \theta')]^2 - [\delta(\theta + \theta')]^2 \} \\ & = \delta_{bc} 2\pi m L \cosh \theta [\delta(\theta - \theta') - \delta(\theta + \theta')]. \end{aligned} \quad (6.7)$$

A further consequence of the low-energy fermionic statistics is that the two-kink amplitudes in (6.3) vanish at $\theta = 0$ (namely when the two particles have the same momentum), and can be written at small rapidity as

$$f_b(\theta, h) \sim C_b(h) \theta. \quad (6.8)$$

The last two equations allow us to calculate the two-kink contribution to the partition function $Z_{11} = \langle B_1(h) | e^{-HR} | B_1(h') \rangle$ in the large R limit as

$$A_{11} 2mL \int \frac{d\theta}{2\pi} \theta^2 e^{-2mR(1+\theta^2/2)} = \frac{A_{11}}{2\sqrt{\pi}} \frac{mL}{(mR)^{3/2}} e^{-2mR}, \quad (6.9)$$

with $A_{11} = \sum_{b \neq 1} C_b^*(h) C_b(h')$. The corresponding force is then

$$\mathcal{F}_{11} \sim -\frac{A_{11}}{\sqrt{\pi}} \frac{m^2}{(mR)^{3/2}} e^{-2mR}, \quad (6.10)$$

in the absence of topologically neutral bound states, and $-g^*(h)g(h')m_B^2 e^{-m_B R}$ if such a bound state is present¹. Notice that the force is attractive for $h = h'$, as for \mathcal{F}_{00} with $u = u'$; this agrees with the general result for identical mirror symmetric boundary conditions. Apart from these two cases, the sign is not determined in general.

6.2.2 Mixed boundary conditions

If we consider boundary conditions $\mathcal{B}_1(h)$ on the upper edge and $\mathcal{B}_0(u)$ on the lower edge, the calculation proceeds as in the previous case, with one important difference. It was found in [38] that when a boundary state contains a two-particle contribution such that the two particles individually contribute single-particle states to the expansion, then the amplitude of the two-particle state has a simple pole at $\theta = 0$. For the state (6.4) this means in particular that for small rapidity

$$f_{abc}(\theta, u) \sim \frac{C_{abc}(u)}{\theta}, \quad (6.11)$$

with $C_{abc} \propto g_{ab}g_{bc}$; this is still consistent with low-energy fermionic statistics since $f_{aba}(\theta, u)$ changes sign when the momenta of the two particles are interchanged ($\theta \rightarrow -\theta$). It follows from the combination of (6.8) and (6.11) that the two-kink contribution to the partition function Z_{10} for mR large reads

$$A_{10} 2mL \int \frac{d\theta}{2\pi} e^{-2mR(1+\theta^2/2)} = \frac{A_{10} mL}{\sqrt{\pi mR}} e^{-2mR}, \quad (6.12)$$

with $A_{10} = \sum_{b \neq 1} C_b^*(h)C_{1b1}(u)$. The force is then

$$\mathcal{F}_{10} \sim -\frac{2A_{10} m^2}{\sqrt{\pi mR}} e^{-2mR}, \quad (6.13)$$

in the absence of neutral bound states, and $-g^*(h)g_1(u)m_B^2 e^{-m_B R}$ otherwise; in writing \mathcal{F}_{10} we are choosing the normalization with $v_1 = 1$ for the boundary state (6.4).

A last possible choice of uniform boundary condition is to take $\mathcal{B}_1(h)$ on the

¹The single-particle contribution to the free energy has been investigated in [119, 122], where its amplitude, including the sign, has been determined for some integrable field theories.

upper edge and $\mathcal{B}_2(h')$ on the lower edge, with the latter choice corresponding to symmetry breaking in the direction of a different vacuum $|\Omega_2\rangle$. It follows from (6.3) that in this case the two boundary states have zero overlap, so that the free energy $-\ln Z_{12}$ is infinite. This corresponds to the fact that, in our large R limit, the boundary conditions we are considering lead to phase separation, with an interfacial tension equal to the kink mass m (see Chapter 3) and an excess free energy mL which diverges as $L \rightarrow \infty$.

6.3 Above the critical temperature

We can now consider the case $T > T_c$ of unbroken bulk symmetry. In this case the bulk theory possesses a single, symmetry invariant vacuum $|\Omega\rangle$, and the elementary excitations are no longer topological. In general, they will form a multiplet of particles A_i , with mass \tilde{m} , transforming according to a representation of the symmetry group G . These particles may give rise to bound states, and we denote by B the lightest among those invariant under the action of the group. Normally in a disordered phase the components of the order parameter operator create the elementary excitations A_i , so that the exponential correlation length is $\xi = 1/\tilde{m}$. Concerning the expansion of boundary states on bulk states, it is natural to consider neutral and charged boundary states. Neutral boundary states are those unaffected by the action of the group, and expand as

$$\begin{aligned} |\tilde{\mathcal{B}}_0(u)\rangle &= |\Omega\rangle + \gamma(u)|B(0)\rangle \\ &+ \sum_{ij} \int \frac{d\theta}{2\pi} f_{ij}(\theta, u) |A_i(-\theta)A_j(\theta)\rangle + \dots, \end{aligned} \quad (6.14)$$

where the tilde is used to distinguish (6.14) from the expansion (6.4) below T_c . Comparison with (6.3) then shows that the derivation of the large R behavior of \mathcal{F}_{00} above T_c retraces that of \mathcal{F}_{11} below T_c . The charged state $|\mathcal{B}_i\rangle$, depending on some boundary parameter λ , transforms as the particle A_i under the action of the group, and expands as

$$|\mathcal{B}_i(\lambda)\rangle = |A_i(0)\rangle + \sum_{jk} \int \frac{d\theta}{2\pi} f_{ijk}(\theta, \lambda) |A_j(-\theta)A_k(\theta)\rangle + \dots \quad (6.15)$$

Notice that $Z_{ii} = \langle \mathcal{B}_i | e^{-HR} | \mathcal{B}_i \rangle \propto \tilde{m} L e^{-\tilde{m}R}$ for R large, so that $\mathcal{F}_{ii} \sim -\tilde{m}/L$. We see that the absence of the vacuum contribution in (6.15) makes $L\mathcal{F}_{ii}$ non-extensive in L and non-vanishing as $R \rightarrow \infty$. Since extensivity and large R suppression should be preserved by the boundary state $|\tilde{\mathcal{B}}_1(h)\rangle$ corresponding to the presence of a symmetry-breaking boundary field (the analogue of (6.3) for $T > T_c$), we are led to conclude that this is realized by a superposition of (6.14) and (6.15). Comparing such a superposition to (6.4) we see that the derivation of the large R behavior of the Casimir force above T_c for symmetry-breaking boundary fields acting on both edges retraces that of \mathcal{F}_{00} below T_c .

The dynamics of bulk excitations is known exactly for most universality classes in two dimensions. For example, in the q -state Potts model [49], which exhibits a second-order transition for q up to 4, the high- and low- temperature phases are related by duality, and have the same mass spectrum, with the same mass m for the kinks below T_c and the particles above. These are the only excitations for $q = 2, 3$, while a neutral bound state with mass $\sqrt{3}m$ exists for $q = 4$ [52] and affects the Casimir force in the way we described. The case $q = 3$ provides one of the exceptions we mentioned to the fermionic low-energy behavior of bulk excitations, and this results in modifications of (6.10) and (6.13) that we will detail elsewhere. For the Ising model ($q = 2$), the exact relations satisfied by the Casimir force in the strip when exchanging high with low temperature and, simultaneously, fixed with free boundary conditions [112, 123], are a duality-enhanced example of the correspondences we obtained above. Similarly, it follows from our analysis that, for the Ising model with free boundary conditions on both edges of the strip, the Casimir force has the asymptotic form (6.6) below T_c and (6.10) above; this accounts for the asymmetry of the force across T_c studied on the lattice in [97].

Taking as an additional example the XY universality class, characterized by $O(2)$ symmetry, we need to remember that continuous symmetries cannot break spontaneously in two dimensions [124, 125], and that the transition is of the Berezinsky-Kosterlitz-Thouless type [126]. While the low temperature phase renormalizes onto a conformal field theory, our results for massive phases apply above the transition temperature. This disordered phase is described by a field theory with fermionic low-energy behavior and without bound states [127].

Hence, we find in particular the asymptotic result $\mathcal{F}_{00} \propto R^{-3/2} e^{-2mR}$, which can be compared to $R^{(1-D)/2} \exp(-2R/\hat{\xi})$ obtained in [128] from a perturbative calculation in $D = 4 - \epsilon$ dimensions. It is not surprising that the ϵ -expansion does not reproduce for $D = 2$ the prefactor $R^{-3/2}$, which originates from the non-perturbative property (6.8). Concerning the exponential factor, $\hat{\xi}$ should be identified with $\xi = 1/m$.

Several of the arguments used for the strip can be generalized to the case $D > 2$. Boundary states now describe boundary conditions on $(D - 1)$ -dimensional hyperplanes, and can still be expanded on the asymptotic states of the bulk theory [120, 122, 129]. In $D > 2$ also continuous symmetries can break spontaneously, but the presence of massless (Goldstone) particles in the expansion of the boundary states will prevent exponential decay of the force below¹ T_c . For phases with spontaneously broken discrete symmetry the force still decays exponentially, but the elementary particle excitations are no longer kinks and the analysis differs substantially from the case $D = 2$. The symmetry considerations we made above for the case $T > T_c$ should instead hold in general. A limitation for the asymptotic analysis in $D > 2$ is that the low-energy behavior of the amplitudes of two-particle states (the analogue of (6.8) and (6.11) above) is not known; in principle simulation results for the force can be used to investigate this point. On the other hand, when the decay of the force $\mathcal{F}_{ud} = L^{1-D} \partial_R \ln Z_{ud}$ is ruled by a single-particle term, the large R suppression is D -independent. For example, for the $O(n)$ model with a boundary field h on both boundaries, the force is expected to decay as $\alpha_D(h) \xi^{-D} e^{-R/\xi}$ above T_c , with $\alpha_D(h)$ a pure number and ξ the exponential correlation length.

6.4 Summary

In summary, we studied the decay of the thermodynamic Casimir force on an infinitely long strip whose width R is much larger than the bulk correlation length. The analysis exploits the expression of the boundary conditions in terms of the particle excitations of the bulk theory. Using low energy properties of two-dimensional field theory we determined the exact form of the large- R suppression,

¹See the profile of the force determined in [130] for the three-dimensional $O(n \rightarrow \infty)$ case.

and showed that it depends in distinctive ways on the symmetry properties of the boundary conditions. The possibility to detect symmetry classes of boundary conditions from the functional form of the decay of the force contrasts with what happens in the opposite limit (R much smaller than the correlation length), in which boundary conditions only affect numerical amplitudes. We also discussed which features specific of the bulk universality class may affect the decay of the force. The different nature of the bulk excitations above and below the critical temperature was shown to induce in general a different behavior of the force in the two regimes. On the other hand, the large- R suppression does not change when exchanging spontaneously broken with disordered phases and, at the same time, symmetry-breaking with symmetry-preserving boundary conditions, a circumstance that must be regarded as a weaker, but more general, version of duality relations known for the Ising model. The formalism makes transparent that the sign of the force at large R depends on the boundary parameters if these are different on the two edges of the strip, and is attractive if they are identical. Finally we discussed how several of our arguments extend to higher dimensions and yield specific predictions.

Acknowledgements

Desidero esprimere i miei più calorosi ringraziamenti al mio relatore, il *Prof. Gesualdo Delfino*, per avermi dato l'opportunità di apprendere una delle più affascinanti ed eleganti aree della Fisica Teorica lavorando al suo fianco, e in definitiva, per avermi guidato in quella che è stata la più edificante e sublime di tutte le esperienze culturali che abbia mai intrapreso. Di non secondaria importanza è stata la sua cordialità, comprensione e sincera vicinanza umana, specialmente nei momenti in cui le vicissitudini della vita interferiscono con il percorso accademico. Un grazie di cuore.

Ringrazio inoltre il Dr. Raul Santachiara e il Prof. Andrea Cappelli per aver accettato il ruolo di referre per la mia tesi.

Colgo l'occasione per ringraziare tutti gli afferenti al gruppo di Fisica Statistica, in primis il suo direttore, *Prof. Giuseppe Mussardo*, per aver creato una stimolante atmosfera di scambio di idee e crescita intellettuale nel campo della Fisica Statistica (e non solo), della quale il nostro caro Paese sentiva tanto bisogno. E aggiungo, grazie per aver scelto Trieste.

Un ringraziamento speciale è dedicato a *Laura*, per essermi stata vicina nei momenti più difficili, per avermi supportato e sopportato nei giorni più irritabili e per aver creduto in me, anche quando era la sola a farlo. Una nota di merito spetta al piccolo *Tullio Livio*, che ha saputo mantenerci uniti nei giorni più tormentati, il tutto nonostante la sua incontenibile energia e incredibile produzione di "entropia domestica".

Vorrei dedicare un sentito ringraziamento anche a tutti coloro che con il loro aiuto materiale, supporto morale o con la semplice vicinanza,

anche inconsapevole, hanno contribuito al raggiungimento di questo traguardo. Siete tanti e non posso elencarvi tutti.

Concludo con dei ringraziamenti di caratura più “metafisica” dei precedenti. Ringrazio: la *SISSA* e il *SISSA Medialab* per le innumerevoli iniziative culturali che mi hanno offerto, la città di Trieste, le sue atmosfere e i suoi caffè, *Trenitalia* e *Ferrovie dello Stato* per le memorabili ore di lavoro spese traballando da Pontedera a Trieste e viceversa, la città di Firenze e il *GGI* (Galileo Galilei Institute for Theoretical Physics) per le meravigliose passeggiate e riflessioni a cielo aperto, le mie care terre in Toscana; e di nuovo *Trieste*, città che Amo follemente e mai dimenticherò.

AS,

Stuttgart, 18-06-2016

Bibliography

- [1] G. Delfino and J. Viti. Phase separation and interface structure in two dimensions from field theory. *J. Stat. Mech.*, page P10009, (2012). [i](#), [27](#), [48](#)
- [2] G. Delfino and A. Squarcini. Interfaces and wetting transition on the half plane. Exact results from field theory. *J. Stat. Mech.*, page P05010, (2013). [i](#)
- [3] G. Delfino and A. Squarcini. Exact theory of intermediate phases in two dimensions. *Annals of Physics*, 342:171, (2014). [i](#)
- [4] G. Delfino and A. Squarcini. Phase separation in a wedge. Exact results. *Phys. Rev. Lett.*, 113:066101, (2014). [i](#)
- [5] G. Delfino and A. Squarcini. Multiple phases and vicious walkers in a wedge. arXiv:1509.00310v1. [i](#)
- [6] G. Delfino and A. Squarcini. Bulk and boundary effects on the decay of the thermodynamic Casimir force. *Europhys. Lett.*, 109:16001, (2015). [i](#)
- [7] L. D. Landau and E. M. Lifshitz. *Statistical Physics*, volume 5 of *Landau and Lifshitz Course of Theoretical Physics*. Elsevier, third edition, (1980). [1](#), [2](#)
- [8] M. Hillert. *Phase Equilibria, Phase Diagrams and Phase Transformations*. Cambridge University Press, second edition, (2008). [2](#)
- [9] P. Papon and J. Leblond and P. H. E. Meijer. *The Physics of Phase Transitions*. Springer, second edition, (2006). [2](#)

- [10] H. E. Stanley. *Introduction to Phase Transition and Critical Phenomena*. International Series of Monographs on Physics. Oxford University Press, (1971). [3](#)
- [11] J. Cardy. *Scaling and Renormalization in Statistical Physics*, volume 5 of *Cambridge Lecture Notes in Physics*. Cambridge University Press, (1996). [3](#)
- [12] S. Dietrich. Wetting Phenomena. In C. Domb and J.L. Lebowitz, editors, *Phase Transitions and Critical Phenomena*, volume 12, page 1. Academic Press, London, (1988). [3](#), [33](#), [34](#), [63](#), [85](#)
- [13] G. Forgacs, R. Lipowsky and T. M. Nieuwenhuizen. The behavior of interfaces in ordered and disordered systems. In C. Domb and J. L. Lebowitz, editor, *Phase Transitions and Critical Phenomena*, volume 14, chapter 2. Academic Press, London, (1991). [3](#), [63](#)
- [14] M. Schick. An Introduction to Wetting Phenomena. In J. Chavrolin and J.-F. Joanny and J. Zinn-Justin, editor, *Liquids at Interfaces*, page 415. Elsevier, Amsterdam, (1990). [3](#), [63](#), [85](#)
- [15] P.-G. de Gennes. Wetting: statics and dynamics. *Rev. Mod. Phys.*, 57:827, (1985). [3](#), [4](#), [63](#), [72](#), [85](#)
- [16] D. Bonn and J. Eggers and J. Indekeu and J. Meunier and E. Rolley. Wetting and spreading. *Rev. Mod. Phys.*, 81:739, (2009). [3](#), [8](#), [63](#), [71](#), [72](#), [85](#)
- [17] D. Bonn and D. Ross. Wetting transitions. *Rep. Prog. Phys.*, 64:1085, (2001). [3](#), [13](#), [63](#)
- [18] P.-G. de Gennes and F. Brochard-Wyart and D. Quéré. *Capillarity and Wetting Phenomena: Drops, Bubbles, Pearls, Waves*. Springer, (2010). [3](#)
- [19] Thomas Young. An Essay on the Cohesion of Fluids. *Philosophical Transactions of the Royal Society of London*, 95:65–87, (1805). [4](#)

- [20] J. Pellicer and J. A. Manzanares and S. Mafé. The physical description of elementary surface phenomena: Thermodynamics versus mechanics. *American Journal of Physics*, 63(6):542–547, (1995). [4](#)
- [21] J. W. Cahn. Critical point wetting. *Journal of Chemical Physics*, 66:3667, (1977). [5](#), [11](#), [13](#)
- [22] B. Widom. Surface Tension of Fluids. In C. Domb and M.S. Green, editors, *Phase Transitions and Critical Phenomena*, volume 2, page 79. Academic Press, London, (1972). [5](#), [11](#)
- [23] K. Binder. Critical Behaviour at Surfaces. In C. Domb and J.L. Lebowitz, editors, *Phase Transitions and Critical Phenomena*, volume 8, page 1. Academic Press, London, (1983). [5](#)
- [24] H. W. Diehl and D. M. Kroll and H. Wagner. The Interface in a Ginsburg-Landau-Wilson Model: Derivation of the Drumhead Model in the Low-Temperature Limit. *Zeitschrift für Physik B*, 36:329–333, (1980). [6](#)
- [25] D. Nelson and T. Piran and S. Weinberg, editor. *Statistical Mechanics of Membranes and Surfaces*. World Scientific, second edition, (2004). [6](#)
- [26] K. R. Mecke and S. Dietrich. Effective Hamiltonian for liquid-vapor interfaces. *Physical Review E*, 59:6766, 1999. [7](#)
- [27] J. O. Indekeu. Wetting phase transitions and critical phenomena in condensed matter. *Physica A*, 389:4332–4359, (2010). [8](#)
- [28] A. O. Parry, C. Rascón, Nelson Rei Bernardino, and J. M. Romero-Enrique. 3D Short-Range Wetting and Nonlocality. *Physical Review Letters*, 100:136105, 2008. [8](#)
- [29] A. O. Parry and C. Rascón. The Trouble with Critical Wetting. *Journal of Low Temperatures Physics*, 157:149–173, (2009). [8](#)
- [30] D. Ross, D. Bonn, and J. Meunier. Observation of short-range critical wetting. *Nature*, 400:737, (1999). [8](#)

- [31] H. W. Diehl. Field-theoretic approach to critical behaviour at surfaces. In C. Domb and J.L. Lebowitz, editors, *Phase Transitions and Critical Phenomena*, volume 10, page 75. Academic Press, London, (1986). [8](#), [10](#), [63](#)
- [32] D. Jasnow. Renormalization Group Theory of Interfaces. In C. Domb and J.L. Lebowitz, editors, *Phase Transitions and Critical Phenomena*, volume 10, page 270. Academic Press, London, (1986). [10](#)
- [33] A. O. Parry, C. Rascón, Nelson Rei Bernardino, and J. M. Romero-Enrique. Derivation of a non-local interfacial Hamiltonian for short-range wetting: II. General diagrammatic structure. *Journal of Physics: Condensed Matter*, 19:416105(21pp), (2007). [10](#)
- [34] J. S. Rowlinson and B. Widom. *Molecular Theory of Capillarity*. Oxford University Press, Oxford and New York, (1982). [11](#)
- [35] H. Nakanishi and M. E. Fisher. Multicriticality of wetting, pre-wetting, and surface transitions. *Phys. Rev. Lett.*, 49:1565, (1982). [13](#)
- [36] R. J. Eden and P. V. Landshoff and D. I. Olive and J. C. Polkinghorne. *The Analytic S-Matrix*. Cambridge University Press, (1966). [17](#), [65](#), [68](#), [70](#), [88](#), [93](#)
- [37] S. Coleman and J. Mandula. All Possible Symmetries of the S Matrix. *Phys. Rev.*, 159:1251, (1967). [20](#)
- [38] S. Ghoshal and A. B. Zamolodchikov. Boundary S Matrix and Boundary State in Two-Dimensional Integrable Quantum Field Theory. *Int. J. Mod. Phys.*, A9:3841; [Erratum ibidem, 4353], (1994). [22](#), [23](#), [66](#), [67](#), [70](#), [94](#), [95](#), [107](#), [108](#), [111](#)
- [39] A. Fring and R. Köberle. Factorized scattering in the presence of reflecting boundaries. *Nucl. Phys. B*, 421:159, (1994). [22](#)
- [40] D. B. Abraham. Surface Structures and Phase Transitions - Exact Results. In C. Domb and J.L. Lebowitz, editors, *Phase Transitions and Critical*

- Phenomena*, volume 10, page 1. Academic Press, London, (1986). [25](#), [63](#), [73](#), [86](#)
- [41] M. E. Fisher. Walks, Walls, Wetting, and Melting. *J. Stat. Phys.*, 34:667, (1984). [25](#), [86](#), [98](#)
- [42] B. Berg, M. Karowski and P. Weisz. Construction of Green's functions from an exact S matrix. *Phys. Rev. D*, 19:2477, (1979). [30](#)
- [43] F. A. Smirnov. *Form Factors in Completely Integrable Models of Quantum Field Theory*. World Scientific, (1992). [30](#), [67](#)
- [44] G. Delfino and J. Cardy. Universal amplitude ratios in the two-dimensional q -state Potts model and percolation from quantum field theory. *Nucl. Phys. B*, 519:551, (1998). [30](#), [68](#)
- [45] G. Delfino and J. Viti. Universal properties of Ising clusters and droplets near criticality. *Nucl. Phys. B*, 840:513, (2010). [30](#)
- [46] D. B. Abraham. Capillary Waves and Surface Tension: An Exactly Solvable Model. *Phys. Rev. Lett.*, 47:545, (1981). [31](#)
- [47] L. Greenberg and D. Ioffe. On an invariance principle for phase separation lines. *Ann. Inst. H. Poincaré Probab. Statist.*, 41:871, (2005). [33](#)
- [48] M. Campanino, D. Ioffe and Y. Velenik. Fluctuation Theory of Connectivities for Subcritical Random Cluster Models. *Ann. Probab.*, 36:1287, (2008). [33](#)
- [49] F. Y. Wu. The Potts model. *Rev. Mod. Phys.*, 54:235, (1982). [43](#), [44](#), [94](#), [113](#)
- [50] R. J. Baxter. *Exactly Solved Models in Statistical Mechanics*. Academic Press, New York, (1982). [43](#)
- [51] G. Delfino. Parafermionic excitations and critical exponents of random cluster and $O(n)$ models. *Annals of Physics*, 1:333, (2013). [43](#)

- [52] L. Chim and A. B. Zamolodchikov. Integrable field theory of the q -state Potts model with $0 < q < 4$. *Int. J. Mod. Phys. A*, 7:5317, (1992). [44](#), [48](#), [113](#)
- [53] G. Delfino. First-order phase transitions and integrable field theory. The dilute q -state Potts model. *Nucl. Phys. B*, 554:537, (1999). [44](#), [94](#), [95](#)
- [54] C. M. Fortuin and P. W. Kasteleyn. On the random-cluster model: I. Introduction and relation to other models. *Physica*, 57:536; *J. Phys. Soc. Jpn. Suppl.*, 26 (1969) 11, (1972). [49](#)
- [55] G. Delfino and J. Cardy. The field theory of the $q \rightarrow 4^+$ Potts model. *Phys. Lett. B*, 483:303, (2000). [49](#), [94](#), [95](#)
- [56] B. M. McCoy and T. T. Wu. Two-dimensional Ising field theory for $T < T_c$: String structure of the three-point function. *Phys. Rev. D*, 18:1243, (1978). [49](#)
- [57] D. B. Abraham and P. J. Upton. Droplet singularity. *Phys. Rev. Lett.*, 70:1567, (1993). [49](#)
- [58] L.-F. Ko and M.E. Fisher. The shapes of bowed interfaces in the two-dimensional Ising model. *J. Stat. Phys.*, 58:249, (1990). [49](#)
- [59] G. Delfino and P. Grinza. Universal ratios along a line of critical points. The Ashkin-Teller model. *Nucl. Phys. B*, 682:521, (2004). [50](#), [51](#), [53](#)
- [60] L. P. Kadanoff and A. C. Brown. Correlation functions on the critical lines of the Baxter and Ashkin-Teller models. *Ann. Phys.*, 121:318, (1979). [50](#)
- [61] A. B. Zamolodchikov and Al. B. Zamolodchikov. Factorized S matrices in two-dimensions as the exact solutions of certain relativistic Quantum Field Models. *Ann. Phys.*, 120:253, (1979). [50](#), [51](#)
- [62] G. Delfino. Off-critical correlations in the Ashkin-Teller model. *Phys. Lett. B*, 450:196, (1999). [53](#)

- [63] G. Andrews, R. Baxter and J. Forrester. Eight-vertex SOS model and generalized Rogers-Ramanujan-type identities. *J. Stat. Phys.*, 35:193, (1984). [55](#)
- [64] A. LeClair. Restricted sine-Gordon theory and the minimal conformal series. *Phys. Lett. B*, 230:103, (1989). [55](#)
- [65] G. Delfino. Correlators in integrable quantum field theory: the scaling RSOS models. *Nucl. Phys. B*, 583:597, (2000). [55](#)
- [66] N. M. Temme. Error Functions, Dawson’s and Fresnel Integrals. In F. W. J. Olver, D. W. Lozier, R. F. Boisvert, C. W. Clark, editor, *NIST Handbook of Mathematical Functions*, chapter 7. Cambridge University Press, (2010). [56](#), [57](#), [80](#)
- [67] O. Schramm. Scaling limits of loop-erased random walks and uniform spanning trees. *Israel J. Math.*, 118:221; *Electron. Commun. Probab.* 8 (2001) paper no. 12, 2000. [60](#), [61](#)
- [68] J. Cardy. SLE for theoretical physicists. *Ann. Phys.*, 318:81–118, (2005). [60](#), [61](#)
- [69] M. Bauer and D. Bernard. 2D growth processes: SLE and Loewner chains. *Phys. Rep.*, 432:115, (2006). [61](#)
- [70] K. Binder, D. P. Landau and M. Muller. Monte Carlo Studies of Wetting, Interface Localization and Capillary Condensation. *J. Stat. Phys.*, 110:1411, (2003). [63](#)
- [71] D. B. Abraham. Solvable Model with a Roughening Transition for a Planar Ising Ferromagnet. *Phys. Rev. Lett.*, 44:1165, (1980). [63](#), [69](#), [73](#), [86](#), [91](#)
- [72] Z. Bajnok and L. Palla and G. Takács. On the boundary form factor program. *Nucl. Phys. B*, 750:179–212, (2006). [67](#), [70](#)
- [73] D. B. Abraham and M. E. Issigoni. Phase separation at the surface of an Ising ferromagnet. *J. Phys. A*, 13:L89, (1980). [69](#)

- [74] A. A. Belavin and A. M. Polyakov and A. B. Zamolodchikov. Infinite conformal symmetry in two-dimensional quantum field theory. *Nucl. Phys. B*, 241:333, (1984). [72](#)
- [75] J. Cardy. Conformal invariance and surface critical behavior. *Nucl. Phys. B*, 240:514, (1984). [72](#)
- [76] S. Dietrich and M. N. Popescu and M. Rauscher. Wetting on structured substrates. *J. Phys.: Condensed Matter*, 17:S577, (2005). [85](#)
- [77] P. Pfeifer and Y. J. Wu and M. W. Cole and J. Krim. Multilayer adsorption on a fractally rough surface. *Phys. Rev. Lett.*, 62:1997, (1989). [85](#)
- [78] L. D. Gelb and K. E. Gubbins and R. Radhakrishnan and M. Sliwinski-Bartkowiak. Phase separation in confined systems. *Rep. Prog. Phys.*, 62:1573, (1999). [85](#)
- [79] C. Rascón and A. O. Parry. Geometry-dominated fluid adsorption on sculpted solid substrates. *Nature (London)*, 407:986, (2000). [85](#)
- [80] E. H. Hauge. Macroscopic theory of wetting in a wedge. *Phys. Rev. A*, 46:4994, (1992). [85](#), [93](#)
- [81] D. B. Abraham and A. O. Parry and A. J. Wood. Drumhead model of 2D wetting, filling and wedge covariance. *Europhys. Lett.*, 60:106, (2002). [86](#)
- [82] C. Rascón and A. O. Parry. Covariance for Cone and Wedge Complete Filling. *Phys. Rev. Lett.*, 94:096103, (2005). [86](#)
- [83] A. O. Parry and C. Rascón. An interpretation of covariance relations for wetting and wedge filling transitions. *J. Chem. Phys.*, 132:204704, (2010). [86](#)
- [84] L. Bruschi and A. Carlin and G. Mistura. Complete Wetting on a Linear Wedge. *Phys. Rev. Lett.*, 89:166101, (2002). [86](#)
- [85] G. Gallavotti. The phase separation line in the two-dimensional Ising model. *Commun. Math. Phys.*, 27:103, (1972). [86](#)

- [86] D. B. Abraham and P. Reed. Phase Separation in the Two-Dimensional Ising Ferromagnet. *Physical Review Letters*, 33:377–379, 1974. [86](#)
- [87] D. B. Abraham and P. Reed. Interface profile of the Ising ferromagnet in two dimensions. *Commun. Math. Phys.*, 49(1):35–46, (1976). [86](#)
- [88] D. B. Abraham and F. T. Latrémolière. Path-Summation Representations in Planar Uniaxial Ferromagnets. *Physical Review Letters*, 77:171–174, 1996. [86](#)
- [89] D. B. Abraham and A. Maciolek. Filling Transition: Exact Results for Ising Corners. *Phys. Rev. Lett.*, 89:286101, (2002). [86](#)
- [90] D. B. Abraham and A. Maciolek. Exact results for corner filling on a quadratic lattice. *Physical Review E*, 72:031601–14, 2005. [86](#)
- [91] D. B. Abraham and V. Mustonen and A. J. Wood. Triangular lattice solution for filling in a wedge. *Europhys. Lett.*, 63(3):408, 2003. [86](#)
- [92] K. Rejmer and S. Dietrich and M. Napiorkowski. Filling transition for a wedge. *Phys. Rev. E*, 60:4027, (1999). [86](#)
- [93] A. O. Parry and C. Rascón and A. J. Wood. Universality for 2D Wedge Wetting. *Phys. Rev. Lett.*, 83:5535, (1999). [86](#)
- [94] A. O. Parry and C. Rascón and A. J. Wood. Critical Effects at 3D Wedge Wetting. *Phys. Rev. Lett.*, 85:345, (2000). [86](#)
- [95] A. Malijevský and A. O. Parry. Critical Point Wedge Filling. *Phys. Rev. Lett.*, 110:166101, (2013). [86](#)
- [96] G. Delfino. Fields, particles and universality in two dimensions. *Ann. Phys.*, 360:477, (2015). [87](#), [90](#)
- [97] D. B. Abraham and A. Maciolek. Surface states and the Casimir interaction in the Ising model. *Europhys. Lett.*, 101:20006, (2013). [94](#), [113](#)

- [98] G. Schehr, S. N. Majumdar, A. Comtet, and J. Randon-Furling. Exact Distribution of the Maximal Height of p Vicious Walkers. *Phys. Rev. Lett.*, 101:150601, (2008). [98](#)
- [99] H. B. G. Casimir. On the attraction between two perfectly conducting plates. *Proc. K. Ned. Akad. Wet.*, 51:793, (1948). [105](#)
- [100] M. E. Fisher and P.-G. de Gennes. Phénomènes aux parois dans un mélange binaire critique. *C. R. Acad. Sci. Paris B*, 287:207, (1978). [105](#)
- [101] R. Garcia and M. H. W. Chan. Critical Fluctuation-Induced Thinning of ^4He Films near the Superfluid Transition. *Phys. Rev. Lett.*, 83:1187, (1999). [105](#)
- [102] M. Fukuto, Y. F. Yano and P. S. Pershan. Critical Casimir Effect in Three-Dimensional Ising Systems: Measurements on Binary Wetting Films. *Phys. Rev. Lett.*, 94:135702, (2005). [105](#), [106](#)
- [103] A. Ganshin, S. Scheidemantel, R. Garcia, and M. H. W. Chan. Critical Casimir Force in ^4He Films: Confirmation of Finite-Size Scaling. *Phys. Rev. Lett.*, 97:075301, (2006). [105](#)
- [104] C. Hertlein, A. Gambassi, S. Dietrich, and C. Bechinger. Direct measurement of critical Casimir forces. *Nature*, 451:172, (2008). [105](#)
- [105] F. Soyka, O. Zvyagolskaya, C. Hertlein, L. Helden and C. Bechinger. Critical Casimir Forces in Colloidal Suspensions on Chemically Patterned Surfaces. *Phys. Rev. Lett.*, 101:208301, (2008). [105](#)
- [106] D. Bonn, J. Otwinowski, S. Sacanna, H. Guo, G. Wegdam and P. Schall. Direct Observation of Colloidal Aggregation by Critical Casimir Forces. *Phys. Rev. Lett.*, 103:156101, (2009). [105](#)
- [107] U. Nellen, L. Helden and C. Bechinger. Tunability of critical Casimir interactions by boundary conditions. *Europhys. Lett.*, 88:26001, (2009). [105](#)
- [108] O. Kenneth and I. Klich. Opposites Attract: A Theorem about the Casimir Force. *Phys. Rev. Lett.*, 97:160401, (2006). [106](#)

- [109] C. P. Bachas. Comment on the sign of the Casimir force. *J. Phys. A*, 40:9089, (2007). [106](#)
- [110] O. Vasilyev and A. Gambassi and A. Maciolek and S. Dietrich. Monte Carlo simulation results for critical Casimir forces. *Europhys. Lett.*, 80:60009, (2007). [106](#)
- [111] F. M. Schmidt and H. W. Diehl. Crossover from Attractive to Repulsive Casimir Forces and Vice Versa. *Phys. Rev. Lett.*, 101:100601, (2008). [106](#)
- [112] D. B. Abraham and A. Maciolek. Casimir Interactions in Ising Strips with Boundary Fields: Exact Results. *Phys. Rev. Lett.*, 105:055701, (2010). [106](#), [113](#)
- [113] J. Cardy. Universal critical-point amplitudes in parallel-plate geometries. *Phys. Rev. Lett.*, 65:1443, (1990). [106](#)
- [114] J. Cardy. Effect of boundary conditions on the operator content of two-dimensional conformally invariant theories. *Nucl. Phys. B*, 275:200, (1986). [106](#)
- [115] T. W. Burkhardt and T. Xue. Density profiles in confined critical systems and conformal invariance. *Phys. Rev. Lett.*, 66:895, (1991). [106](#)
- [116] S. L. Veatch, P. Cicuta, P. Sengupta, A. Honerkamp-Smith, D. Holowka and B. Baird. Critical Fluctuations in Plasma Membrane Vesicles. *ACS Chem. Biol.*, 3:287, (2008). [106](#)
- [117] B. B. Machta, S. L. Veatch and J. Sethna. Critical Casimir Forces in Cellular Membranes. *Phys. Rev. Lett.*, 109:138101, (2012). [107](#)
- [118] A. Le Clair, G. Mussardo, H. Saleur and S. Skorik. Boundary energy and boundary states in integrable quantum field theories. *Nucl. Phys. B*, 453:581, (1995). [107](#)
- [119] Z. Bajnok, L. Palla and G. Takacs. Finite size effects in quantum field theories with boundary from scattering data. *Nucl. Phys. B*, 716:519, (2005). [107](#), [111](#)

- [120] Z. Bajnok, L. Palla and G. Takacs. Casimir force between planes as a boundary finite size effect. *Phys. Rev. D*, 73:065001, (2006). [107](#), [114](#)
- [121] G. Delfino and J. Viti. Crossing probability and number of crossing clusters in off-critical percolation. *J. Phys. A*, 45:032005, (2012). [107](#)
- [122] Z. Bajnok and L. Palla and G. Takács. Boundary one-point function, Casimir energy and boundary state formalism in $D + 1$ dimensional QFT. *Nucl. Phys. B*, 772:290, (2007). [111](#), [114](#)
- [123] R. Evans and J. Stecki. Solvation force in two-dimensional Ising strips. *Phys. Rev. B*, 49:8842, (1994). [113](#)
- [124] N. D. Mermin and H. Wagner. Absence of Ferromagnetism or Antiferromagnetism in One- or Two-Dimensional Isotropic Heisenberg Models. *Phys. Rev. Lett.*, 17:1133, (1966). [113](#)
- [125] P. C. Hohenberg. Existence of Long-Range Order in One and Two Dimensions. *Phys. Rev.*, 158:383, (1967). [113](#)
- [126] J. M. Kosterlitz and D. J. Thouless. Ordering, metastability and phase transitions in two-dimensional systems. *J. Phys. C*, 6:1181, (1973). [113](#)
- [127] A. B. Zamolodchikov. Exact S -Matrix associated with self-avoiding polymer problem in two dimensions. *Mod. Phys. Lett. A*, 6:1807, (1991). [113](#)
- [128] M. Krech and S. Dietrich. Finite-size scaling for critical films. *Phys. Rev. Lett.*, 66:345 [Erratum 67, 1055 (1991)], (1991). [114](#)
- [129] G. Delfino. Order parameter profiles in presence of topological defect lines. *J. Phys. A*, 47:132001, (2014). [114](#)
- [130] H. W. Diehl, D. Gruneberg, M. Hasenbusch, A. Hucht, S. B. Rutkevich and F. M. Schmidt. Exact thermodynamic Casimir forces for an interacting three-dimensional model system in film geometry with free surfaces. *Europhys. Lett.*, 100:10004, (2012). [114](#)